MACROPHAGE INVOLVEMENT IN THE REMODELING OF AN EXTRACELLULAR MATRIX SCAFFOLD

by

Jolene E. Valentin

B.S. in Materials Science and Engineering, University of Florida, 2003

Submitted to the Graduate Faculty of

Swanson School of Engineering in partial fulfillment

of the requirements for the degree of

Doctor of Philosophy

University of Pittsburgh

2009

UNIVERSITY OF PITTSBURGH

SWANSON SCHOOL OF ENGINEERING

This dissertation was presented

by

Jolene E. Valentin

It was defended on

November 2, 2009

and approved by

Sanjeev G. Shroff, PhD, Professor, Department of Bioengineering

William R. Wagner, PhD, Professor, Department of Bioengineering

Mervin C. Yoder, MD, Professor, Department of Pediatrics

Dissertation Director: Stephen F. Badylak, DVM, MD, PhD, Professor, Department of Surgery

MACROPHAGE INVOLVEMENT IN THE REMODELING OF AN EXTRACELLULAR MATRIX SCAFFOLD

Jolene E. Valentin, Ph.D.

University of Pittsburgh, 2009

The remodeling response to extracellular matrix (ECM) scaffold materials such as porcine small intestinal submucosa (SIS) is characterized by intense mononuclear cell infiltration during the first 4 weeks post-implantation. Persistence of macrophages in wounds is typically diagnosed as chronic inflammation with downstream formation of scar tissue and/or foreign body reaction, but ECM scaffolds remodel into organized site-specific tissue. Macrophages can express either proinflammatory (M1) or immunomodulatory and tissue remodeling (M2) phenotypes. Processing methods used during the manufacturing of ECM scaffolds can influence macrophage phenotype and downstream remodeling outcome.

In the first study, human monocyte-derived macrophages were cultured on SIS and carbodiimide (CDI) crosslinked SIS in 20% and 6% oxygen concentrations. Macrophage phenotype was evaluated by expression of M1 (*CXCL10* and *CCR7*) and M2 (*ARG-1*, *CCL13*, *CCL18*, and *MRC-1*) gene markers, and secretion of CXCL10, CCL13, CCL18, and MMP9. Macrophages cultured on SIS expressed an M2 profile, while macrophages cultured on CDI-SIS expressed a mixed M1/M2 profile. No consistent patterns were observed when comparing oxygen concentrations.

The second study used radioactive ^{14}C-labeled scaffolds to measure ECM scaffold degradation in a rodent model of musculoskeletal reconstruction with and without the depletion of macrophages. Tissues were characterized by expression of M1 (*iNOS* and *IFN-γ*) and M2

(*ARG-1* and *IL-10*) gene markers, and cell surface markers CD68 (pan-macrophage), CCR7 (M1), and CD163 (M2). Results showed that macrophages are required for early and rapid degradation of SIS scaffolds, and that CDI-SIS is resistant to macrophage-mediated degradation. Furthermore, depletion of macrophages resulted in an attenuated inflammatory response and slowed the rate of scaffold degradation.

The third study determined the contractile response and histomorphologic appearance of tissue repaired with SIS, CDI-SIS, or autologous tissue at 26 weeks after implantation. Contractile properties and fatigue resistance of remodeled tissue and of contralateral native tissue were assessed using an in-situ methodology. Muscle fiber-type distribution, blood vessel density and distribution, and innervation were determined. The tissue repaired with SIS showed complete replacement by tissue that histologically and functionally resembled native muscle. CDI-SIS was characterized by chronic inflammatory response and produced little to no measurable tetanic force output.

TABLE OF CONTENTS

LIST OF TABLES

LIST OF FIGURES

PREFACE

Throughout my graduate school career and during the completion of my Dissertation, I have been blessed by countless individuals who have helped shape me into the scientist that I am today. I wish to extend my immense gratitude to Dr. Stephen Badylak, who took a chance on a Florida Gator and provided a structured, intense, and challenging mentorship in the multidiscipline field of tissue engineering and regenerative medicine. Dr. Badylak provided all the tools and personnel in a world-class laboratory setting that enabled infinite opportunities and growth of scientific creativity. I owe immense gratitude to the members of the Badylak Laboratory – past and present – who have supported me from conception to completion of my Dissertation. I have been privileged to work with passionate and intelligent scientists, including Dr. Ann Stewart-Akers, Dr. Thomas Gilbert, Dr. Danny Freytes, and Jennifer DeBarr, who have been very supportive professionally and personally.

Thank you to all of my wonderful friends, who have enriched my life with the blessings of unconditional love, belief in my capabilities, and have given me a lighter heart when things were difficult: Rebecca Mayton, Lisa MacDonald, Jennifer Engleson, to name a few.

I could not have survived without the support and love of my family: my husband Dimas, my mother Roberta Hodge, and my most inspirational angel of all, my daughter Elizabeth Maria. Thank you for providing a rock-solid ground for me to stand on, a shoulder to lean on, and words of wisdom to inspire me. I also want to thank my God and Savior Jesus Christ, whom I owe my life and accomplishments during the most challenging and soul-searching time of my life.

ACRONYMS

^{14}C	Carbon 14
ARG1	Arginase Type 1
BSA	Bovine Serum Albumin
CCL	Chemokine (C-C Motif) Ligand
CCR	Chemokine (C-C Motif) Receptor
CD	Cluster of Differentiation
CDI	Carbodiimide
CPM	Counts per Minute
CXCL	Chemokine (C-X-C Motif) Ligand
DAB	Diaminobenzidine
ECM	Extracellular Matrix
ELISA	Enzyme-Linked ImmunoSorbent Assay
GM-CSF	Granulocyte Macrophage Colony Stimulating Factor
H&E	Hematoxylin and Eosin
IFN-γ	Interferon-gamma
Ig	Immunoglobulin
IL	Interleukin
iNOS, NOS2	Inducible Nitric Oxide Synthase Type 2
IV	Intravenous
LPS	Lipopolysaccharide
LSC	Liquid Scintillation Counting

M1	Type 1 Macrophage
M2	Type 2 Macrophage
M-CSF	Macrophage Colony Stimulating Factor
MMP	Matrix Metalloproteinase
MRC1	Mannose Receptor C Type 1
NBF	Neutral Buffered Formalin
NO	Nitric Oxide
PBMC	Peripheral Blood Mononuclear Cells
PBS	Phosphate Buffered Saline
Rh	Recombinant Human
RT-PCR	Reverse Transcriptase Polymerase Chain Reaction
SEM	Scanning Electron Microscopy
SIS	Small Intestinal Submucosa
TBS	Tris Buffered Saline
TGF-β	Transforming Growth Factor-beta
Th	Helper T-cells
TNF-α	Tumor Necrosis Factor-alpha
VEGF	Vascular Endothelial Growth Factor
UBM	Urinary Bladder Matrix

1.0 NATURALLY OCCURRING EXTRACELLULAR MATRIX AS A BIOLOGIC SCAFFOLD MATERIAL

Tissue engineering and regenerative medicine approaches to tissue reconstruction include the use of scaffolding materials composed of mammalian extracellular matrix (ECM) to promote cell attachment, migration, proliferation, and spatial organization [1-8]. Naturally occurring ECM scaffolds remodel into functional tissues in numerous preclinical and clinical studies, including dermal [9-14], cardiac [15-20], gastroesophageal [21-23], urological [24-30], and musculotendinous [31-42] applications. The purported advantages of using ECM-derived scaffolds include their natural three-dimensional ultrastructure and their diverse composition of structural and functional proteins, including collagen, elastin, growth factors, and proteoglycans [3, 43-52]. During the past decade, off-the-shelf biologic scaffold materials composed of ECM have become available for the repair and reconstruction of damaged or missing tissues (Table 1). These ECM-based products differ in the species of origin (e.g., human, bovine, equine, or porcine), tissue source (e.g., dermis, fascia lata, pericardium, or small intestine), and the processing techniques used to prepare each device for human clinical use. The marketing literature for these devices may claim host acceptance and intact functionality; however, there usually are marked differences in the amount and temporal appearance of inflammatory cells, the morphologic structural integrity of the devices over time, and the type of host tissue that replaces or surrounds the ECM devices (Appendix A). It is not clear how these differences can alter the

host tissue remodeling response, but the temporal sequence of remodeling events, including the rapidity of scaffold degradation and extent of new tissue deposition, would logically be predictive of the functional outcome.

Table 1: A partial list of ECM products commercially available for human clinical use.

Product	Company	Species /Tissue of Origin	Processing	Clinical Indication
AlloDerm	Lifecell	Human skin	Natural	Abdominal wall, breast, ENT/head & neck, grafting
AlloPatch HD™	Musculoskeletal Transplant	Human dermis	Natural	Tendon repair
Axis™ dermis	Mentor	Human dermis	Natural	Pelvic organ prolapse
CuffPatch™	Arthrotek®	Porcine SIS	Crosslinked	Soft tissues, rotator cuff repair
DuraDAPT™	Pegasus Biologicals	Equine pericardium	Crosslinked	Dura matter repair after craniotomy
Dura-Guard®	Synovis Surgical	Bovine pericardium	Crosslinked	Spinal and cranial repair
Durasis®	Cook SIS	Porcine SIS	Natural	Dura matter repair
Durepair®	TEI Biosciences	Fetal bovine skin	Natural	Cranial or spinal dura repair
FasLata®	Bard	Cadaveric fascia lata	Natural	Urologic repair
GraftJacket®	Wright Medical Technology	Human dermis	Proprietary	Soft tissues, rotator cuff, foot ulcer repair
Mosaic®	Medtronic, Inc.	Porcine heart valve	Crosslinked	Aortic & mitral bioprostheses
Oasis®	Healthpoint	Porcine SIS	Natural	Partial & full thickness wounds
OrthADAPT™	Pegasus Biologicals	Equine pericardium	Crosslinked	Soft tissue repair in orthopedics
Pelvicol®	Bard	Porcine dermis	Crosslinked	Vaginal prolapsed, urethral sling
Peri-Guard®	Synovis Surgical	Bovine pericardium	Crosslinked	Pericardial and soft tissue repair
Prima™	Edwards Lifesciences	Porcine heart valve	Crosslinked	Heart valve replacement
PriMatrix™	TEI Biosciences	Fetal bovine skin	Natural	Wound management
Restore™	DePuy Orthopaedics®	Porcine SIS	Natural	Soft tissues, rotator cuff repair
Stratasis®	Cook SIS	Porcine SIS	Natural	Treatment of urinary incontinence
SurgiMend™	TEI Biosciences	Fetal bovine skin	Natural	Repair of soft tissue membranes
Surgisis®	Cook SIS	Porcine SIS	Natural	Soft tissue repair
Suspend™	Mentor	Human fascia lata	Natural	Urethral sling
TissueMend®	TEI Biosciences	Fetal bovine skin	Natural	Rotator cuff repair
Vascu-Guard®	Synovis Surgical	Bovine pericardium	Crosslinked	Reconstruction of blood vessels in neck, legs, arms
Veritas®	Synovis Surgical	Bovine pericardium	Crosslinked	Soft tissue repair
Xenform™	TEI Biosciences	Fetal bovine skin	Natural	Colon, rectal, and vaginal prolapse, urethral sling
Zimmer Collagen Patch®	Tissue Science Laboratories	Porcine dermis	Crosslinked	Soft connective tissue repair

1.1 MECHANISMS OF ECM SCAFFOLD REMODELING

Biologic scaffolds composed of ECM can promote the site-appropriate tissue reconstruction of injured tissues through mechanisms that include angiogenesis [5, 22, 28, 46, 48], the recruitment of multipotential progenitor cells to the site of tissue reconstruction [2, 7, 8, 53], the release of antimicrobial peptides [16, 19, 54-57], and activation of the alternative pathway of immunity [58-62]. There is convincing evidence that host-mediated degradation of ECM scaffolds is typically completed within eight to twelve weeks and is necessary to realize the full beneficial effects of ECM-mediated tissue remodeling [40, 42, 63], but the mechanisms by which such scaffold degradation occurs have been largely ignored. Further work is needed to better understand the cellular mechanisms of biologic scaffold remodeling and to correlate such findings with the methods by which the materials are processed and with the eventual clinical outcome. This thesis examines the role and phenotype of macrophages involved in the degradation and "processing" of scaffold materials, and investigates the relationship between early remodeling events and downstream characteristics of the remodeled scaffold materials.

1.1.1 Importance of ECM Scaffold Degradation

The evaluation of scaffold degradation is usually based on the histomorphologic appearance of the implantation site and the ability of the investigator to recognize intact devices. Unless molecular or radioactive labeling of the devices is performed to quantify the rate of scaffold degradation, it is possible that remnants of the remodeled scaffold materials remain at the site and are incorporated into the new host tissue even when histologic evaluation fails to recognize their presence. The only scaffold material for which quantitative data exists for *in vivo*

degradation is the non-crosslinked form of small intestinal submucosa (SIS). Those studies used carbon 14 (^{14}C)-proline to radiolabel the total collagen content of SIS to quantitatively determine the rate of degradation and to track the fate of the degradation products of SIS scaffolds following placement in canine models of Achilles tendon and urinary bladder repair [40, 63]. The ^{14}C-labeled SIS materials showed approximately 50% degradation by 20 days and complete elimination and concomitant replacement with host cells and new ECM deposition by 60-90 days [63, 64].

Rapid degradation emphasizes the importance placed upon the source and type of cells that must populate the scaffold, secrete new ECM, and participate in tissue remodeling. Also significant to the remodeling process, molecules that are encoded or bound within the cryptic sites of the matrix are released upon structural or compositional changes to the ECM parent molecules [65], and these low molecular weight 'matricryptic' fragments, in concert with other signals such as growth factors, have biologic activity such as chemoattractant activity for primary endothelial cells, bone marrow-derived cells, multipotential progenitor cells, inflammatory cells, and other cell types [2, 5, 7, 66, 67]. The degradation products of ECM scaffolds also show mitogenic activity for progenitor cells [7] and antimicrobial activity against Gram-negative Escherichia coli and Gram-positive Staphylococcus aureus [16, 19, 54-56, 68]. In clinical applications, non-crosslinked ECM scaffolds are the only grafts that are indicated for contaminated wounds because of the antibacterial effects associated with their degradation [68]. At least a portion of the host biologic response to ECM-derived materials is associated with and/or caused by the degradation products of the scaffold itself. Conversely, the lack of degradation of a biologic scaffold material would logically suggest that such downstream effects would not occur.

1.1.2 Cellular Response

1.1.2.1 Mononuclear Cell Response

Mononuclear cells are commonly observed and are expected participants in the host response to all biomaterials, including those that are used as scaffolds for tissue reconstruction. The term "mononuclear cell' is a generic morphologic description for a population of cells with a single nucleus, usually having a round or oblong shape, and variable amounts of cytoplasm. Mononuclear cells are typically associated with phagocytic capability, and are assumed to participate in chronic inflammation with downstream consequences of necrosis, fibrosis with encapsulation, some degree of scar tissue formation, or a combination of the three [69, 70]. A variety of cell types are virtually indistinguishable upon routine examination of peripheral blood or tissue sections, although various progenitor cells [71-78], circulating fibrocytes [79-82], blood monocytes [83], and others [84-86] fit the morphologic description of a classic mononuclear cell. Clearly, the conventional term 'mononuclear cell' is not always sufficient to fully describe the host response of ECM scaffolds or predict the eventual tissue remodeling outcome.

1.1.2.2 Recruitment of Progenitor Cells

ECM scaffolds including SIS are capable of inducing site-specific remodeling with differentiated tissue structures such as skeletal [35, 42] and smooth muscle [27], myocardium [17], specialized epithelium [21, 22], and well-organized connective tissue [8, 32, 40]. Recent studies have shown that bone marrow-derived progenitor cells are recruited to the site of ECM remodeling and participate in the differentiation of site-appropriate tissue structures [8, 53]. A percentage of these bone marrow progenitor cells differentiate into functional cells that secrete collagen and remain in the remodeled tissue after inflammation has subsided [8]. Beattie and colleagues

investigated the chemotactic properties of tissue harvested during the first 14 days after repair with a urinary bladder matrix (UBM) ECM scaffold in a murine model of Achilles tendon reconstruction [2]. The results showed that multipotential progenitor cells (MRL blastema cells [7]) preferentially migrated toward the tendons repaired with UBM compared to tendons repaired with autologous tissue or uninjured normal tendons. The recruitment of progenitor cells toward degrading ECM scaffolds is an area of scientific interest in understanding the mechanisms for constructive remodeling.

1.1.2.3 Maintenance of Differentiated Cell Phenotype

The ultrastructure of ECM is synthesized and continually maintained by the resident cell population of most tissues and organs, and serves to support and direct cells in a highly defined and specialized microenvironment [67, 87-89]. A variety of cell types, including NIH 3T3 fibroblasts [90], primary human bladder urothelial and smooth muscle cells [91], primary tracheal chondrocytes and epithelial cells [unpublished data], human pancreatic islets [92], and primary human epidermal cells [6], maintain tissue-specific phenotypes when cultured on the surface of scaffold materials derived from ECM. Sellaro et al. demonstrated that hepatic sinusoidal endothelial cells (SECs) co-cultured with hepatocytes on the surface of materials composed of liver-derived ECM maintained a differentiated phenotype to a greater degree and for a longer duration of culture than substrates composed of purified collagen type I, or ECM derived from the urinary bladder (UBM) or small intestinal submucosa (SIS) [87]. This study suggests that for some cell populations such as SECs the origin of the tissue or organ from which the ECM is derived may make a significant difference in the modulation or maintenance of specialized phenotypes. It is evident that ECM scaffolds are more suitable for supporting tissue-

specific phenotypes for differentiated cells compared to scaffolds composed of individual components of ECM such as collagen.

1.1.3 Oxygen Diffusion

The passive diffusivity of oxygen through a biomaterial is one of many factors associated with cell viability, metabolic activity, and the rapidity with which cells can successfully populate a scaffold material. The amount of oxygen available to the remodeling site will be determined by the surrounding microenvironment including the local vascular network. At the time of surgical placement of a biomaterial, the existing vasculature is limited to the outer boundaries; a factor which likely slows cell migration into the scaffold in the early stages of remodeling and has an effect on cell behavior due to a hypoxic environment [93]. A study by Valentin et al. showed that oxygen diffusion through ECM materials is at least partially dependent on the complexity of the collagen fiber arrangement and ultrastructure, including the presence of a basement membrane [94]. Oxygen diffusivity would logically become less important as scaffold remodeling proceeds with the deposition of plasma proteins, the secretion of host neo-ECM, the population of host cells occupying the material, and the development of new vascular networks. Stated differently, the remodeling characteristics after ECM scaffold implantation may be partially attributed to the ability of the biologic material to diffuse oxygen in the early stages of the host response, coupled with relatively rapid degradation, and subsequent release of angioinductive matrix-bound growth factors. It has been shown that component growth factors such as vascular endothelial growth factor (VEGF), transforming growth factor-beta (TGF-β), and basic fibroblast growth factor (bFGF) are incorporated within SIS and that active forms of these factors survive the processing and terminal sterilization steps that are used to disrupt cell membranes and cytoplasmic

organelles, denature cytoplasmic proteins, and largely eliminate these components from the remaining ECM [4, 48, 49, 95, 96]. These growth factors are released during scaffold degradation and stimulate angiogenesis, mitogenesis, and cellular differentiation during tissue remodeling. Biologic scaffold devices composed of ECM material other than SIS may also retain growth factor activity following device preparation, but few published studies to that effect are available [51].

1.1.4 Role of Mechanical Loading on ECM Remodeling

The physical properties of scaffold materials prior to implantation are important determinants of clinical success, and are usually used as predictors of the clinical utility of the device. Equally if not more important however, is the change in the physical properties of the scaffold during the remodeling process. The degradation rate of non-chemically crosslinked ECM appears to be compatible with the rate of new host tissue deposition, such that the scaffold retains sufficient strength to serve as a functional replacement until the host can deposit new host tissue [17, 35, 38, 97]. However, there is a measureable loss of strength that occurs prior to transfer of mechanical function to the new host tissue. For Achilles tendon [98], medial collateral ligament [31, 99], abdominal body wall [97], urinary bladder [27, 100], and esophageal [21] repair, the strength of non-crosslinked ECM scaffolds decreased as a result of scaffold degradation, but the mechanical properties of the new host tissue subsequently increased to anatomically site appropriate levels when mechanical load was applied from the onset of scaffold placement.

A study by Boruch et al. utilized a canine model of partial cystectomy to demonstrate the importance of physiologic biomechanical load to constructive remodeling [27]. A defect was created in the anterior dome of the urinary bladder and repaired with either an SIS or UBM

scaffold. The animals were then divided according to the duration of post-operative catheterization. The bladders from animals that received an indwelling catheter for 28 consecutive days post-surgery showed evidence of contraction and a lack of urothelization at the site of scaffold placement. The bladders from animals that received the catheter for only 24 hours post-surgery demonstrated a constructive host remodeling response, characterized by complete urothelialization along the luminal surface, vascularity, innervation, and islands of smooth muscle bundles. This study showed that exposure of ECM scaffolds to a physiologic-appropriate pattern of mechanical loading (cyclic distention) promoted constructive remodeling. In a similar fashion, a study that utilized a rabbit model of Achilles tendon repair ascertained that joint immobilization during the remodeling period resulted in delayed scaffold degradation, the deposition of disorganized connective tissue, and a lack of cellular infiltration within the ECM remodeling site [44]. These studies suggest that the reconstruction of ECM scaffolds into functional tissue is dependent upon a combination of temporally associated events, including timely scaffold degradation, cellular infiltration, and early exposure to site-appropriate mechanical loading.

1.1.5 Summary

Scaffold materials composed of intact ECM provide structural and biofunctional support to hematopoietic cells, fibroblasts, and other site appropriate cell types. ECM-based bioscaffolds retain the essential structural and functional molecules of their tissue of origin when decellularization is conducted by appropriate and effective methods. The beneficial biologic effects of ECM scaffold degradation and the associated loss of scaffold mechanical strength would suggest that a balance of these seemingly mutually exclusive events is necessary to realize

functional tissue reconstruction. The relationship between the host cellular response during the early stages of remodeling and the mechanical properties of the completely remodeled tissue is not fully understood. A goal of this dissertation is to investigate the associated between the early host mononuclear cell response after ECM scaffold placement and the functionality of remodeled tissue in an established rat model of musculoskeletal repair [36, 42].

2.0 HOST RESPONSE TO SCAFFOLD MATERIALS

The classic paradigm of mammalian inflammation associates neutrophils with an active, acute, or persistent host inflammatory response and associates mononuclear cells with a subacute to chronic type of inflammatory response. The host response may further develop into a foreign body reaction by surface-adherent macrophages that fuse together to form multinucleate giant cells until the foreign body is degraded or surrounded by a fibrous capsule. However, the traditional model of the inflammatory response to biomaterials does not adequately describe the temporal observations of ECM scaffold remodeling.

2.1 ROLE OF MACROPHAGES IN THE HOST RESPONSE

2.1.1 Historical Perspective

Mononuclear phagocytes (monocytes and macrophages) are found in most tissues of the body and are vital participants in the innate and acquired immune system. Circulating monocytes are the precursors to tissue macrophages, and are borne out of the bone marrow from a common myeloid progenitor. Upon release into the peripheral blood, monocytes circulate for several minutes to days before entering the tissues [101]. Monocytes are capable of differentiating into

morphologically and functionally heterogeneous effector cells, including resident tissue macrophages and inflammatory macrophages.

Resident tissue macrophages perform specified functions that are required for different anatomical locations. A few examples include: alveolar macrophages in the lung, which are responsible for local defense against pathogenic and particulate matter [102, 103]; Langerhans cells that populate the epidermis [103]; osteoclasts that remodel bone [103]; splenic macrophages and Kupffer cells in the liver, which foster the clearance of blood-borne pathogens [103]; and intestinal macrophages, which reside in the lamina propria of the small intestine and are characterized by high phagocytic and bactericidal activity, low production of co-stimulatory cytokines, and a lack of innate response expression, including the primary receptor for LPS, CD14 [85, 86].

During the inflammatory response, blood monocytes are recruited to the wounded tissue by adhering to vessel endothelium and following local haptotactic and chemotactic gradients before differentiating into macrophages [102]. Macrophages, both resident and newly recruited, are the major producer of chemokines in wounded tissue, and are likely instrumental in the subsequent recruitment of additional macrophages.

Conventional knowledge suggests that mononuclear macrophages follow neutrophils into a site of inflammation over time, phagocytose cellular debris and foreign material, and finally exit from the site of inflammation. The prolonged presence of a large population of mononuclear macrophages at the site of tissue repair is usually indicative of, and routinely diagnosed as, chronic inflammation with granulation tissue formation, with likely downstream outcomes such as necrosis, fibrosis with encapsulation, and/or some degree of scarring [70, 104]. Extensive research has shown that macrophages exhibit plasticity, i.e. the phenotype of macrophages can

change depending upon the local environment [78, 84, 103, 105-111]. Macrophages were once considered to be either classically activated or alternatively activated, but there is substantial heterogeneity in macrophage phenotype, due in part to the broad role that macrophages play in the inflammatory response and in the maintenance of tissue homeostasis. The thesis investigates the phenotypic profile of macrophages in the site of ECM scaffold remodeling in order to give a more accurate and complete description of the host response.

2.1.2 Macrophage Phenotypes

Mononuclear macrophages play an important role in modulating the inflammatory response to foreign materials, infection, and allergy through the synthesis and secretion of cytokines, chemokines, and growth factors [102]. Influenced by the local tissue and exposure to immunological microenvironment signals such as cytokines and microbial products, macrophages acquire distinctive morphological and functional characteristics. Macrophages perform critical functions in tissue repair, including collagen degradation and organization, promotion of angiogenesis, and other constructive processes [102], and act as effector cells in adaptive immune responses, such as in orchestrating helper T cells through the presentation of antigens [112].

Macrophage phenotype is classified according to gene expression, cell surface receptor expression, and secretion of cytokines. Macrophages that are induced to a classical activation profile by microbial products such as LPS or Th1 cytokines including interferon-gamma (IFN-γ) and tumor necrosis factor-alpha (TNF-α) are termed M1 macrophages [108, 112]. M1 macrophages synthesize and release proinflammatory factors such as IL-1β, IL-6, IL-12, and TNF-α [113, 114], produce high concentrations of nitric oxide (NO) and reactive oxygen

intermediates (ROI), and produce type-1 chemokines such as CXCL-10, CXCL11, and CCL5. M1 macrophages are associated with microbicidal activity, tumor resistance, and cytotoxic tissue damage. By contrast, macrophages that are induced by IL4 or IL10 and promote a type-2 response are called M2 macrophages. At least three distinct forms of M2 macrophages have been identified, and are categorized by the inducing agent: M2a macrophages, which are induced by IL-4 and IL-13, are classified as alternatively activated macrophages and drive type-2 responses; M2b macrophages, which are exposed to agonists of Toll-like receptors (TLRs) or IL-1R, are immunoregulatory and drive type-2 responses; and M2c macrophages, induced by IL-10 and glucocorticoid hormones, suppress immune responses and participate in matrix deposition and tissue remodeling (Figure 1) [108]. In general, M2 macrophages produce IL-10, transforming growth factor-beta (TGF-β), and type-2 chemokines such as CCL13 and CCL18 [108]. In particular, IL-10 is described as an immunosuppressive cytokine that functions to inhibit the production of proinflammatory cytokines and chemokines such as CXCL10, IL-1α/β IL-6, IL-12, and TNF, while amplifying the expression of their antagonists [115]. The expression of scavenger receptors such as the mannose receptor (CD206) and CD163 is strongly induced in macrophages by anti-inflammatory stimuli such as glucocorticoids and IL-10, and suppressed by proinflammatory mediators such as LPS, IFN-γ, and TNF-α [115-117]. M2 macrophages support parasite encapsulation and eradication, participate in the promotion of tumor growth and progression [118, 119], scavenge debris, and promote angiogenesis, tissue repair and homeostasis. M2 macrophages enhance fibrogenesis of mesenchymal cells (fibroblasts) by secreting soluble profibrogenic mediators such as TGF-β and platelet-derived growth factor (PDGF), while M1 macrophages inhibit fibrogenesis by releasing fibrolytic factors including matrix metalloproteinases (MMPs) and TNF-α [113]. The phenotype of macrophages involved in

the degradation and "processing" of ECM scaffold materials is likely dependent upon the local tissue and cellular environment, and has the potential to affect downstream characteristics of the remodeled scaffold materials. The body of work contained in this thesis examines the phenotypic profile of macrophages and determines its impact on the duration, magnitude, and overall outcome of the host response.

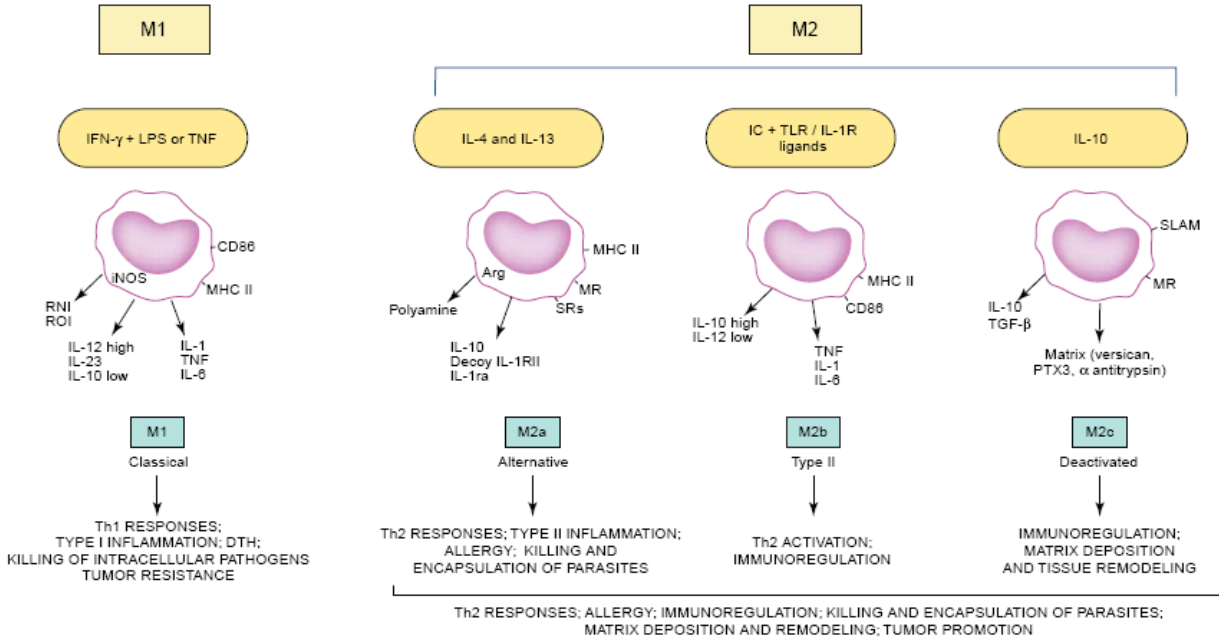

Figure 1: Inducers, secreted products, and functional properties of macrophage populations polarized toward either an M1 phenotype or an M2 phenotypes. Reprinted from [108], with permission from Elsevier.

The amino acid L-arginine plays an essential role in wound healing. Macrophages metabolize L-arginine in one of two distinct and competitive pathways (Figure 2). Macrophages from the M1 profile metabolize L-arginine through inducible nitric oxide synthase (iNOS; NOS2), which converts L-arginine to NO and L-citrulline, and results in a decrease of collagen synthesis by fibroblasts. M2 macrophages metabolize L-arginine via arginase, a critical enzyme that converts arginine to urea and L-ornithine [112]. L-ornithine is the substrate for two enzyme

pathways important in cell proliferation and collagen production during tissue repair, ornithine decarboxylase and ornithine aminotransferase, which increases concentrations of polyamines and L-proline, respectively [120, 121]. The reciprocal pathways of L-arginine metabolism may be a good predictor of how macrophages affect the outcome of inflammation.

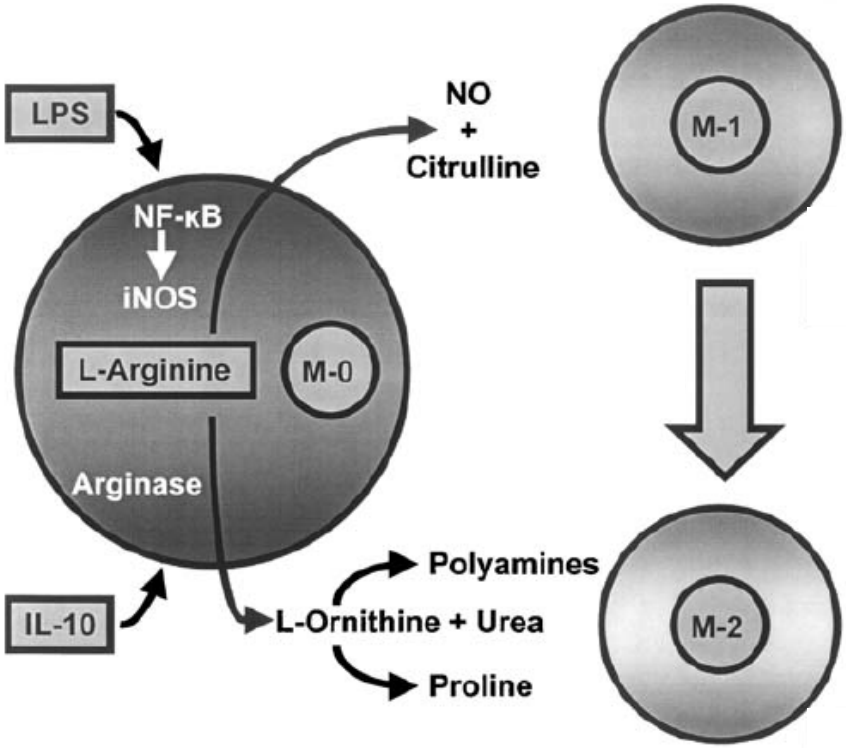

Figure 2: Schematic of the L-arginine pathway. Reproduced with permission from [122], the Biochemical Society [http://www.biochemsotrans.org]

Caution is required when defining the M1/M2 classification scheme against rigid boundaries to what is, in reality, a broad spectrum that lies between the two extremes of polarization. Separating macrophages into only M1 or M2 macrophages risks an oversimplification of a continuum of diverse phenotypes that may be involved in ECM scaffold remodeling, since it is unlikely that macrophage phenotype is uniform throughout the remodeling

site. In addition, it is unclear whether M1 or M2 macrophages are terminally differentiated, have the ability to switch their phenotype, or become quiescent in response to micro environmental fluxuations in cytokine concentrations [109]. This dissertation will work within the confines of the current knowledge of the M1/M2 paradigm, but the complex milieu of ECM scaffold remodeling and the macrophage response is not fully understood.

2.2 CONSTRUCTIVE REMODELING VERSUS FOREIGN BODY RESPONSE

Constructive remodeling is best defined as a modification of the default wound healing mechanism away from scarring and toward regeneration and restoration of function. The cellular response to naturally derived ECM scaffold materials may not follow the conventional pattern of inflammation and can differ for each device, depending on the source of the material and the processing techniques which may include crosslinking with chemical agents. In a recent study that compared the host tissue response to five ECM products currently marketed for orthopedic applications, it was shown that an intense mononuclear macrophage response in the early post implantation period was a consistent finding (Appendix A) [42]. However, the long term remodeling outcome differed greatly for each product. The remodeled tissue showed chronic inflammation, fibrosis, scarring, and encapsulation (i.e., "foreign body response") with some devices, and the formation of organized, site-appropriate tissue (i.e., "constructive remodeling") for other devices.

One hallmark of constructive remodeling is the presence of highly differentiated tissue structures (i.e., urothelium and smooth muscle bundles in the reconstruction of the urinary bladder after partial cystectomy and repair with ECM [27], and a continuous intact mucosal layer

of the esophagus and islands of skeletal muscle bundles after reinforcement of the cervical esophageal anastomoses with UBM [22]). Several mechanisms of ECM scaffold-mediated constructive remodeling have been attributed to site-appropriate mechanical loading from the onset of scaffold placement (Section 1.1.4), rapid and complete scaffold degradation (Section 1.1.1), concurrent new host ECM deposition (1.1.2), and bioactive growth factors found within ECM scaffolds [47-49, 95, 96] or low molecular-weight peptides generated from the degradation products of ECM scaffolds (Section 1.1.1).

2.2.1 Native (Non-crosslinked) ECM Scaffolds

Although xenogeneic and allogeneic cellular antigens elicit an aggressive host inflammatory response or immune-mediated rejection, the components of ECM are conserved among mammalian species and are therefore well-tolerated by the recipient. The ideal processing techniques for ECM scaffolds decellularize the native tissue through mechanical, chemical, and/or enzymatic methods while minimally changing the biological properties and three dimensional ultrastructure [123]. Scaffold materials composed of intact ECM provide structural and biofunctional support to hematopoietic cells, fibroblasts, and other site-appropriate cell types [1, 4, 53, 90, 124, 125]. The remodeling characteristics of tissue repaired with native ECM scaffolds typically include such features as cellular infiltration and differentiation, scaffold degradation, new host ECM deposition, and the development of organized, site-specific tissue structures that resemble the native tissue in structure and function [43].

2.2.1.1 Lymphocyte Response

The immune response is a primary constituent of the host recognition to injury and implanted materials. Lymphocytes and helper T-cells (Th) in particular modulate the adaptive immune response through secreted cytokines [126]. One paradigm of lymphocyte biology classifies Th cells into two categories based on the secretion of specific cytokines related to macrophage activation. Th1 cells produce IFN-γ, TNF-α, and IL-12, and are thought to cause macrophage activation, differentiation of T-cells to a cytotoxic (CD8+) phenotype, and graft rejection. In contrast, Th2 cells produce IL-4, IL-5, IL-6 and IL-10, cytokines that inhibit macrophage activation [112, 127, 128]. SIS is the only ECM scaffold for which the Th1/Th2 response has been examined. In a study by Allman et al., mice were implanted subcutaneously with SIS, xenogeneic muscle tissue, or syngeneic muscle tissue to determine the host tissue and cellular response [58]. The xenogeneic tissue showed histological evidence of necrosis, granuloma formation, and encapsulation; these remodeling features are indicative of graft rejection. The syngeneic tissue and the SIS graft remodeled into organized tissue, and the inflammatory response was resolved, consistent with graft acceptance. In addition, SIS-ECM induced a Th2-restricted immune response, as evidenced by suppression of IFN-γ and upregulation of IL-4. Palmer and colleagues investigated whether the presence of TGF-β in SIS influenced human Th cell activation and differentiation *in vitro* [129]. This study showed that SIS inhibited Th1 expansion and cytokine production of IL-12 and IFN-γ in a TGF-β dependent manner and induced Th1 cell apoptosis. Furthermore, SIS also inhibited Th2 expansion, which was not rescued with exogenous TGF-β. These studies and others [10, 130, 131] may explain why there are no documented cases of immune-mediated rejection with SIS scaffolds.

2.2.1.2 Macrophage Response

Mononuclear macrophages are commonly observed and are expected participants in the innate host inflammatory response to biomaterials, including those that are used as scaffolds for tissue reconstruction. A recently published study by our laboratory showed that the phenotype of mononuclear macrophages that participate in the host response to biologic scaffolds can differ markedly and that the method of material processing was an important variable [60]. In this study, the surgical sites in which the SIS device was placed showed an intense mononuclear cell response at 1, 2 and 4 weeks and infiltration of these cells between the individual layers of the multilaminate SIS device. These mononuclear cells were predominantly of an M2 phenotype (i.e., CD163+) at all timepoints (Figure 3A). By 16 weeks there was no evidence of the SIS-ECM device and the surgical site was characterized by organized collagenous connective tissue, skeletal muscle tissue, and occasional CD163+ mononuclear cells (Figure 4A). This study suggests that the M2 macrophage response was associated with an organized, site-appropriate tissue-remodeling outcome and an absence of persistent inflammation. Furthermore, the presence of a cell population that is typically associated with cytotoxicity and inflammation (i.e., "macrophages") was not necessarily predictive of the long term remodeling outcome.

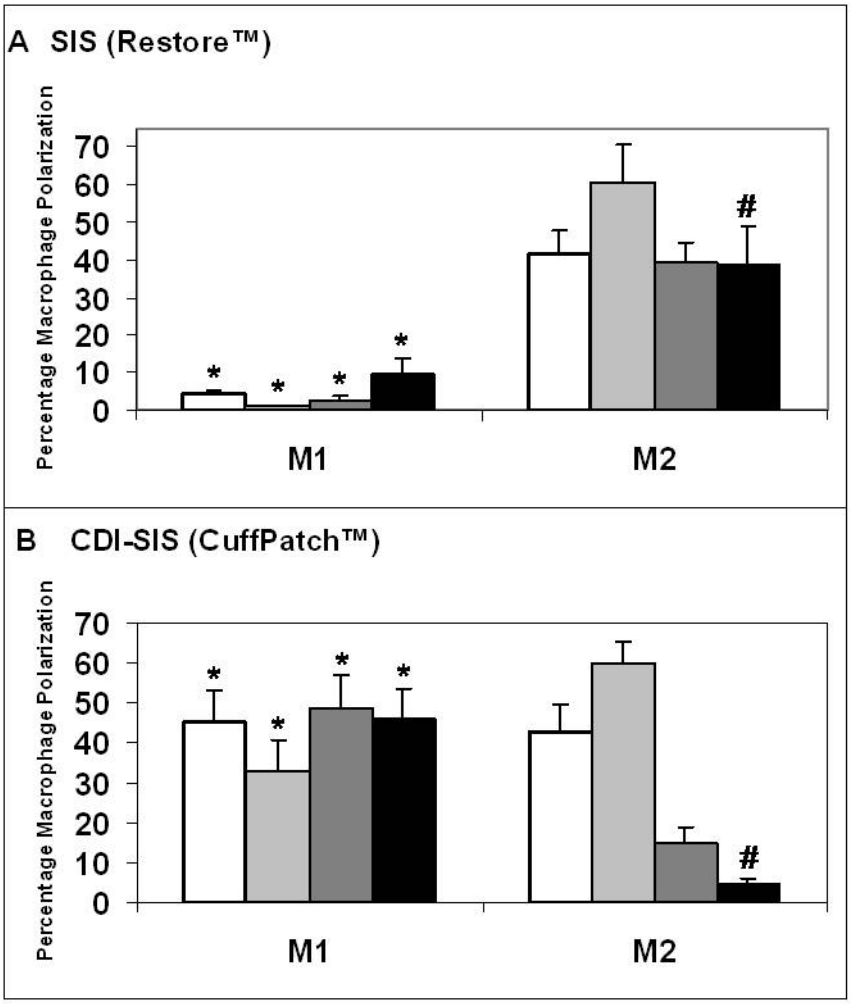

Figure 3: The macrophage polarization percentages for (A) SIS and (B) carbodiimide crosslinked SIS (CDI-SIS) at 1 (white bars), 2 (light grey bars), 4 (dark grey bars), and 16 (black bars) weeks post-implantation in a rodent model of musculoskeletal repair. Mean ± standard error of the mean; *$p < 0.001$ and #$p < 0.03$. Reproduced from [60], with permission from Liebert Publishing.

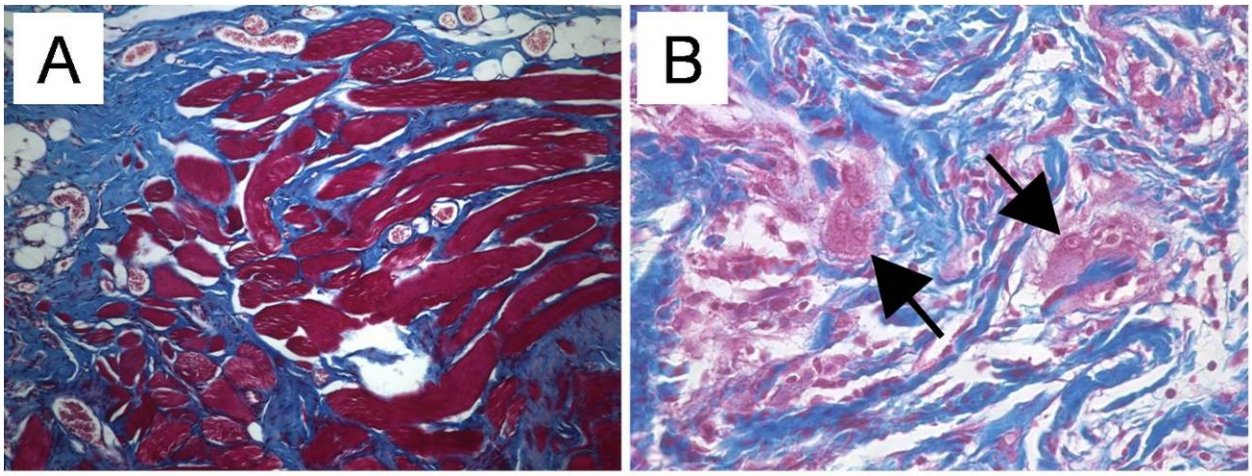

Figure 4: Masson's trichrome staining at 16 weeks post-surgery in a rodent model of musculoskeletal repair. (A) Photomicrograph of completely remodeled SIS device. Blood vessels, scattered skeletal muscle fibers, and organized collagen completely replaced the SIS device (100X). (B) Photomicrograph of carbodiimide crosslinked SIS device. A dense mononuclear cell response can be observed with the presence of multinucleate giant cells (arrows) and fibrosis around the scaffold material (400X). Reproduced from [60], with permission from Liebert Publishing.

2.2.2 Chemically Crosslinked ECM Scaffolds

The clinical utility of ECM scaffolds depends upon the ability of the scaffold material to provide adequate mechanical support to the injured or missing tissue being repaired. A common approach for increasing the strength of biologic scaffolds composed of ECM or components of ECM (e.g., purified type I collagen) has been the use of chemical crosslinking agents such as carbodiimide [13, 132-134], isocyanate [135] or glutaraldehyde [136-138]. While chemical crosslinking increases the mechanical strength of the scaffold, it also necessarily alters the kinetics of degradation and has a deleterious effect on the biologic activity of the degradation products. ECM scaffolds that are processed using chemical crosslinking methodologies [132,

139-141] are more likely to elicit a host response that is consistent with a synthetic material; that is, the response is characterized by chronic inflammation, minimal scaffold degradation, and fibrous encapsulation [142-146].

2.2.2.1 Macrophage Response

Crosslinking agents, such as carbodiimide (CDI), are often included in the processing of biologic materials to impart added strength and to slow the degradation rate (see Table 1). Collagen constitutes approximately 90% of the total protein content in many biologic scaffolds used in tissue engineering and regenerative medicine, including SIS. Collagen materials subjected to carbodiimide treatment show intra- and interhelical crosslinks of the tropocollagen molecules, which would logically change the surface architecture on a molecular level [147]. A recent study by Brown et al. showed that distinct structural changes in the arrangement of collagen fibers and minimal changes in the molecular composition of the surface of UBM scaffolds resulted from the use of carbodiimide as a crosslinking agent [148]. Macrophages are clearly affected by the surface topology and molecular organization of biomaterials, and the cell-surface interaction can change the quantity and identity of secreted proinflammatory cytokines and chemokines [149], the gene expression pattern [150], and downstream remodeling events [145, 146]. Chemical crosslinking can also lead to “frustrated phagocytosis” by macrophages [69], which may in turn affect their M1/M2 phenotype. In a recently published study by our laboratory, chemical crosslinking of the SIS scaffold with carbodiimide resulted in a switch from an M2 dominant profile to an M1 dominant profile (Figure 3B) and a change in the long-term (16 week) remodeling outcome from constructive remodeling to chronic inflammation (Figure 4B). Carbodiimide crosslinking was associated with an M1 response, long-term inflammation and the formation of multinucleate giant cells and scar tissue.

2.3 SUMMARY

This dissertation expands the knowledge of macrophage phenotype outlined in Section 2.1.2 to include ECM scaffold remodeling as a way to develop a better understanding of constructive remodeling. Although this work limits the test articles to a single form of biologic scaffold material (SIS), the principles may also be applied to all scaffold materials, including synthetic and biologic materials.

3.0 CENTRAL HYPOTHESIS AND SPECIFIC AIMS

The goal of this dissertation is to examine the phenotypic profile and contribution of macrophages to ECM remodeling in an animal model of musculoskeletal tissue reconstruction. The central hypothesis of this dissertation is that the phenotype of macrophages during the early stages of the remodeling process will predict downstream structural and functional properties of SIS remodeled tissue. Because of its extensive characterization and excellent remodeling properties in many soft tissue applications, SIS represents the prototype for naturally derived scaffold materials for studying the host response to bioactive scaffold materials and will be used for the proposed studies; however, the learned principles will likely be relevant for most, if not all, ECM-based bioscaffolds.

Specific Aim 1. To determine the phenotype of macrophages following contact with a biologic scaffold composed of small intestinal submucosa (SIS). Monocytes are active and important participants in the inflammation cascade, and have the ability to differentiate toward a proinflammatory (M1) macrophage or tissue remodeling and immunoregulatory (M2) macrophage. The present study will evaluate the phenotype of macrophages that are cultured on the surfaces of SIS scaffolds that differ only in the presence or absence of chemical crosslinking. Evidence suggests that low oxygen tension found in areas of inflammation can affect the

macrophage phenotype. To mimic the wound healing environment, atmospheric (20% oxygen) and low oxygen (6% oxygen) tensions will be compared.

The specific aim was based on the hypothesis that monocytes will differentiate toward macrophages that express an M2-like phenotype when in direct contact with non-crosslinked SIS, while monocytes in direct contact with crosslinked SIS will differentiate toward an M1-like macrophage phenotype.

Specific Aim 2: To determine the necessity of participation of macrophages for the degradation of SIS scaffolds. Macrophages efficiently respond to tissue injury and participate in the repair process. Phagocytosis is the hallmark of macrophage functionality. The constructive remodeling of SIS in past studies has always been associated with complete and relatively rapid degradation of the scaffold. In addition, the degradation products of ECM scaffolds have shown chemotactic and antimicrobial properties. By eliminating or significantly reducing the macrophage involvement in the host response, the benefits attributed to ECM degradation may not be realized.

The hypothesis of the second specific aim is that depletion of macrophages will result in prolonged graft presence and a pro-inflammatory tissue cytokine profile at the site of scaffold placement.

Specific Aim 3: To determine the histomorphology and functionality of SIS scaffolds when used for the reconstruction of musculoskeletal tissue in a rat model. The default inflammatory response following muscle injury may initiate the process of scar tissue formation or promote reconstruction and repair. Previous studies have shown that specimens harvested

from one to sixteen weeks after implantation in a rodent model of musculoskeletal repair contain a macrophage response that may be useful in predicting the ultimate tissue functionality [60, 151]. To date, the contractility of the repaired tissue in the abdominal wall repair model has not been investigated. The third aim will determine the *in situ* contractile properties and the histomorphologic characteristics of abdominal wall muscle tissue after repair with ECM scaffolds at the 6 month timepoint. In previous preclinical models, by 6 months the SIS grafts are completely remodeled with functioning, site specific tissue [8, 21, 24, 36, 40, 63].

The hypothesis of the third specific aim is that abdominal wall muscle that is repaired with a noncrosslinked ECM scaffold will show contractile responses and histomorphologic characteristics comparable to the native muscle wall, while the crosslinked ECM scaffold will show little, if any, contractile forces and a histomorphologic profile that represents a foreign body reaction rather than a constructive remodeling response.

4.0 SPECIFIC AIM 1: TO DETERMINE THE PHENOTYPE OF MACROPHAGES FOLLOWING CONTACT WITH A BIOLOGIC SCAFFOLD COMPOSED OF SMALL INTESTINAL SUBMUCOSA

4.1 INTRODUCTION

Previous studies have shown that ECM scaffolds derived from mammalian organs are excellent substrates for a variety of cell types, including the survival and outgrowth of primary neurons [152], the maintenance of human hepatocytes phenotype [87], the differentiation and functional characteristics of cardiomyocytes [153, 154], and the survival and proliferation of fibroblasts [125] and endothelial cells [3, 124]. The response of macrophages seeded onto ECM substrates may mimic the differentiation phenotype of macrophages involved in ECM scaffold remodeling in an *in vivo* setting. Therefore, macrophages seeded onto crosslinked and non-crosslinked ECM scaffolds may show altered expressions of various inflammatory-related markers in such a way that would be predictive of the constructive remodeling response observed *in vivo*.

The objective of Specific Aim 1 was to characterize the protein and gene expression profile of human monocyte-derived macrophages when in direct contact with ECM scaffolds harvested from the small intestinal submucosa. The monocytes were selected by negative depletion to avoid the possible activation of the cell surface by bound antibodies. Cell culture was performed in atmospheric (20% oxygen) and low oxygen (6%) atmosphere. An enclosed cell

culture system (BioSpherix, Ltd., NY) was utilized so that all cell culture procedures for low oxygen experiments were performed and maintained in a controlled environment.

4.2 MATERIALS AND METHODS

4.2.1 Isolation and Preparation of Extracellular Matrix Scaffolds Derived from the Small Intestinal Submucosa (SIS)

4.2.1.1 Preparation of SIS

Established protocols for preparing the SIS scaffold material used in this study have been previously described [155] but are briefly reviewed below. The tissue from which the ECM bioscaffolds were prepared was harvested from the small intestine of market weight pigs (180 – 270 kg). Immediately after euthanasia, the mesenteric tissues were removed. After rinsing, the tunica serosa, tunica muscularis externa, and the luminal portion of the tunica mucosa were mechanically removed. The tunica submucosa and the basilar portion of the tunica mucosa including the muscularis mucosa and the stratum compactum of the lamina propria were left intact, and these layers represented SIS. The SIS material was placed in a solution of 0.1% (v/v) peracetic acid (Sigma Chemical Co., St. Louis, MO), 4% (v/v) ethanol (Pharmco Products (Brookfield, CT), and 95.9% (v/v) sterile deionized water and shaken for 2 hours. The SIS material was then washed twice with phosphate buffered saline (PBS) at pH 7.4 and twice with deionized water for 15 minutes each to remove residual peracetic acid. The test article was then lyophilized and terminally sterilized with ethylene oxide at a dosage of 500 mg/L/h for 16 hours.

4.2.1.2 Preparation of Carbodiimide crosslinked SIS-ECM

The SIS scaffolds designated as CDI-SIS were prepared by immersing the sheets of SIS in a solution of 10 mM carbodiimide (CDI) (Sigma) in 90% acetone/10% deionized water (v/v) for 24 hours. To determine crosslinking efficacy, 6 samples each of SIS and CDI-SIS were digested in 27.3 U/mL bacterial collagenase type I (Sigma) for 72 hours at 37°C. The amino acids released in the supernatant were quantified in triplicate by the ninhydrin assay according to the manufacturer's protocol. The CDI-SIS scaffolds were lyophilized and terminally sterilized by exposure to ethylene oxide at a dose of 500 mg/L/h for a 16 hour cycle.

4.2.2 Human Monocyte Isolation and Culture

Buffy coats prepared from six healthy human donors were obtained from the Central Blood Bank (Pittsburgh, PA). Peripheral blood mononuclear cells (PMBCs) were isolated using density gradient centrifugation (Lymphocyte Separation Media, Gibco, Carlsbad, CA; RPMI media, MediaTech, Inc., Manassas, VA). Monocytes were separated from PBMCs by immuno-magnetic depletion of T cells, natural killer cells, B cells, dendritic cells, and basophils using the Monocyte Isolation Kit II (Miltenyi Biotec, Bergisch Gladbach, Germany). Monocyte preparations were greater than 95% CD14+/CD115+, as indicated by flow cytometry.

4.2.2.1 Differentiation of Monocytes into Macrophages

Freshly isolated monocytes were cultured in RPMI media supplemented with 10% heat-inactivated FBS (Gibco) and 1% penicillin/streptomycin (Gibco). Cultures were maintained at 37°C in a humidified atmosphere containing 5% CO_2 in either 20% oxygen/75% nitrogen or 6% oxygen/89% nitrogen environment. On day 3, cells were washed and fresh medium was added.

To stimulate the monocytes into M0 macrophages, macrophage-colony stimulating factor (M-CSF) (100 ng/mL, R&D Systems, Minneapolis, MN) was included in the medium from day 0 to day 7. To stimulate the M0 macrophages into M1 macrophages, granulocyte macrophage (GM)-CSF (1 ng/mL) (R&D Systems); IFN-γ (20 ng/mL) (R&D Systems); and LPS (10 ng/mL) (R&D Systems) were added to the medium at day 7. To stimulate the M0 macrophages into M2 macrophages, IL-10 (50 ng/mL) (R&D Systems) or IL-4 (20 ng/mL) (R&D Systems) was included in the medium on day 7. The supernatants and macrophages were collected on day 8.

4.2.2.2 Culture of Monocytes on SIS, CDI-SIS, or Tissue Culture Plastic (TCP)

Freshly isolated monocytes were cultured in triplicate on the following substrates: tissue culture-treated plastic (TCP), the luminal surface of SIS (i.e., stratum compactum), or the luminal surface of CDI-SIS. Stainless steel tissue culture rings with inner area of 1.5 cm^2 were placed on the SIS and CDI-SIS scaffolds. Pressure was applied to create a seal and to hold the sheets of ECM on the bottom of the well. The scaffolds were incubated in 1 mL of XVIVO-15 media (BioWhittaker, Lonza, Walkersville, MD) supplemented with 10% heat-inactivated FBS and 1% penicillin/streptomycin at 37°C and 5% CO_2 for at least 4 hours prior to cell seeding, at which point the media was replaced just before adding the cells. The cells were seeded within the tissue culture rings at a density of 0.4 x 10^6 cells/cm^2. After 8 hours the tissue culture rings were removed. The cells were grown on the substrates for 18 hours, 72 hours, or 168 hours at 37°C and 5% CO_2, in 20% or 6% oxygen atmospheres. Eighteen hours prior to collecting the supernatant and harvesting the samples, the cell-seeded scaffolds were placed in a new well and fresh XVIVO-15 serum-free media was added (Figure 5).

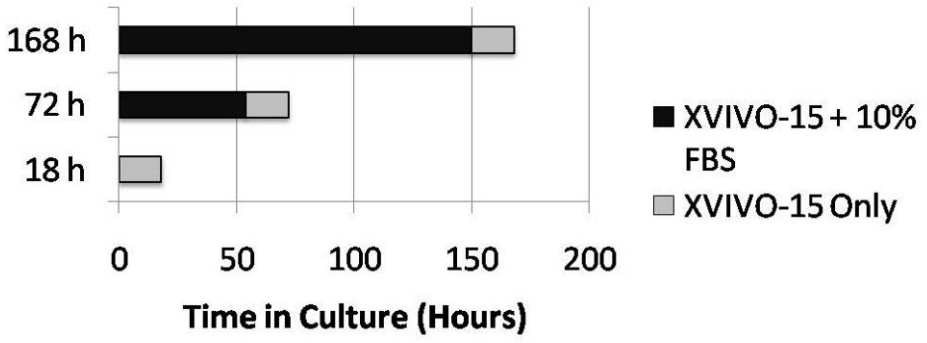

Figure 5: Schematic of culture conditions.

4.2.3 Scanning Electron Microscopy

Samples were fixed overnight at 4°C with 2.5% glutaraldehyde (TAAB Laboratories Ltd., Aldermaston, Berkshire, UK) in PBS. After 3 PBS washes, the tissues were immersed in 1% osmium tetroxide (Electron Microscopy Sciences, Hatfield, PA) in PBS, dehydrated through a graded series of ethanol washes, from 30% - 100%, and then critical point dried by soaking the samples in hexamethyldisazane (Ted Pella Inc., Redding, CA) for 15 minutes. The samples were allowed to air dry, then immediately attached to aluminum SEM specimen mounting stubs (Electron Microscopy Sciences) and sputter coated with a 7-nm layer of gold-palladium (Cressington 108 Sputter Coater, Cressington Scientific Instruments, Cranberry, PA). Following processing, the samples were visualized using a JEM 6335F SEM (JEOL, Peabody, MA).

4.2.4 mRNA Isolation and Quantitative Real Time RT-PCR Analysis

Total RNA was isolated and purified using the AllPrep DNA/RNA Mini Kit (Qiagen, Valencia, CA) according to the manufacturer's instructions. RNA concentration and purity was determined by Nanodrop ND-1000 Spectrophotometer. RNA was stored at -20°C until further use. cDNA

was synthesized from 100 ng of total RNA in a volume of 20 μL using a Superscript RT III kit (Invitrogen, Carlsbad, CA) according to the manufacturer's instructions.

Quantitative real time RT-PCR was performed using primers specific for genes known to be strong indicators of either an M1 (nitric oxide synthase 2 [*NOS2*], *CXCL11, CXCL10* and *CCR7*) or M2 (arginase type 1 [*ARG1*], *CCL13, CCL18,* and mannose receptor C type 1 [*MRC1*]) type macrophage response [122, 156] (Table 2). Primers were either custom designed using Beacon Designer 7.2 primer design software (PREMIER Biosoft International, Palo Alto, CA) and purchased from Operon Biotechnologies (Huntsville, AL) or predesigned primers were purchased from Real Time Primers (Elkins Park, PA). Primers for the housekeeping gene ribosomal protein L13A (*RPL13A*) were purchased as part of a housekeeping gene primer kit (Human Housekeeping Gene Primer Set, Real Time Primers), and was used to normalize reactions. One μL of cDNA was mixed with the appropriate primers and 2X SYBR Green Master Mix in a total volume of 25 μL. All reactions were performed in triplicate and were monitored using an iQ5 Real-Time Detection System (BioRad, Hercules, CA).

Relative expression of each gene was calculated using the comparative Ct method [157, 158]. The value of the threshold cycle (Ct) for the gene of interest was subtracted from the value of the threshold cycle for the housekeeping gene for each sample (ΔCt, sample) and for the freshly isolated monocytes of the respective donor (ΔCt, monocyte). For samples that did not reached threshold by the 40^{th} cycle, the analytical value of the threshold cycle was designated as 40. Relative expression to the donor-specific monocyte population was then calculated as $2^{(\Delta\Delta Ct)}$, where

$\Delta\Delta Ct = (\Delta Ct, sample) - (\Delta Ct, monocyte)$.

Table 2: Sequences of Human-Specific Primer Sets Used in Real Time Analysis

Gene Name	Gene Symbol	Sequence (5' – 3')	Accession
Nitric oxide synthase type 2	*NOS2**	F: ACAAGCCTACCCCTCCAGAT R:TCCCGTCAGTTGGTAGGTTC	NM_000625
CXCL11	*CXCL11**	F: AGAGGACGCTGTCTTTGCAT R:AGATGCCCTTTTCCAGGACT	NM_005409
CXCL10	*CXCL10*	F: GAATCGAAGGCCATCAAGAA R:GCTCCCCTCTGGTTTTAAGG	NM_001565
CCR7	*CCR7*	F: GTGGTGGCTCTCCTTGTCAT R:ATAGGGAGGAACCAGGCTTT	NM_001838
Arginase type 1	*ARG1**	F:CAAGGTGGCAGAAGTCAAG R:GGTTGTCAGTGGAGTGTTG	NM_000045
CCL13	*CCL13*	F: ACATGAAAGTCTCTGCAGTGCTTC R:AGTAGATGGGACGTTGAGTGCAT	NM_005408
CCL18	*CCL18*	F:ACAAAGAGCTCTGCTGCCTC R:CCCACTTCTTATTGGGGTCA	NM_002988
Mannose receptor C type 1	*MRC1*	F:GGCGGTGACCTCACAAGTAT R:ACGAAGCCATTTGGTAAACG	NM_002438
Ribosomal protein L13A	*RPL13A**	F: CCTGGAGGAGAAGAGGAAAGAGA R:TTGAGGACCTCTGTGTATTTGTCAA	NM_012423.2

*Purchased from Real Time Primers

4.2.5 Measurement of DNA Content

Total DNA was isolated using the AllPrep DNA/RNA Mini Kit (Qiagen, Valencia, CA) according to the manufacturer's instructions. Total DNA was quantified using the commercially available Quant-iT PicoGreen dsDNA Kit (Invitrogen-Molecular Probes, Eugene, OR) according to the manufacturer's instructions. Each sample was measured in triplicate.

4.2.6 Protein Analysis of Supernatant

The supernatants from the macrophage cultures were cleared through centrifugation, snap frozen in liquid nitrogen and stored at -80°C. SearchLight® Biomarker Testing Service (Aushon Biosystems, Billerica, MA) was utilized to determine the concentration of MMP9, CXCL10, CCL13, and CCL18 in the supernatant. SearchLight Array Technology uses a multiplexing sandwich-ELISA system based on chemiluminescent detection of analytes (information from www.aushon.com). The concentrations of each protein for SIS in media, CDI-SIS in media, and media only were subtracted from the concentrations detected for each sample. The protein amounts were then normalized to DNA content of each sample.

4.2.7 Nitric Oxide Analysis of Supernatant

The supernatants from macrophage cultures from two donors were prepared as described in Section 4.2.6. The concentration of nitric oxide (NO) was determined using the Griess Reagent (Sigma) according to the manufacturer's instructions. Each sample was measured in triplicate.

4.2.8 Statistical Methods

All values are presented as mean ± standard error. For the mRNA expression and MMP9 protein concentration, a generalized linear model was used to determine statistical significance of the factors scaffold (SIS, CDI-SIS, and TCP), time (18, 72, and 168 hours), and oxygen concentration (6% and 20%), and the interaction between these factors. The data were transformed using natural log for the statistical analysis. Results were transformed back to the

original scale for presentation. The post-hoc Tukey's (HSD) procedure was used to determine which pairs of levels of factors were significantly different when a main effect was statistically significant. For the CXCL10, CCL13, and CCL18 protein concentration data, the Kruskal-Wallis model was used to determine statistical significance, followed by the post-hoc Mann-Whitney procedure. Statistical analysis was performed using SAS 7.2 software. A p value of < 0.05 was considered statistically significant.

4.3 RESULTS

4.3.1 Crosslinking Efficacy

The ninhydrin assay showed a greater concentration of free amino acids in the supernatants from SIS compared to CDI-SIS (547.1 ± 99.2 vs. 16.6 ± 7.4 μM/mg, $p < 0.01$), confirming that the CDI-SIS scaffolds were more resistant to collagenase degradation than the SIS scaffolds.

4.3.2 Macrophage Morphology on Substrates

For the M1-induced macrophages, several cells showed a flattened, 'fried egg' morphology, while the remaining cells showed a spindle-shaped morphology. The M2-induced macrophages remained mostly spherical, and the cell membrane showed a rippled appearance (Figure 6). Macrophages attached to the surfaces of SIS and CDI-SIS by 18 hours, and by 72 and 168 hours macrophages were concentrated in areas of topographical complexity. The macrophages in contact with SIS showed a rounded morphology at 72 hours, and by 168 hours the macrophages

coated the surface of the fibers (Figure 7). The macrophages in contact with CDI-SIS at 168 hours showed a mixed morphologic appearance of rounded cells and flattened cells in areas that showed a raised surface (Figure 8). The macrophages cultured with complete media only showed a mixture of rounded, spindled cells and flattened cells at 72 hours, and by 168 hours the majority of macrophages showed a flattened morphology. There were no obvious differences in the morphology of the macrophages when comparing the oxygen concentrations.

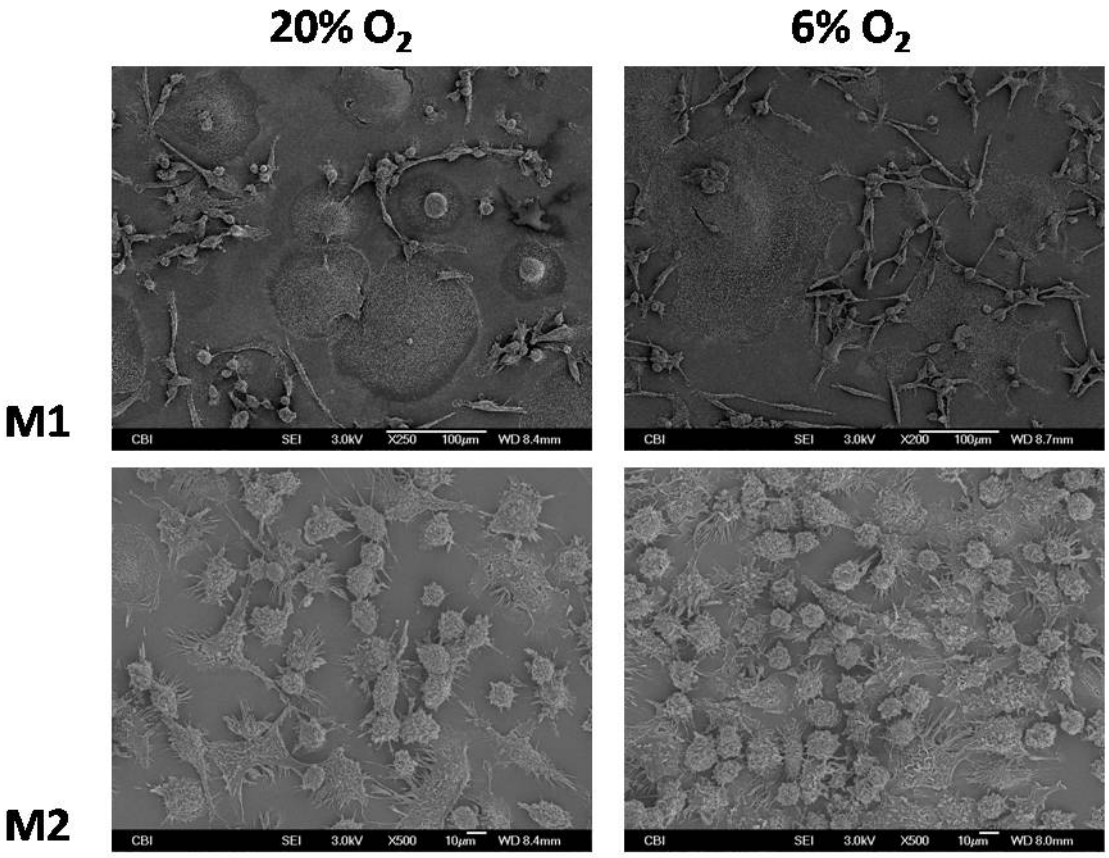

Figure 6: Comparison of morphologic appearance of M1 and M2-differentiated macrophages at 168 hours in 20% and 6% oxygen concentrations.

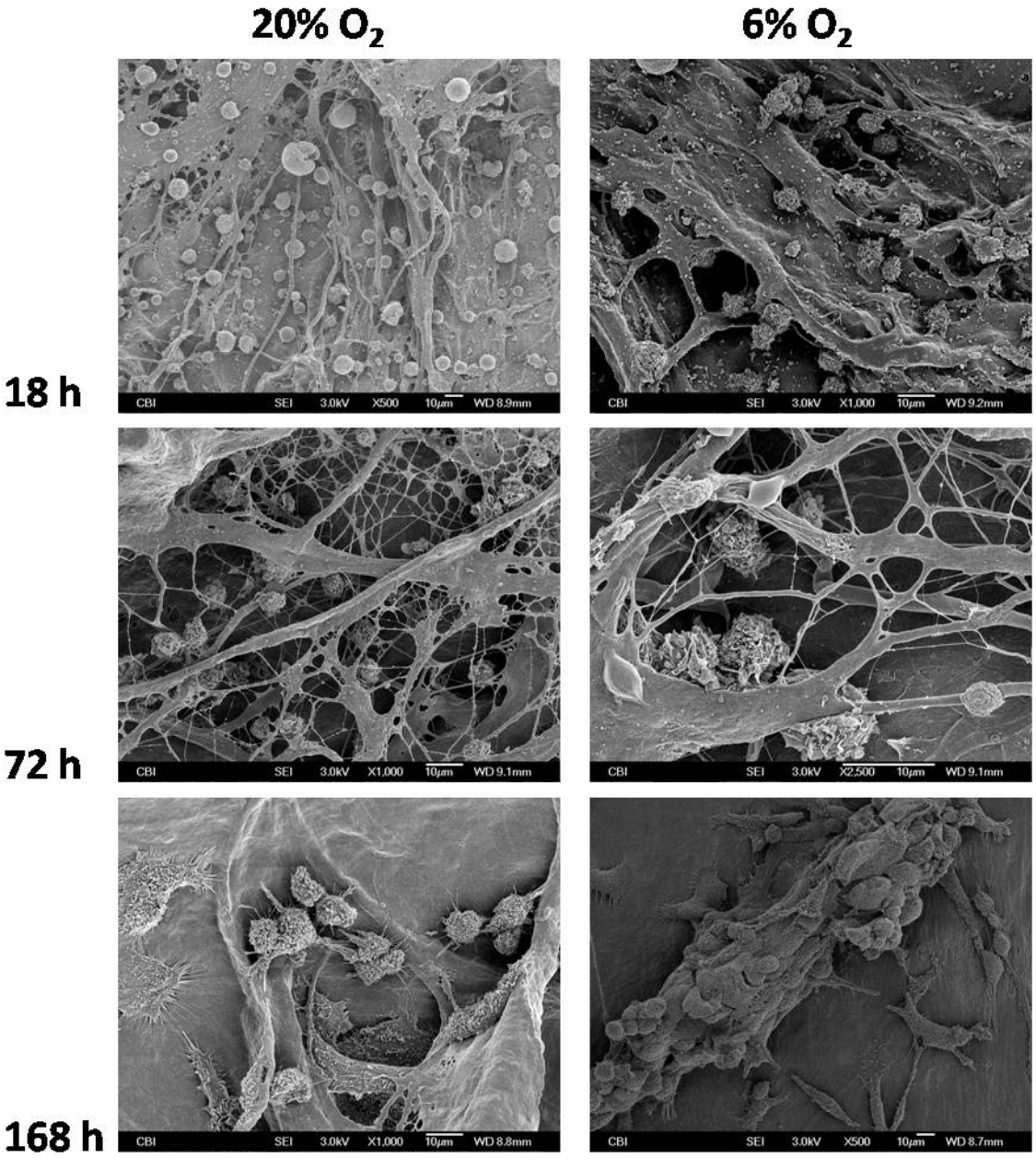

Figure 7: Comparison of morphologic appearance of macrophages on the luminal surface of SIS at 18, 72, and 168 hours in 20% and 6% oxygen concentrations.

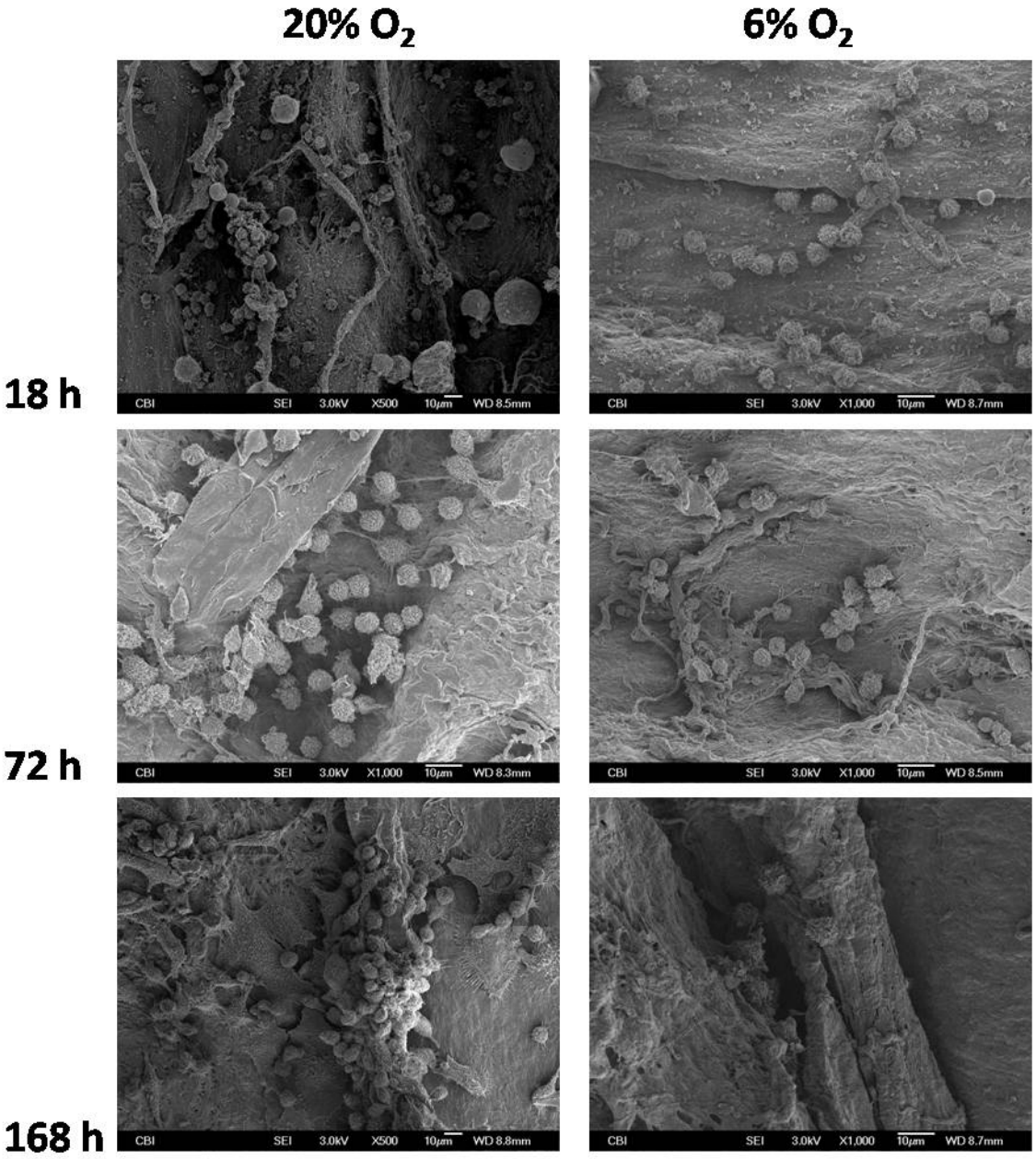

Figure 8: Comparison of morphologic appearance of macrophages on the luminal surface of CDI-SIS at 18, 72, and 168 hours in 20% and 6% oxygen concentrations.

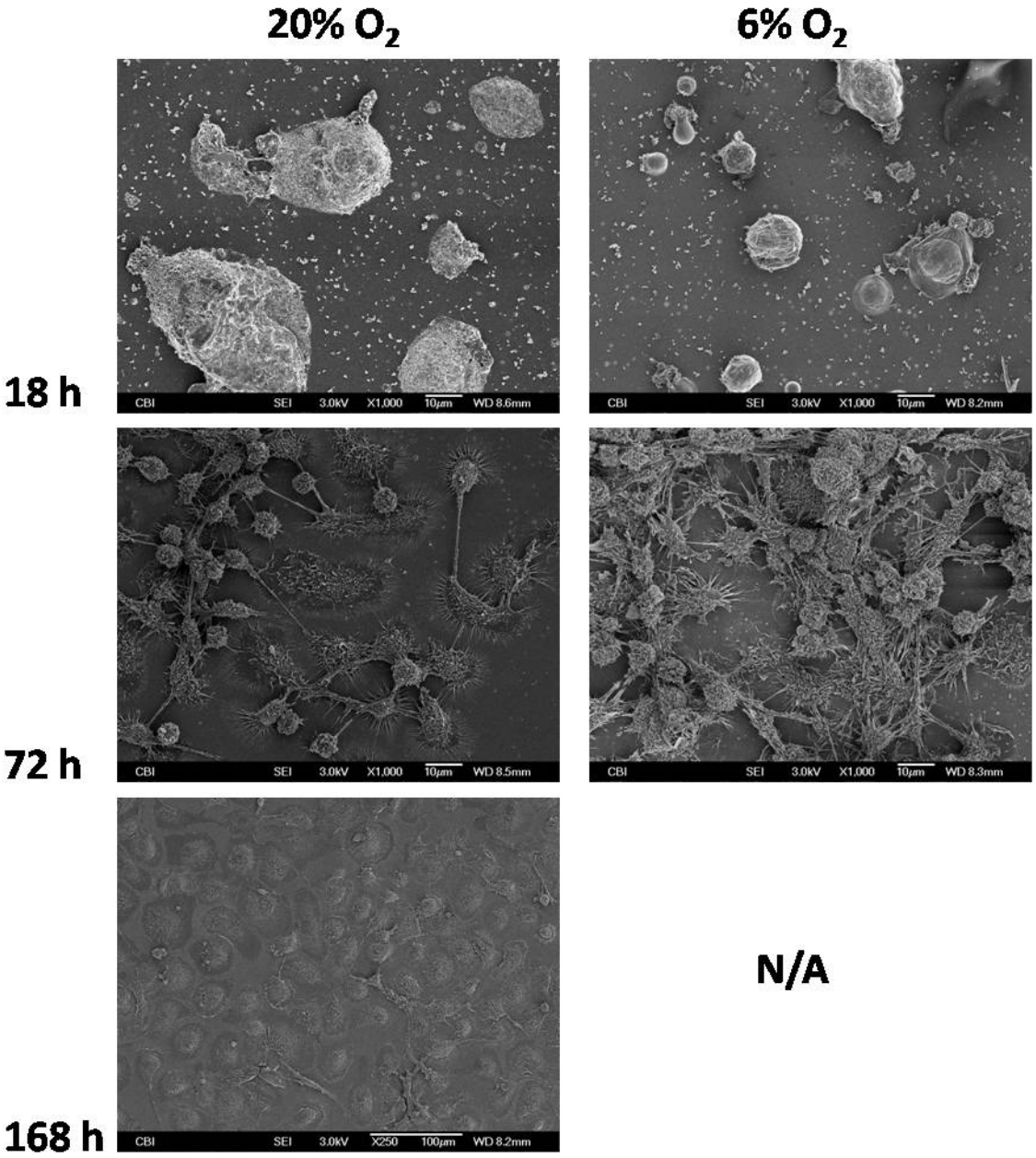

Figure 9: Comparison of morphologic appearance of macrophages on glass coverslips in complete media only at 18, 72, and 168 hours in 20% and 6% oxygen concentrations.

4.3.3 Findings of mRNA Analysis

4.3.3.1 *NOS2* and *CXCL11* mRNA Expression

M1 macrophages were the only cells that showed expression of *CXCL11*. No macrophages showed expression of *NOS2*.

4.3.3.2 Donor-specific mRNA Expression of Monocytes

The baseline ΔCt values were determined for each donor (Figure 10). There were marked donor-specific differences for *CXCL10*, *CCR7* and *CCL13*.

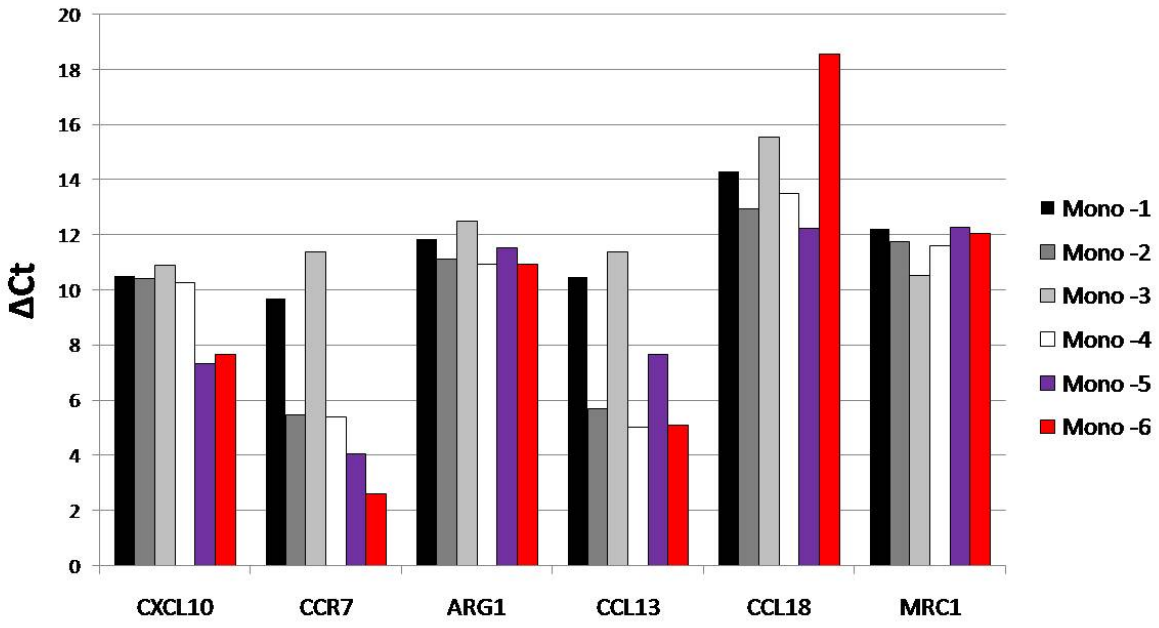

Figure 10: Baseline threshold cycle for each gene was subtracted from the threshold cycle for the housekeeping gene (ΔCt) from each donor of the isolate monocytes (Mono-#).

4.3.3.3 mRNA Expression for M0, M1, and M2-induced Macrophages

The mRNA expression for the M1 (*CXCL10* and *CCR7*) and M2 (*CCL13, CCL18,* and *MRC1*) markers used in the study was determined for M0, M1, and M2 macrophages (Figure 11). Compared to M2 macrophages, M1 macrophages showed higher expression of *CXCL10* and *CCR7*, with the exception of M2 macrophages induced by IL-10 and cultured in 6% oxygen, and lower expression of *CCL13*, *CCL18,* and *MRC1*. *CXCL10* showed an increased ratio toward the M1 phenotype, and *CCR7* and *CCL18* showed an increased ratio toward the M2 phenotype in 20% oxygen compared to 6% oxygen (Table 3). *CCL13* and *MRC1* did not show appreciable differences in expression with respect to oxygen tension.

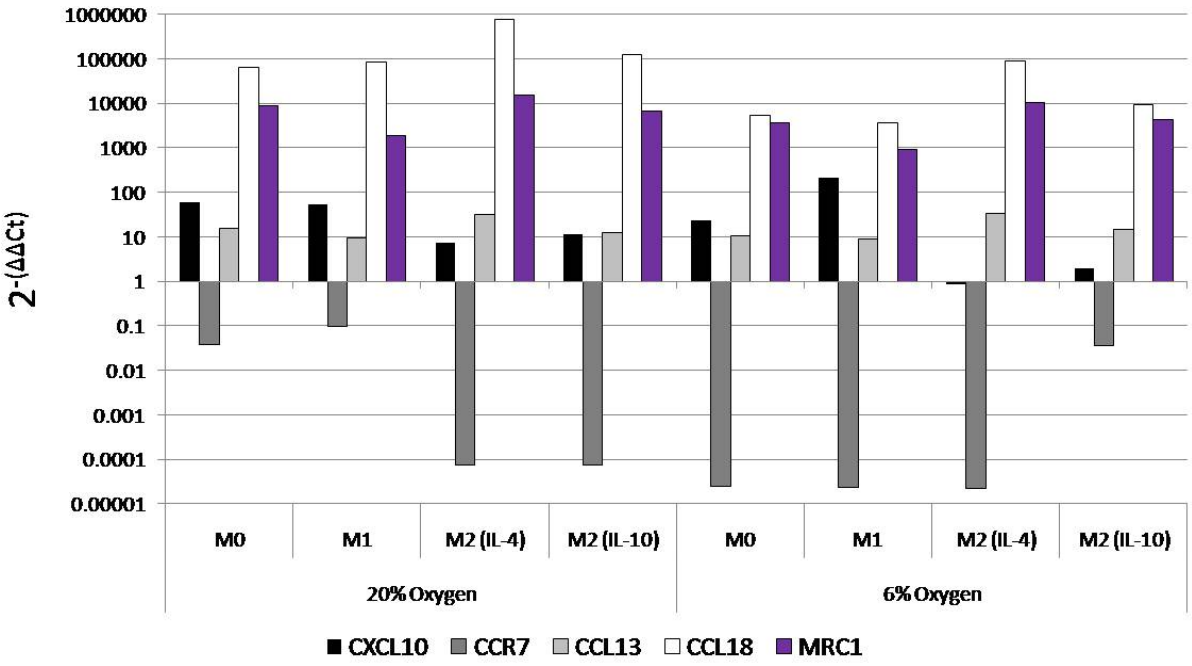

Figure 11: mRNA expression for M0, M1, and M2-induced macrophages cultured in 20% and 6% oxygen.

Table 3: Genes differentially expressed in M1 vs. M2 macrophages.

Gene	O_2 %	M1:M2 (IL-4)	M1:M2 (IL-10)
CXCL10	20%	7.3	4.6
	6%	252.5	108.4
CCR7	20%	1252	1296.1
	6%	1.1	-1541.4
CCL13	20%	-3.4	-1.3
	6%	-3.9	-1.6
CCL18	20%	-8.8	-1.5
	6%	-25.1	-25.7
MRC1	20%	-8.3	-3.7
	6%	-11.4	-4.7

4.3.3.4 Effect of Substrate and Oxygen Tension on *CXCL10* mRNA Expression

The statistically significant effects were for scaffold ($P<0.003$) and time ($P<0.0001$). Further analysis indicated that expression was higher for macrophages cultured on TCP compared to SIS and CDI-SIS, and expression was highest at 18 hours compared to 72 and 168 hours (Figure 12). No statistically significant effects were found for oxygen concentration.

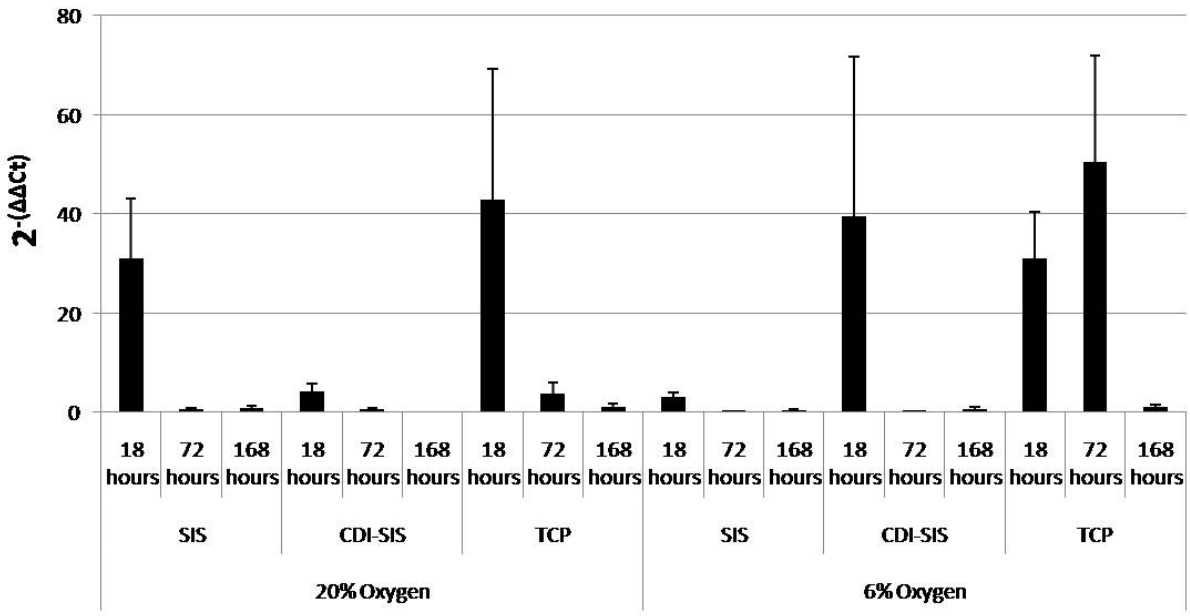

Figure 12: *CXCL10* mRNA expression in macrophages cultured on SIS, CDI-SIS, and TCP at 18, 72, and 168 hours in 20% and 6% oxygen.

4.3.3.5 Effect of Substrate and Oxygen Tension on *CCR7* mRNA Expression

The statistically significant effects were for scaffold ($P<0.0002$) and time ($P<0.0001$). Further analysis indicated that macrophages cultured on CDI-SIS showed higher expression compared to macrophages cultured on SIS and TCP, and expression was highest at 18 hours and lowest at 168 hour (Figure 13). No statistically significant effects were found for oxygen concentration.

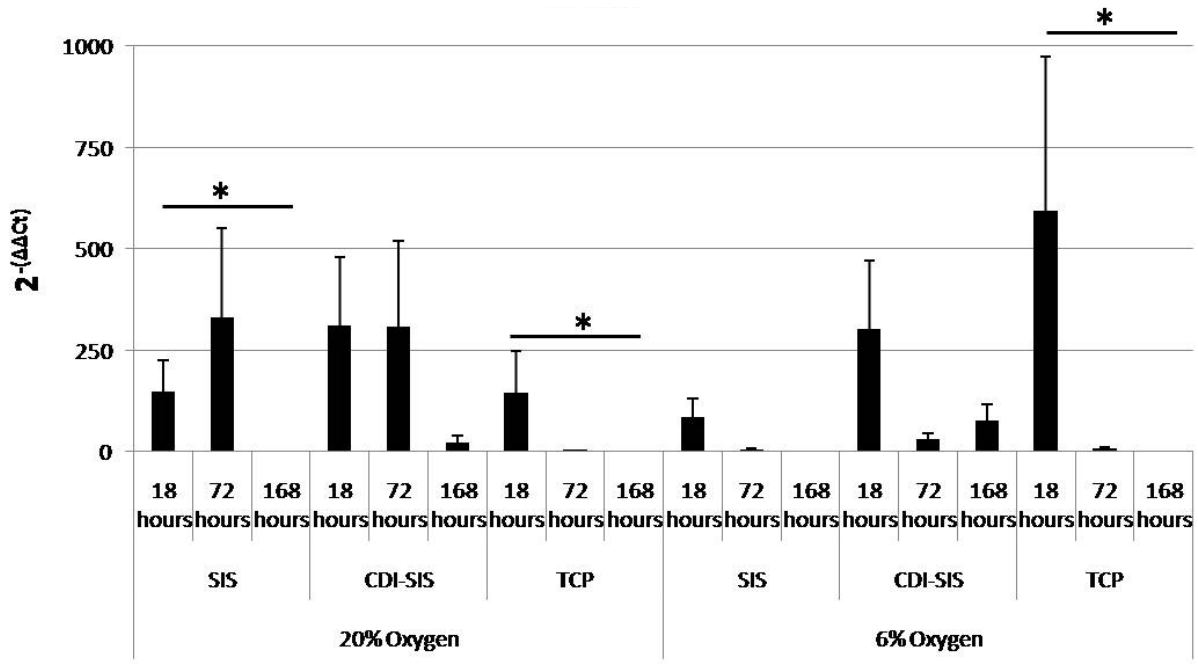

Figure 13: *CCR7* mRNA expression in macrophages cultured on SIS, CDI-SIS, and TCP at 18, 72, and 168 hours in 20% and 6% oxygen. * indicates statistical significance ($p < 0.05$) between timepoints within a scaffold group.

4.3.3.6 Effect of Substrate and Oxygen Tension on *ARG1* mRNA Expression

The statistically significant effect was for time ($P<0.0001$). Further analysis indicated that expression was lowest at 168 hours compared to 18 and 72 hours for all substrates (Figure 14). No statistically significant effects were found for scaffold or oxygen concentration.

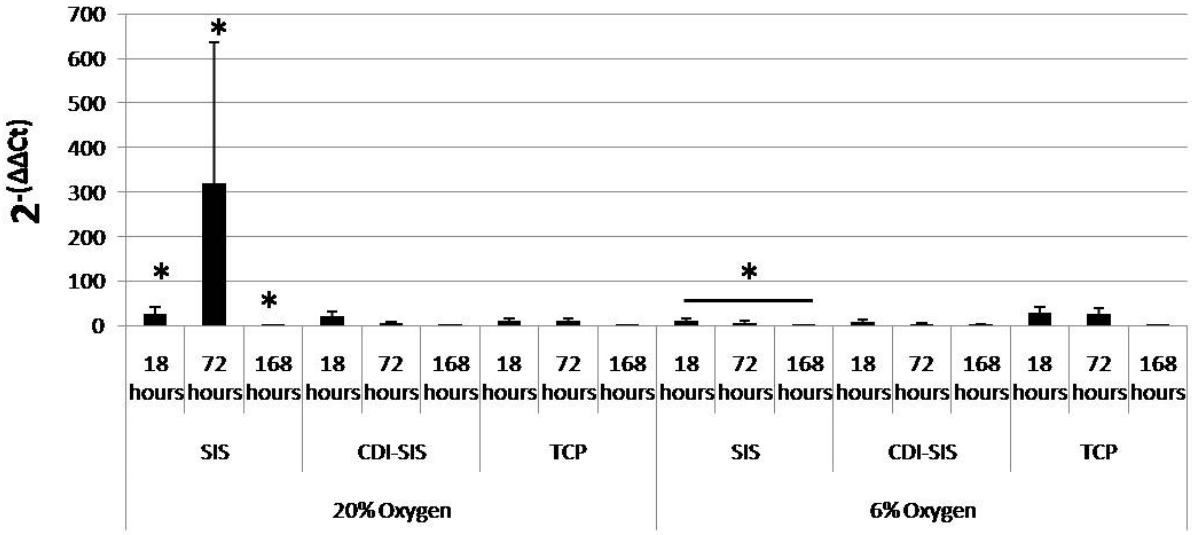

Figure 14: *ARG1* mRNA expression in macrophages cultured on SIS, CDI-SIS, and TCP at 18, 72, and 168 hours in 20% and 6% oxygen. * indicates statistical significance ($p < 0.05$) between timepoints within a substrate group.

4.3.3.7 Effect of Substrate and Oxygen Tension on *CCL13* mRNA Expression

The statistically significant effects were for scaffold ($P<0.011$), time ($P<0.0001$), and scaffold by time interaction ($P<0.006$). Further analysis indicated that macrophages cultured on SIS and CDI-SIS showed higher expression compared to TCP, and expression was greatest at 18 hours compared to 72 and 168 hours (Figure 15). No statistically significant effects were found for oxygen concentration.

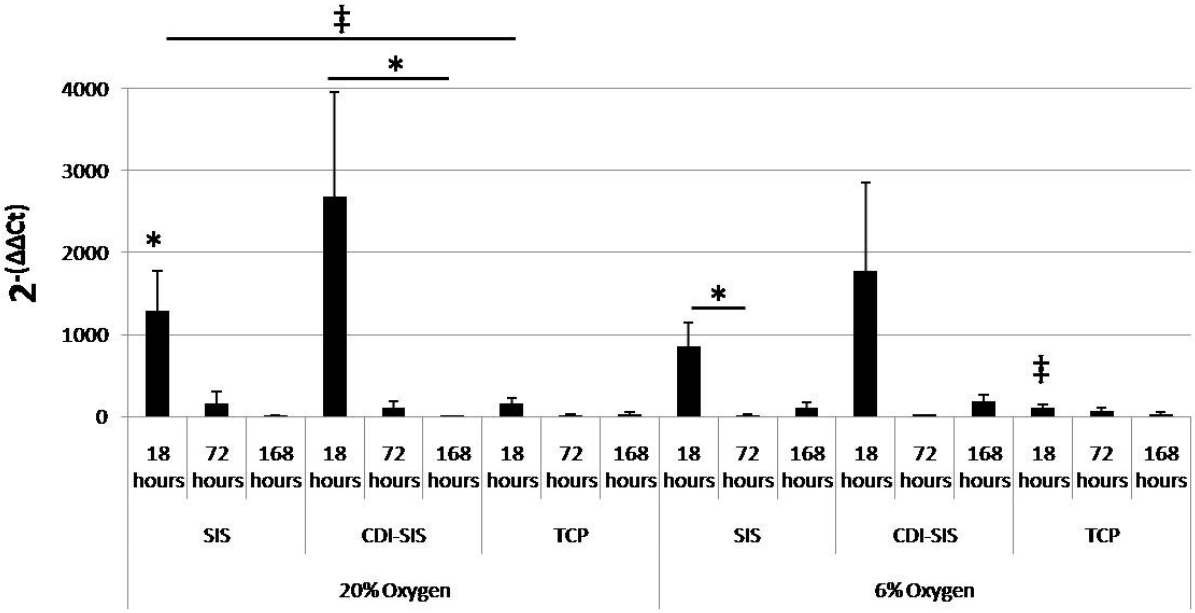

Figure 15: *CCL13* mRNA expression in macrophages cultured on SIS, CDI-SIS, and TCP at 18, 72, and 168 hours in 20% and 6% oxygen. * indicates statistical significance ($p < 0.05$) between timepoints within a substrate group, and ‡ indicates statistical significance between substrate groups within a timepoint.

4.3.3.8 Effect of Substrate and Oxygen Tension on *CCL18* mRNA Expression

The statistically significant effects were for scaffold ($P<0.03$), time ($P<0.0001$), oxygen concentration ($P<0.02$), oxygen concentration by time ($P<0.03$), and scaffold by time interaction ($P<0.0007$). Further analysis indicated that macrophages cultured on SIS showed higher expression compared to macrophages cultured on CDI-SIS, and the 18 hour timepoint was significant compared to 72 and 168 hours (Figure 16).

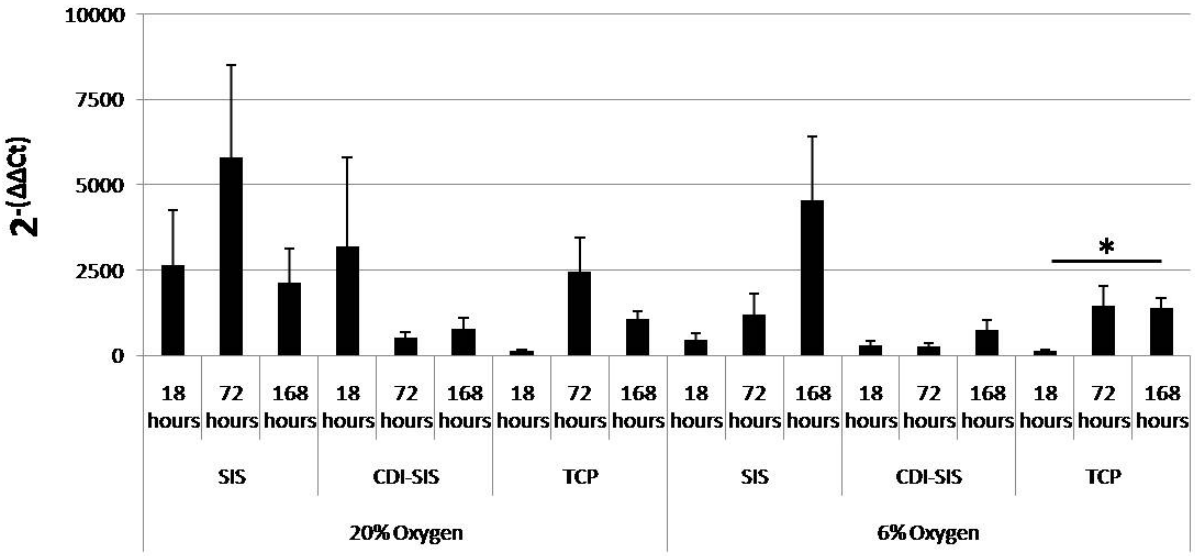

Figure 16: *CCL18* mRNA expression in macrophages cultured on SIS, CDI-SIS, and TCP at 18, 72, and 168 hours in 20% and 6% oxygen. * indicates statistical significance ($p < 0.05$) between timepoints within a substrate group.

4.3.3.9 Effect of Substrate and Oxygen Tension on *MRC1* mRNA Expression

The statistically significant effects were for scaffold ($P<0.0005$) and oxygen concentration by time interaction ($P<0.05$). Further analysis indicated that macrophages cultured on TCP showed significance compared to macrophages cultured on SIS and CDI-SIS (Figure 17). No statistically significant effects were found for time.

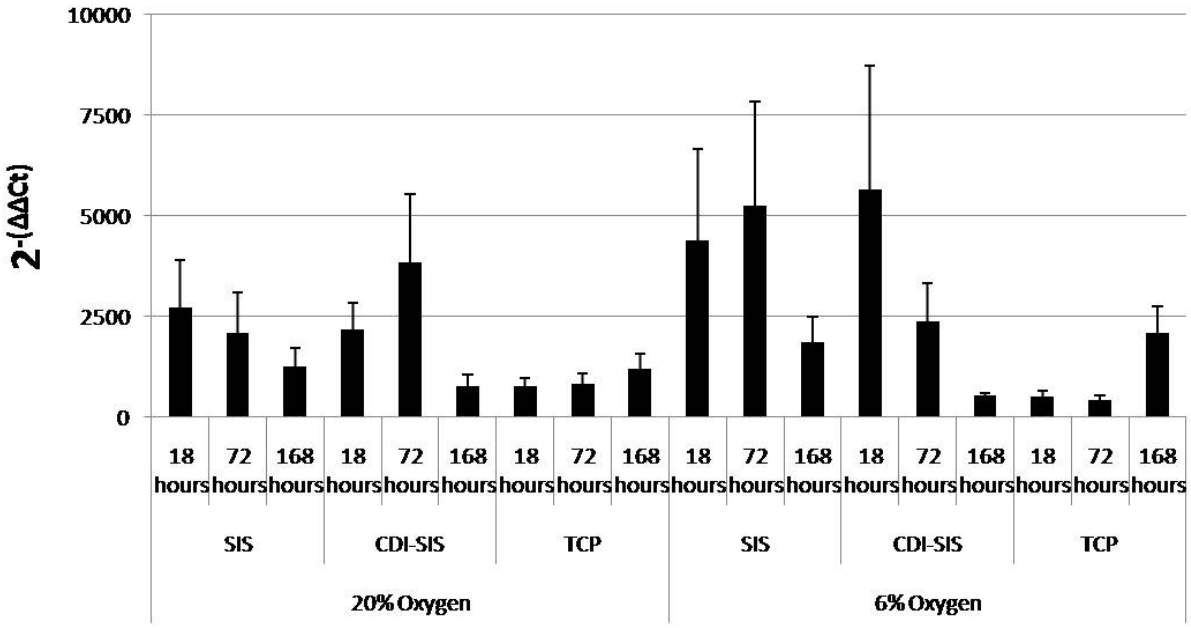

Figure 17: *MRC1* mRNA expression in macrophages cultured on SIS, CDI-SIS, and TCP at 18, 72, and 168 hours in 20% and 6% oxygen.

4.3.3.10 Summary of mRNA Findings

The M1 markers *CXCL10* and *CCR7* showed a higher expression for macrophages cultured on CDI-SIS and TCP compared to SIS. These findings are comparable to the expression levels of M1 and M2-induced macrophages (Section 4.3.3.3). The M2 marker *ARG1* did not show significance with respect to substrate or oxygen tension. The M2 markers *CCL13* and *CCL18* showed a higher mRNA expression for macrophages cultured on SIS compared to macrophages cultured on TCP. The expression of *CCL13* and *CCL18* was not affected by oxygen tension for the M1 and M2-induced macrophages nor for the macrophages cultured on the test substrates. The M2 marker *MRC1* showed a higher mRNA expression for macrophages cultured on SIS and CDI-SIS, irrespective of oxygen concentration. These findings are comparable to mRNA expression in M1 and M2-induced macrophages. In general, these results show that macrophages

express an M2-like phenotype when in cultured on SIS, while macrophages cultured on CDI-SIS or TCP express a mixed M1/M2-like phenotype.

4.3.4 Findings of Protein Analysis

4.3.4.1 Protein Concentration Findings for M0, M1, and M2-induced Macrophages

The protein concentrations for MMP9 and the M1 (CXCL10) and M2 (CCL13 and CCL18) markers used in the study were determined for M0, M1, and M2 macrophages (Figure 18). MMP9 was expressed in equal amounts for all induced macrophages irrespective of oxygen tension. M1 macrophages showed a higher expression of CXCL10 and a lower expression of CCL13 and CCL18 compared to M2 macrophages. Comparing oxygen tension, the lower oxygen tension showed a trend toward a more polarized expression of M1 and M2 markers (Table 4).

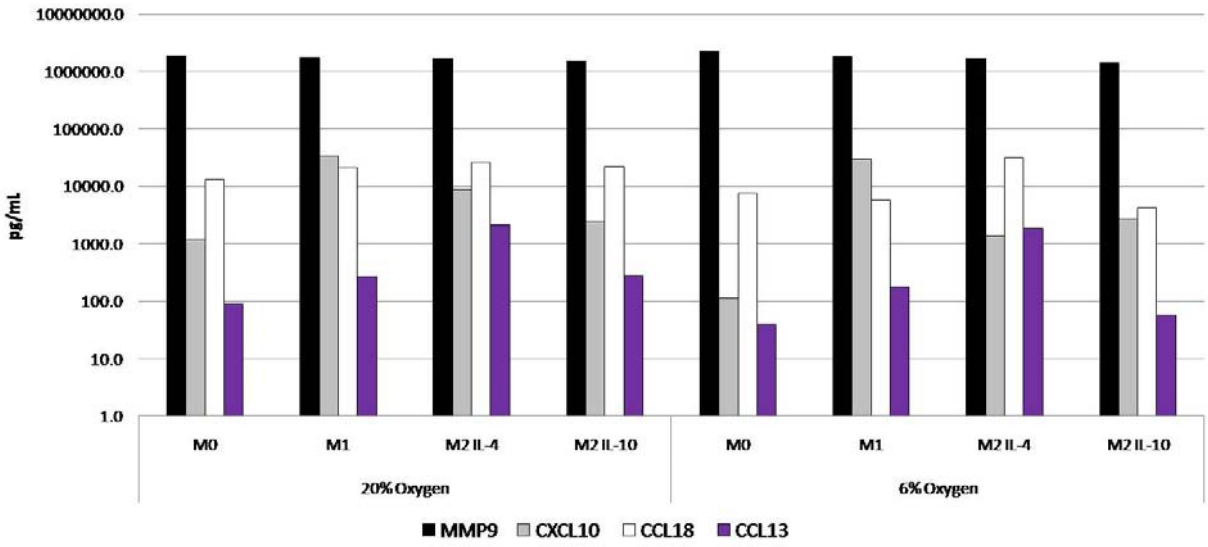

Figure 18: Protein levels in supernatants from M0, M1, and M2-induced macrophages at 168 hours in 20% and 6% oxygen.

Table 4: Proteins differentially expressed in M1 vs. M2 macrophages.

Protein	O_2 %	M1:M2 (IL-4)	M1:M2 (IL-10)
MMP9	20%	1.0	1.1
	6%	1.1	1.3
CXCL10	20%	3.9	13.7
	6%	21.3	10.9
CCL13	20%	-8.1	-1.0
	6%	-10.9	3.0
CCL18	20%	-1.2	-1.0
	6%	-5.5	-1.4

4.3.4.2 Effect of Substrate and Oxygen Tension on MMP9 Protein Concentration

The statistically significant effects were for scaffold ($P<0.0005$), time ($P<0.0001$), and scaffold by time interaction ($P<0.02$). Further analysis indicated that macrophages cultured on SIS showed significance compared to macrophages cultured on CDI-SIS and TCP, and protein concentration was highest at 168 hours and lowest at 18 hours (Figure 19). No statistically significant effects were found for oxygen concentration.

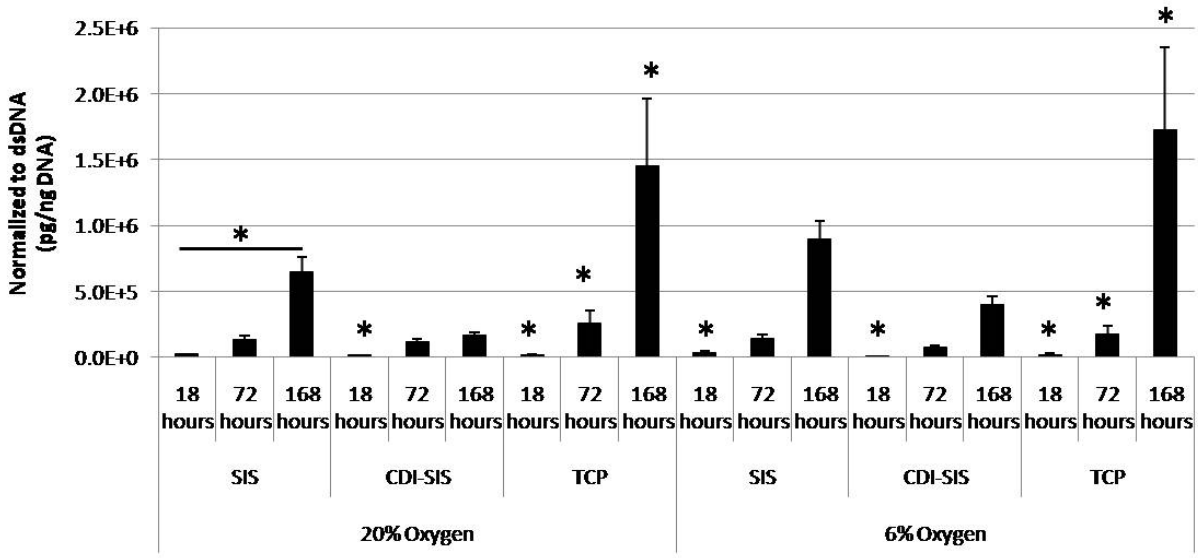

Figure 19: Concentration of MMP9 in supernatants from macrophages cultured on SIS, CDI-SIS, and TCP at 18, 72, and 168 hours in 20% and 6% oxygen. * indicates statistical significance ($p < 0.05$) between timepoints within a substrate group.

4.3.4.3 Effect of Substrate and Oxygen Tension on CXCL10 Protein Concentration

Macrophages cultured on SIS showed the lowest concentration of CXCL10 at 18 hours in 6% oxygen, and macrophages cultured on CDI-SIS showed the lowest concentration at 168 hours in 20% oxygen (Figure 20). Macrophages cultured on TCP showed the highest concentration at 18 hours in 20% oxygen, and 72 hours in 6% oxygen. No statistically significant effects were found for oxygen concentration.

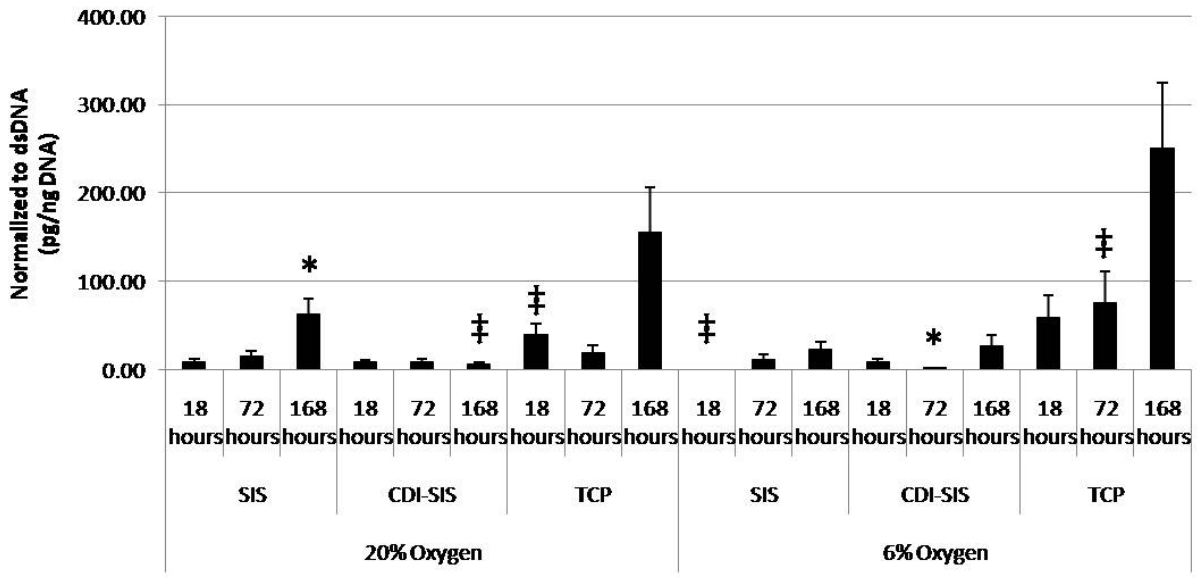

Figure 20: CXCL10 concentration in supernatants from macrophages cultured on SIS, CDI-SIS, and TCP at 18, 72, and 168 hours in 20% and 6% oxygen. * indicates statistical significance ($p < 0.05$) between timepoints within a substrate group, and ‡ indicates statistical significance between substrate groups within a timepoint.

4.3.4.4 Effect of Substrate and Oxygen Tension on CCL13 Protein Concentration

For most substrates, CCL13 concentration increased with time. Macrophages cultured on SIS showed the highest expression at 72 hours compared to macrophages cultured on CDI-SIS and TCP, while macrophages cultured on CDI-SIS showed the lowest expression at 72 and 168 hours compared to SIS and TCP (Figure 21). No statistically significant effects were found for oxygen concentration.

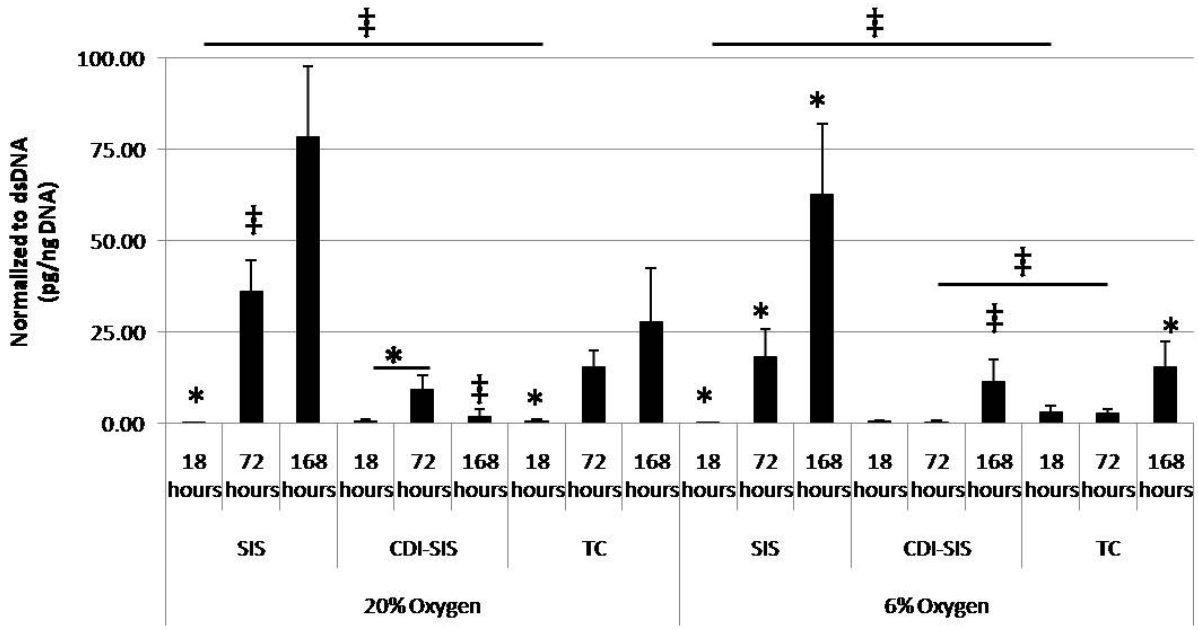

Figure 21: Concentration of CCL13 in supernatants from macrophages cultured on SIS, CDI-SIS, and TCP at 18, 72, and 168 hours in 20% and 6% oxygen. * indicates statistical significance ($p < 0.05$) between timepoints within a substrate group, and ‡ indicates statistical significance between substrate groups within a timepoint.

4.3.4.5 Effect of Substrate and Oxygen Tension on CCL18 Protein Concentration

For all substrates the concentration of CCL18 increased with time. Macrophages cultured on CDI-SIS showed the lowest concentration of CCL18 compared to macrophages cultured on SIS and TCP (Figure 22). No statistically significant effects were found for oxygen concentration.

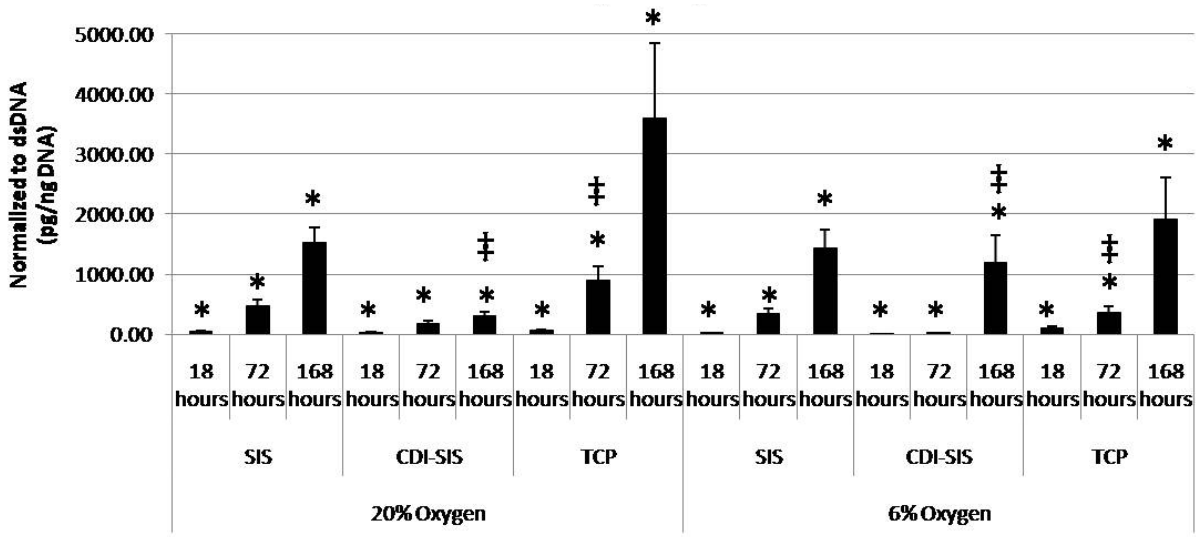

Figure 22: Concentration of CCL18 in supernatants from macrophages cultured on SIS, CDI-SIS, and TCP at 18, 72, and 168 hours in 20% and 6% oxygen. * indicates statistical significance ($p < 0.05$) between timepoints within a substrate group, and ‡ indicates statistical significance between substrate groups within a timepoint.

4.3.4.6 Summary of Protein Analysis

The protein levels of MMP9 were higher for macrophages cultured on SIS and TCP compared to CDI-SIS. The M1 cytokine marker CXCL10 showed a higher protein concentration for macrophages cultured on TCP compared to SIS and CDI-SIS. These findings are comparable to the concentration levels of M1 and M2-induced macrophages (Section 4.3.4.1). The M2 markers CCL13 and CCL18 showed higher protein concentration in the supernatant from macrophages cultured on SIS compared to CDI-SIS. The concentration of CCL13 was not affected by oxygen tension for the M1 and M2-induced macrophages nor for the macrophages cultured on the test substrates. Contradicting the findings from the M1 and M2-induced macrophages, the concentration of CCL18 for macrophages cultured on the test substrates was not affected by the

oxygen tension. In general, these results show correlation with the gene expression profiles in Section 4.3.3, although most of the gene markers were elevated at the 18 hour timepoint while the protein levels were elevated at 168 hours.

4.3.5 Findings of Nitric Oxide Concentration Analysis

There was little to no detectable nitric oxide in the supernatants from the M1 or M2-induced macrophages or the macrophages cultured on SIS, CDI-SIS, or TCP.

4.4 DISCUSSION

The results of the present study support the hypothesis of Specific Aim 1, in that macrophages cultured on the luminal surface of SIS showed an M2-like phenotype, while macrophages cultured on the surfaces of CDI-SIS and TCP showed a mixed M1/M2-like phenotype. Of interest, macrophages cultured on substrates that showed higher mRNA expression for *CXCL10* and *CCL18* also showed higher protein concentrations for the same marker, although expression of the mRNA markers peaked at 18 hours and protein concentrations peaked at 168 hours.

It is common practice to compare the relative ratio of *iNOS* to *ARG1* as a way to determine macrophage function and phenotype for murine and rodent macrophages *in vitro* and *in vivo*. However, species differences do exist, and the methods that are used to stimulate macrophages may have a significant impact on the results. A study by Chiang and colleagues showed that resident peritoneal cells (PECs) from C3H/HeN mice stimulated *in vivo* with i.p. injections of LPS or IFN-γ showed opposing expression of iNOS and arginase, while PECs that

were harvested prior to stimulating in culture with LPS showed almost no expression of *iNOS* but did show detectable levels of *ARG1* expression [159]. Several studies by Pham et al. determined that primary human monocyte-derived macrophages do not readily produce NO in culture, and that protein kinase C-eta (PKC-η) is at least one requirement for the development of *iNOS* expression [160, 161]. In the present study *iNOS* expression was absent and no NO was detected in the supernatant from cultures of human monocyte-derived macrophages.

A finding of the present study was that for most markers the macrophages cultured on the test substrates did not show an increased polarization toward either an M1 or M2 profile in a lower oxygen tension. Low oxygen tension is a crucial physiological signal in wound healing by altering gene expression and metabolic activity, and induces marked changes in the proliferation rate, migration, differentiation, and secretory activity of most cells, including tumor associated macrophages, osteoblasts, chondrocytes, and stem cells [93, 107]. Previous studies have shown that monocytes and macrophages cultured in hypoxia up-regulate the transcription factors hypoxia-inducible factor 1 and 2 (HIF), which in turn activates a broad array of markers for monocyte recruitment including endothelial cell adhesion molecules and proangiogenic factors VEGF and angiopoietin-2 [162]. Hypoxia is also known to inhibit macrophage migration, chemotaxis, and proliferation [163, 164]. Work by Csete et al. has shown that various stem cell populations including rat fetal-derived neural crest stem cells, adult murine skeletal satellite cells, and rat marrow-derived mesenchymal stem cells cultivated in lower oxygen tensions show enhanced proliferation, reduced apoptosis, and enhanced differentiation into lineage-specific phenotypes [165]. Studies in our laboratory have complemented Csete's results by showing that murine blastema (MRL-B) cells and human perivascular stem cells (MG-71) increased rate of proliferation and retained chemotactic and mitogenic properties to ECM digests when cultured in

low oxygen compared to atmospheric oxygen (data not published). The migration, chemotactic, or proliferative capacities of the monocyte-derived macrophages to SIS or CDI-SIS were outside the scope of the present study, but such an endeavor would be worthy of pursuit.

Although the present study does not demonstrate a direct link between macrophages cultured on ECM substrates and *in vivo* remodeling, the findings in the present study coupled with the *in vivo* macrophage response observed in previous studies [60, 151] support the concept that the macrophage phenotype during ECM scaffold remodeling may contribute to the long-term outcome.

4.5 FUTURE STUDIES

Future investigations may develop a macrophage-mediated protocol for producing ECM digest products, which may be a more physiologic method than digestion protocols that use acid/heat or pepsin. Experiments would utilize the Boyden chamber assay to study the chemotactic properties of these digests for progenitor cell lines such as MRL blastema cells or mesenchymal stem cells.

Another prospective study may investigate the specificity of ECM scaffolds to the resident tissue macrophages that normally resided in the organ of origin. It would be interesting to show whether monocytes-derived macrophages adopt a profile that is more similar to the resident tissue macrophage rather than inflammatory macrophage phenotype. Such substrates/ macrophage combinations may include Kupffer macrophages cultured on liver-derived ECM or intestinal macrophages cultured on SIS.

Further investigation is also warranted to understand the phenotypic changes that occur when macrophages are exposed to mechanical loading. Applying a stretching protocol to

macrophages in direct contact with ECM scaffolds may alter the gene expression profile of markers important for remodeling, such as MMPs, collagen production, and angiogenic growth factors.

5.0 SPECIFIC AIM 2: TO DETERMINE THE NECESSITY OF PARTICIPATION OF MACROPHAGES FOR THE DEGRADATION OF SIS-ECM SCAFFOLDS

It is intuitive and logical that phagocytic cells such as macrophages play an important role in ECM scaffold degradation but definitive studies to address the issue have not been reported. The concept of ECM scaffold degradation as a critical determinant of constructive tissue remodeling becomes even more clinically relevant when considering the widespread use of commercially available ECM materials that have been subjected to chemical and physical methods designed specifically to prevent scaffold degradation and increase the mechanical strength of the materials [132]. A recent study that compare several commercially available ECM scaffold materials has shown that the methods used to process these scaffolds, especially chemical methods to create molecular crosslinks, have marked effects upon host macrophage phenotype surrounding the ECM scaffold and downstream remodeling events (see sections 2.2.1.2 and 2.2.2.1) [60].

The objective of Specific Aim 2 was to determine the contribution of mononuclear macrophages to the degradation and early remodeling events that follow the implantation of ECM scaffolds for the purpose of tissue reconstruction. This objective was accomplished by evaluating the degradation and remodeling response of native and chemically crosslinked ECM in a rat model of abdominal wall repair with and without macrophage depletion. Both of the scaffolds tested in the study mimic products that are used clinically for augmentation of the rotator cuff [166]. Macrophage depletion was accomplished by administration of clodronate-

containing liposomes that are subjected to phagocytosis by circulating monocytes. Apoptosis of monocytes occurs when intracellular clodronate reaches a threshold concentration [167-169]. Liposomes do not cross the vascular-endothelial barrier, so only circulating monocytes are affected. Stated differently, resident tissue macrophages remain unaffected by the clodronate treatment.

5.1 MATERIALS AND METHODS

5.1.1 Overview of Experimental Design

Forty-eight adult rats were randomly divided into three equal groups (n = 16 for each group). A 1.5 cm^2 partial thickness defect was created in the ventro-lateral abdominal wall of each animal. The defect was replaced with one of three different materials: a 10 layer configuration of an ECM biologic scaffold composed of porcine-derived SIS radiolabeled with ^{14}C (^{14}C-SIS); a 10 layer configuration of the same form of porcine-derived ^{14}C-SIS test article except for the use of carbodiimide as a crosslinking agent (^{14}C-X-SIS); or autologous body wall tissue. Each group was divided into 3 sub-groups. Subgroup No.1 was administered clodronate-containing liposomes twice weekly (n=8). Subgroup No.2 was administered PBS-containing liposomes twice weekly (n=4). Subgroup No.3 was administered twice weekly treatments with saline vehicle (n=4). One half of the animals in each subgroup were sacrificed one week after surgery. The remaining animals were sacrificed two weeks following surgery. The implanted scaffold materials plus surrounding host native tissue were explanted and examined by 1) histologic and immunohistochemical methods to determine the participation of blood derived macrophages in

the host response and to characterize the scaffold remodeling response; 2) liquid scintillation counting for ^{14}C content to quantify the extent of SIS scaffold degradation; and 3) real time RT-PCR to determine the effects of macrophage depletion on the M1/M2 profile of the remodeling site.

5.1.2 Test Article Preparation

5.1.2.1 Preparation of ^{14}C-SIS

SIS was manufactured from the small intestine of 26 week old pigs that received weekly injections of 10 μCi of ^{14}C-labeled proline from 3 to 26 weeks of age [63, 64]. The injected proline (or as modified *in vivo* to form hydroxyproline) is integrally incorporated into collagen. Proline and hydroxyproline account for approximately 10% of the amino acids in collagen, and collagen accounts for 90% of the dry weight of SIS. This protocol of ^{14}C-labeled proline administration results in a two to four-log increase in ^{14}C content within porcine ECM and thus serves as a tool for quantification of labeled ECM at the site of interest (Figure 23) [63, 64].

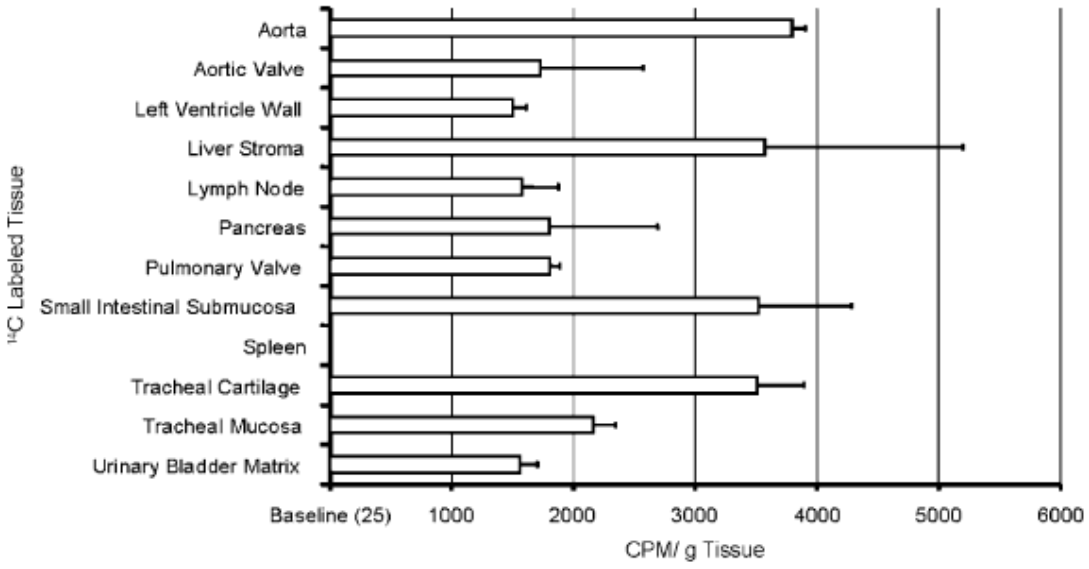

Figure 23: Counts of ^{14}C per minute per gram of labeled porcine tissues using liquid scintillation counting. The more metabolic tissues (aorta, liver, small intestine) tended to have higher levels of ^{14}C at approximately 3500 CPM/g. Reprinted from [64], with permission from Elsevier.

The isolation of SIS from the small intestine has been previously described (4.2.1.1) [155], but is summarized briefly herein. Immediately following euthanasia, the small intestine was harvested and the mesenteric tissues were removed. After rinsing, the tunica serosa, tunica muscularis externa, and the luminal portion of the tunica mucosa including most of the lamina propria were mechanically removed. The remaining layers represented ^{14}C-SIS, and consisted of the tunica submucosa and the basilar portion of the tunica mucosa including the muscularis mucosa and the stratum compactum of the lamina propria. The ^{14}C-SIS material was disinfected and decellularized with 0.1% peracetic acid and rinsed in hypotonic saline. The amount of ^{14}C incorporated in SIS was 3500 counts per minute (CPM) per gram, compared to a background level of 25 CPM [64].

The ^{14}C-SIS scaffolds were constructed by stacking 10 layers of the ECM and subjecting them to a vacuum of 710 to 740 mm Hg for 10 to 12 hours to remove the water and form a

tightly coupled multilaminate device. Ethylene oxide was used for terminal sterilization (500 mg/liter/hr for 16 hours).

5.1.2.2 Preparation of Carbodiimide Crosslinked ^{14}C-SIS

The chemical crosslinking agent used was carbodiimide (CDI), which has been used widely used to crosslink commercially available ECM scaffolds [13, 133, 134]. The SIS scaffolds designated as ^{14}C-X-SIS were prepared by immersing the multilaminate ^{14}C-SIS scaffolds in a solution of 10 mM CDI (Sigma, St. Louis, MO) in 90% acetone/10% deionized water (v/v) for 24 hours. To determine crosslinking efficacy, 8 samples each of ^{14}C-SIS and ^{14}C-X-SIS were digested in triplicate in 27.3 Units/mL bacterial collagenase Type I (Sigma) for 72 hours, and the amino acids released in the supernatant were quantified by the ninhydrin assay according to the manufacturer's protocol. The ^{14}C-X-SIS scaffolds were terminally sterilized by exposure to ethylene oxide at a dose of 500 mg per liter hour for a 16 hour cycle.

5.1.3 Animal Care Compliance

All procedures were performed in accordance with the National Institute of Health (NIH) guidelines for care and use of laboratory animals, and with approval of the Institutional Animal Care and Use Committee (IACUC) and Radiation Safety Office (RSO) at the University of Pittsburgh.

5.1.4 Experimental Animals and Husbandry

Forty-eight adult male Sprague-Dawley rats weighing approximately 300 grams were purchased from Charles River Laboratory (Wilmington, MA). Each animal was housed individually in sterile microisolator cages. The rats were fed a diet of gamma-irradiated Purina rodent chow (LabDiet ProLab Isopro RMH 3000, PMI Nutrition International, St. Louis, MO) and sterile autoclaved water, and were housed individually in an environment maintained at 68° to 76°C for twenty four hours a day and with a light:dark cycle of 12:12 hours.

5.1.5 Surgical Procedure

An established rat model of abdominal wall repair was used to evaluate the host morphologic response to each implanted biomaterial [36]. This model includes muscle tissue, the presence of a variable and multidirectional load, and a clinically obvious failure outcome (i.e., hernia).

Each animal was anesthetized with Isoflurane (2% in oxygen) in an inhalation chamber. The surgical site was clipped, shaved and prepared for sterile surgery with a betadine scrub. Sterile technique was used at all times. A ventral midline abdominal incision was made and the skin and subcutaneous tissue were separated from the underlying muscle tissues on one side of the midline for a distance of approximately 4.0 cm. The incision in the ventral midline of the abdominal skin was retracted to expose the ventral lateral wall adjacent to the linea alba, including the musculotendinous junction of the abdominal wall musculature.

A 1.5 cm x 1.5 cm partial thickness segment consisting of the oblique layers of the abdominal wall was excised leaving the underlying transversalus fascia and peritoneum intact (Figure 24). Uniformity of the defect size and shape was assured by using a fixed size and shape

device on each animal. The defect was then replaced with a size-matched graft of the ^{14}C-SIS device, the ^{14}C-X-SIS device, or the autologous abdominal wall tissue. One 4-0 Prolene suture was placed at each of the four corners of the test article to secure attachment to the adjacent abdominal wall and to demarcate the implant. Securing the test articles in this manner provided a mechanism by which the test article was subjected to the mechanical forces delivered by the adjacent native abdominal wall musculature, while avoiding the predominance of a host tissue reaction to the suture material rather than the test article. A subcuticular placement of 4-0 Vicryl was used to close the skin incision. Each animal was recovered from anesthesia on a heating pad and returned to its housing unit.

Ketoprofen (5 mg per kg of body weight) was administered by subcutaneous injection the day of surgery and for two additional days. Baytril (20 mg) was given orally the day of surgery and for two additional days. The dietary habits, general health status, and the surgical site were monitored daily. Any animal showing signs of infection or uncontrollable pain was immediately euthanized and removed from the study.

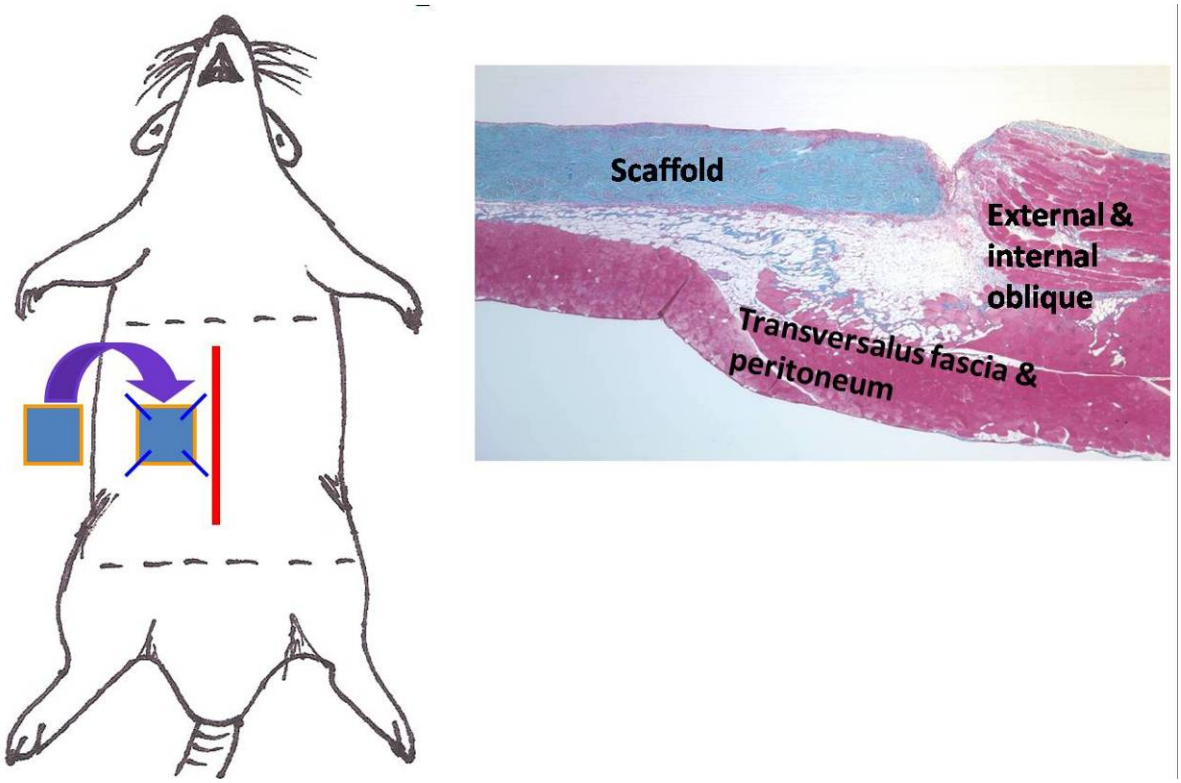

Figure 24: Schematic and histological depiction of the partial thickness abdominal wall defect model (Masson's trichrome, 40X).

5.1.6 *In Vivo* Macrophage Depletion

Clodronate (dichloromethylene bisphosphate, Cl_2MBP, Sigma Aldrich, St. Louis, MO) was encapsulated in multilamellar liposomes, as described [167, 170]. Clodronate was prepared at a concentration of 2.5 grams per 10 mL of PBS solution [170]. In the present study, clodronate liposomes were injected IV in the lateral tail vein to deplete monocytes from the peripheral blood. PBS-encapsulated liposomes labeled with the fluorochrome DiI [71] (Molecular Probes, Eugene, OR) or saline served as the control injections. The volume of each injection was 0.1 ml liposome solution or saline solution per 10 grams of body weight. Injections were given 2 days

and 2 hours prior to surgery. Subsequent injections were then given twice weekly until the predetermined time of sacrifice.

5.1.7 Euthanasia and Specimen Harvest

At the predetermined time of sacrifice, the animals were anesthetized with 5% isoflurane and euthanized by an intracardiac bolus injection of potassium chloride (KCl) to induce cardiac arrest. The surgical site was explanted with an equal amount of adjacent native abdominal wall tissue. The specimens were quartered and prepared by: 1) fixing in 10% neutral buffered formalin for histologic and immunohistochemical analysis; 2) frozen for immunofluorescent imaging studies (i.e., animals treated with DiI-labeled PBS liposomes); 3) frozen for ^{14}C quantification (i.e., animals that received the ^{14}C-SIS and ^{14}C-X-SIS scaffolds); or 4) stored in RNAlater for RNA isolation. Liver and spleen specimens were also harvested and prepared for histology and immunoanalysis to monitor the efficacy of the macrophage depletion protocol.

5.1.8 Quantification of Degradation

The ^{14}C radioactivity of the specimens from animals that received the ^{14}C-SIS and ^{14}C-X-SIS scaffolds was determined by liquid scintillation counting (LSC) using a LSI1800 B-counter (Beckman Coulter, Somerset, NJ). Approximately 80 mg of each specimen was incubated in Solvable (PerkinElmer, Waltham, MA) for 2-4 hours at 50-60 ºC until solubilized. Ten milliliters of scintillation fluid (Ultima Gold, PerkinElmer) was added to each sample, and quantification of ^{14}C was recorded as counts per minute (CPM). Background ^{14}C activity was subtracted from the recorded activity and the CPM were determined for each scaffold.

5.1.9 Histology and Immunohistochemistry

The specimens that were fixed in neutral buffered formalin were embedded in paraffin and serial sections of the embedded tissue specimens were cut at 6 μm intervals for hematoxylin and eosin (H&E) staining and immunohistochemical analysis. The sections were prepared for immunohistochemical staining by deparaffinization with xylene, and rehydration through a graded ethanol series. A heat-mediated antigen retrieval technique that included a 20 minute boil in 0.01M citrate buffer (Spectrum, New Brunswick, NJ), pH 6.0 was used. After cooling, two separate five-minute washes in TBS/Tween20, pH 7.4, followed by one wash in PBS were performed.

5.1.9.1 Antibodies

The primary antibodies used for immunohistochemical staining were mouse anti-rat CD68 (Serotec, Raleigh, NC) at 1:50 dilution in PBS, mouse anti-rat CD163 (Serotec) at 1:50 dilution, and rabbit anti-CCR7 (Cell Applications, Inc., San Diego, CA) at 1:100 dilution. CCR7 is a surface marker indicative of an M1 phenotype, and CD163 is a surface marker representative of an M2 phenotype [60, 108, 151]. The secondary antibody used was biotinylated anti-mouse IgG (H+L) (Vector, Burlingham, CA) at 1:200 dilution for CD68 and CD163, and biotinylated anti-rabbit IgG (H+L) (Vector) for CCR7. Formalin fixed rat spleen served as the positive control tissue for all immunohistochemical procedures.

5.1.9.2 Immunohistochemistry Procedure

To prevent non-specific antibody binding, the slides were incubated for thirty minutes with 2% normal horse serum (Vector) at room temperature. The slides were incubated with 3% hydrogen

peroxide (Spectrum) in methanol for thirty minutes at room temperature to inhibit endogenous peroxidase activity. The slides were incubated with the secondary antibody for thirty minutes at room temperature, followed by horseradish peroxidase solution (Vector) for thirty minutes at 37ºC. Diaminobenzidine (DAB) (Vector) was applied to detect positive staining cells and the slides were counterstained with hematoxylin.

5.1.9.3 Quantitative Analysis of Macrophages

Quantitative analysis of CD68+ cells was conducted independently by two investigators who were blinded to the identity of the tissue specimen. Cells immunopositive for CD68 were counted for each tissue specimen in ten microscope fields at 400X magnification at the host-implant interface.

5.1.9.4 Analysis of M1/M2 Ratio

Quantitative analysis was conducted independently by two investigators who were blinded to the identity of the tissue specimen and to the antigen being positively identified in each specimen. Immunopositive cells were counted for each specimen in six matched microscope fields at 400X magnification. The percentage of cells expressing an M1 phenotype was calculated by dividing the number of CCR7+ cells by the number of CD68+ cells in each field. The percentage of cells expressing an M2 phenotype was determined by dividing the number of CD163+ cells by the number of CD68+ cells in each field. The mean value for the percentage of cells showing an M1 and M2 phenotype was then calculated by obtaining the average of the six fields for each specimen at each timepoint. A comparison of M1 to M2 was then calculated for each specimen at each timepoint for each field. Values were plotted such that positive values were representative of the predominance of M1 cells among those cells that stained immunopositive

for either M1 or M2 markers. Conversely, a negative value was representative of a predominance of M2 cells. Not all macrophages showed differentiation markers to an M1 or M2 state which accounted for the total number of M1 plus M2 macrophages not necessarily equaling the number of CD68+ cells [171].

5.1.9.5 Immunofluorescence

The frozen tissue sections from animals that received DiI-labeled PBS liposomes were analyzed by fluorescent microscopy to determine the colocalization of DiI-labeled cells with CD68 labeled cells, presumably macrophages that had phagocytosed liposomes. The primary antibody was mouse anti-rat CD68 (Clone ED1, Serotec) at 1:100 dilution in PBS. The secondary antibody used was Alexafluor 488-labeled goat anti-mouse IgG (H+L) (Invitrogen, Carlsbad, CA) at 1:250 dilution. Frozen sections were fixed in ice cold acetone for 5 minutes. After air drying the tissue sections, two separate 5 minute washes in PBS, followed by three washes in PBS-0.1% Tween 20 (Sigma) were conducted. The slides were incubated for 30 minutes with 2% normal goat serum (Vector), and incubated with the primary antibody for 60 minutes at room temperature. The slides were incubated with the secondary antibody for 30 minutes at room temperature, and dehydrated through a graded series of ethanol. The slides were coverslipped with an aqueous medium containing DAPI (Vector).

5.1.10 Gene Expression Analysis

5.1.10.1 RNA Isolation

The section of the explanted tissues stored in RNAlater (Qiagen, Valencia, CA) was stored at 4ºC until RNA isolation was performed. Total RNA was isolated from the specimens using TRI-

Reagent (Molecular Research Center Inc., Cincinnati, OH) according to the manufacturer's instructions. The isolated RNA was then purified using an RNeasy Mini Kit (Qiagen). cDNA was synthesized from 1 μg of total RNA in a total volume of 20 μL using a Superscript RT III kit (Invitrogen) according to the manufacturer's instructions.

5.1.10.2 Quantitative Real Time RT-PCR.

Quantitative real time RT-PCR was performed using primers specific for genes known to be indicators of either a type I response (*iNOS* and *IFN-γ*) or a type II response (*ARG-1* and *IL-10*) (Table 5). Primers were custom designed using Beacon Designer 7.2 primer design software (PREMIER Biosoft International, Palo Alto, CA). The housekeeping gene β glucurodinase (*GUSB*) was used to normalize reactions, and was purchased as part of a housekeeping gene primer kit (Rat Housekeeping Gene Primer Set, Real Time Primers, LLC, Elkins Park, PA). One μL of cDNA was mixed with the appropriate primers and 2X SYBR Green Master Mix (BioRad, Hercules, CA) in a total volume of 25 μL per reaction in triplicate. All reactions were monitored using an iQ5 Real-Time Detection System (BioRad).

Table 5: Sequences of Rat-Specific Primer Sets Used in Real Time Analysis

Gene	Primer
iNOS	Forward: 5'-GAGACGCACAGGCAGAGG-3'
	Reverse: 5'-CAGGCACACGCAATGATGG-3'
IFNγ	Forward: 5'-ATCACTAACTTCTTCAGCAACAG-3'
	Reverse: 3'-CAGAATCAGCACCGACTCC-3'
Arginase	Forward: 5'- CATATCTGCCAAGGACATCG-3'
	Reverse: 5'-GGTCTCTTCCATCACTTTGC-3'
IL-10	Forward: 5'-CACTGCTATGTTGCCTGCTC-3'
	Reverse: 5'-GGTCTGGCTGACTGGGAAC-3'
GUSB	Forward: 5-GTGGGGATAATGACTTGCAG-3'
	Reverse: 5'-GGAACCCCTGGTAGAACAGT-3'

5.1.10.3 Gene Expression

Relative expression of the genes was calculated using the comparative Ct method [157, 158]. The value of the threshold cycle (Ct) for the gene of interest was subtracted from the value of the threshold cycle for the housekeeping gene for each sample (ΔCt, sample) and for native muscle (ΔCt, reference). Relative expression to the native muscle was then calculated as $2^{(\Delta\Delta Ct)}$, where

$$\Delta\Delta Ct = (\Delta Ct, \text{sample}) - (\Delta Ct, \text{reference}).$$

Genes for the enzymes *iNOS* and *ARG-1* use the same substrate, L-arginine (see section 2.1.2). *iNOS* is required for nitric oxide production and is the predominate arginine usage pathway in M1 macrophages. *ARG-1* is inhibitory for *iNOS* and is the predominate arginine usage pathway in M2 macrophages. The relative expression of *iNOS* and *ARG-1* in each specimen was compared using the following equation:

$$\frac{2^{(\Delta\Delta Ct,\ iNOS)}}{2^{(\Delta\Delta Ct,\ ARG\text{-}1)}}$$

Values were then plotted on a log scale such that values greater than 1.0 represented a predominance of the *iNOS* gene expression and values less than 1.0 represented a predominance of *ARG-1* gene expression.

5.1.11 Statistical Analysis

The mean values for CD68+ cells for each group and subgroup was determined and the group values compared using one way analysis of variance (ANOVA). A mixed model ANOVA was used to analyze the immunohistochemical data. The factors were scaffold (autologous, ^{14}C-SIS, and ^{14}C-X-SIS), treatment (clodronate liposomes, PBS liposomes, and saline), time (one week

and two weeks), and area (6 different areas on each slide). A one way ANOVA was used to analyze the gene expression data. Results were considered significant for $p < 0.05$.

5.2 RESULTS

5.2.1 Crosslinking Efficacy

The ninhydrin assay showed a greater concentration of amino acids in the supernatants from ^{14}C-SIS compared to ^{14}C-X-SIS (523.5 ± 40.0 vs. 263.3 ± 74.9 μM/mg, $P < 0.01$), confirming that the ^{14}C-X-SIS scaffolds were more resistant to collagenase degradation than the ^{14}C-SIS scaffolds.

5.2.2 Surgical and Post-operative Outcomes

No complications occurred during the surgical procedures for any animal in this study. All animals assigned to the one week timepoint survived without complication. Five out of the 24 animals with a survival timepoint of two weeks died prior to the scheduled date of sacrifice. All of the animals that died prematurely had been administered clodronate liposomes. None of the animals that were administered the PBS liposomes or saline vector died prematurely. This outcome was not specific to any particular scaffold group. Histopathologic analysis of lung, spleen, and liver tissue specimens from the animals that died prematurely showed widely disseminated foci of parenchymal necrosis associated with colonies of bacteria and an absence of inflammatory cells. These findings were consistent with overwhelming sepsis secondary to

clodronate-induced phagocyte depletion. The animals that died prematurely were replaced in the study, and these replacement animals survived until the study endpoint.

5.2.3 Quantification of Degradation

At 1 and 2 weeks, LSC counts per minute (CPM) of the ^{14}C-SIS graft sites from clodronate-treated animals showed higher levels of ^{14}C when compared to graft sites from PBS liposome or saline treated animals ($p < 0.05$). At 2 weeks, CPM of PBS liposome-treated animals were less than the CPM from saline-treated animals ($p < 0.05$). CPM of ^{14}C-X-SIS graft sites from clodronate liposome, PBS liposome, and saline treated animals were all similar at 1 and 2 weeks, and these ^{14}C levels were also similar to the non-implanted scaffold (Table 6).

Table 6: Quantification of ^{14}C-SIS and ^{14}C-X-SIS Scaffold Degradation, as Measured by LSC

		Clodronate liposomes	*PBS liposomes*	*Saline*
^{14}C-SIS	1 week	$1273.0 \pm 63.3^{a-c}$	683.8 ± 134.9^{c}	468.0 ± 227.6^{c}
	2 weeks	$1214.2 \pm 407.3^{a,b}$	$41.5 \pm 47.3^{b-d}$	$786.0 \pm 215.78^{a,c}$
^{14}C-X-SIS	1 week	1115.1 ± 453.5	1281.0 ± 204.6	1026.6 ± 536.3
	2 weeks	1115.8 ± 355.8	1130.4 ± 156.7	1349.0 ± 204.6
Nonimplanted ^{14}C-SIS	1081.5 ± 112.8 ($n = 7$)			

The CPM were measured for each scaffold. Values reported as mean ± standard deviation.
[a]Significant compared with PBS liposome control ($p < 0.05$).
[b]Significant compared with saline control ($p < 0.05$).
[c]Significant compared with nonimplanted ^{14}C-SIS scaffold ($p < 0.05$).
[d]Significant compared with 1-week data from the same treatment group ($p < 0.05$).

5.2.4 Histopathologic Findings

5.2.4.1 Autologous Tissue Graft

The autologous tissue graft from animals treated with clodronate-containing liposomes showed mild coagulative necrosis of the muscle fibers that were part of the autologous graft tissue, and these fibers were surrounded by partially organized collagenous tissue. Widely scattered mononuclear cells and neutrophils were noted at both the 1 and 2 week time points. The animals that received the saline or PBS liposomes treatment showed that the autologous graft tissue was infiltrated with a dense population of mononuclear cells and a smaller number of neutrophils at 1 and 2 weeks post-implantation. The muscle fiber bundles of the autologous graft tissue showed degeneration and necrosis at 1 week post surgery. By 2 weeks, the tissue specimens of saline-treated animals showed that the tissue graft was almost totally replaced with collagenous tissue with remnants of degenerative or necrotic muscle remaining. The tissues from PBS-liposome treated animals showed remnants of skeletal muscle fibers dispersed within new host ECM and scattered accumulations of adipose tissue (Figure 25).

5.2.4.2 ^{14}C-SIS Scaffold

The animals treated with the clodronate liposomes showed a markedly reduced mononuclear cell response for both timepoints. At 1 week, the scaffold did not adhere to the surrounding host tissue at the time of sacrifice, and at 2 weeks the scaffold was characterized histologically by mononuclear cells in a loosely organized matrix. Neutrophils were present adjacent to the scaffold surface and were occasionally present between the individual layers of the delaminating scaffold.

The surgical sites in which the ^{14}C-SIS device was placed in rats that received either PBS-liposomes or saline showed an abundant mononuclear cell response at 1 and 2 weeks. Animals treated with PBS-liposomes showed that most of the ^{14}C-SIS scaffold was degraded by 2 weeks, a finding that correlated with the ^{14}C levels found at the graft site. The scaffold was replaced with new host ECM and was densely populated by mononuclear cells and blood vessels.

For the saline treated animals, by 2 weeks the scaffold was delaminated and the individual layers at the edges of the scaffold were surrounded by new host ECM. Mononuclear cells were abundant and these cells surrounded and infiltrated the entire scaffold implantation area (Figure 25).

5.2.4.3 ^{14}C-X-SIS Scaffold

Specimens from animals treated with the clodronate liposomes showed almost complete absence of mononuclear cells and a dense population of neutrophils at the implantation site. The scaffold showed no evidence of delamination and appeared to be completely intact. At 1 and 2 weeks the scaffold was loosely attached to the surrounding host tissue.

The animals that received saline or PBS liposomes showed a dense population of mononuclear cells and neutrophils around the ^{14}C-X-SIS material at 1 and 2 weeks. These cells were present at the periphery of the scaffold material with little to no infiltration of cells into the scaffold itself. The layers of the scaffold remained essentially intact, and showed no morphologic evidence of degradation, a finding that was consistent with the LSC data (Figure 25).

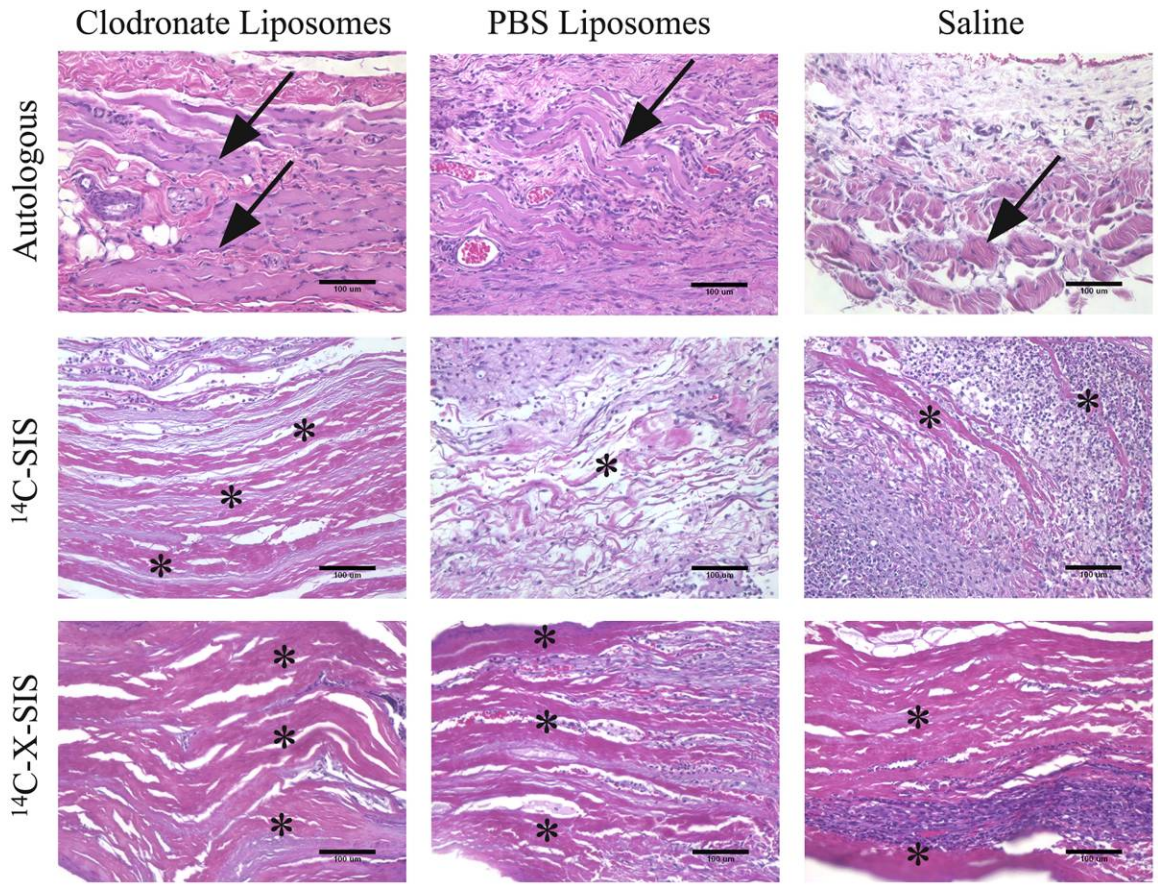

Figure 25: Representative images of autologous, ^{14}C-SIS, and ^{14}C-X-SIS scaffold implantation sites 2 weeks post-implantation. Graft sites from animals treated with clodronate liposomes showed almost no scaffold degradation. Graft sites from animals treated with PBS liposomes or saline show dense accumulations of mononuclear cells for all graft types and scaffold degradation for the autologous and ^{14}C-SIS scaffolds. Arrows point to muscle cells that remained in the autologous tissue graft site. For the ^{14}C-SIS and ^{14}C-X-SIS scaffolds, asterisks (*) indicate the layers of the original multilaminate scaffolds that remain in the implantation site. Sections were stained with H&E. Scale bar = 100 µm.

5.2.5 Immunohistochemical Findings

Macrophage depletion was noted in the spleen of all animals treated with clodronate liposomes at 1 and 2 weeks post-implantation, confirming the effectiveness of the depletion procedure. For each graft type at 1 and 2 weeks, the surgical sites from the clodronate liposome-treated animals showed fewer macrophages (CD68+ cells) than graft sites from PBS liposome and saline-treated animals at both time points for all graft materials ($p < 0.001$) (Figure 26). Animals treated with the DiI-labeled PBS liposomes showed DiI-labeled cells that co-localized with CD68+ cells at the site of tissue remodeling, verifying that liposomes were engulfed by circulating mononuclear cells and that these circulating cells subsequently populated the remodeling site in animals not treated with clodronate (Figure 27).

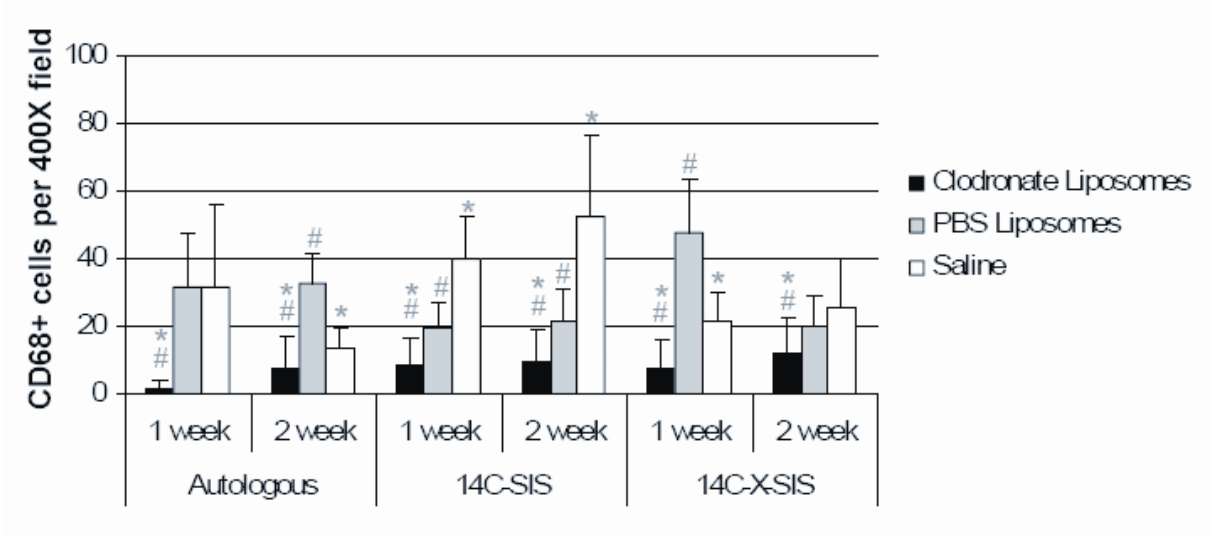

Figure 26: CD68+ cells per 400X field, 10 fields per graft site, examined at the host-implant interface. Data represent mean ± SD. *Significant compared with PBS liposome control ($p < 0.001$); #significant compared with saline control ($p < 0.001$).

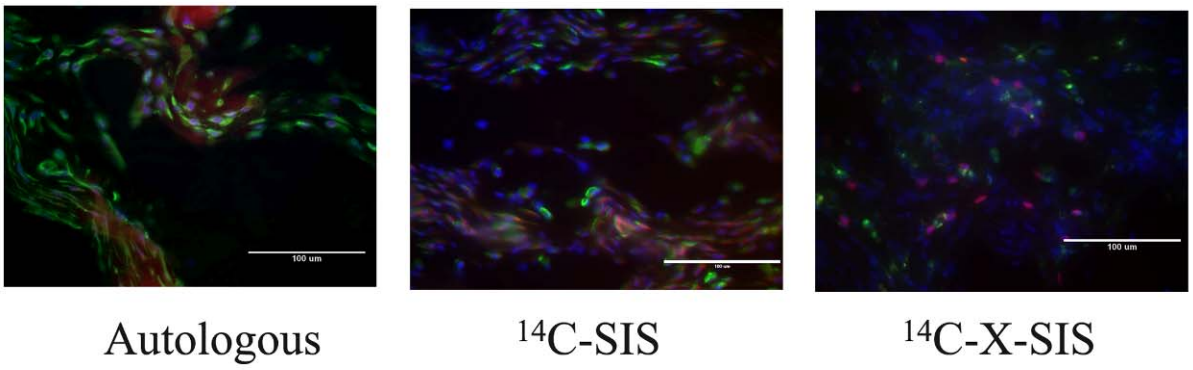

Figure 27: Immunofluorescent images of scaffold sites 2 weeks post-implantation from animals that received IV injections of DiI-labeled PBS liposomes. The distribution of DiI-labeled cells (red), CD68+ macrophages (Alexafluor 488, green), and cell nuclei (DAPI, blue) are shown in merged images. Scale bar = 100 µm.

Representative images of the immunohistochemical staining for each M1/M2 marker at one week post-implantation are shown in Figure 28. A quantitative analysis of the phenotype of the macrophages present in the remodeling autologous tissue graft showed that the polarized macrophages (those expressing either CCR7 or CD163) were a mixed population of CCR7+/CD163+ macrophages for all treatment groups at one week and for the saline treatment group at two weeks, and a predominately M2 (CD163+) response for the clodronate and PBS liposome treatment groups at two weeks (Figure 29A). For the ^{14}C-SIS scaffold, the macrophages expressed mostly an M2 phenotype (CD163+) for all treatment groups at one and two weeks post-implantation (Figure 29B). The macrophages present in the remodeling site of ^{14}C-X-SIS scaffold showed that at one and two weeks a mixed population of macrophages (CCR7+/CD163+) was present for all treatment groups (Figure 29C).

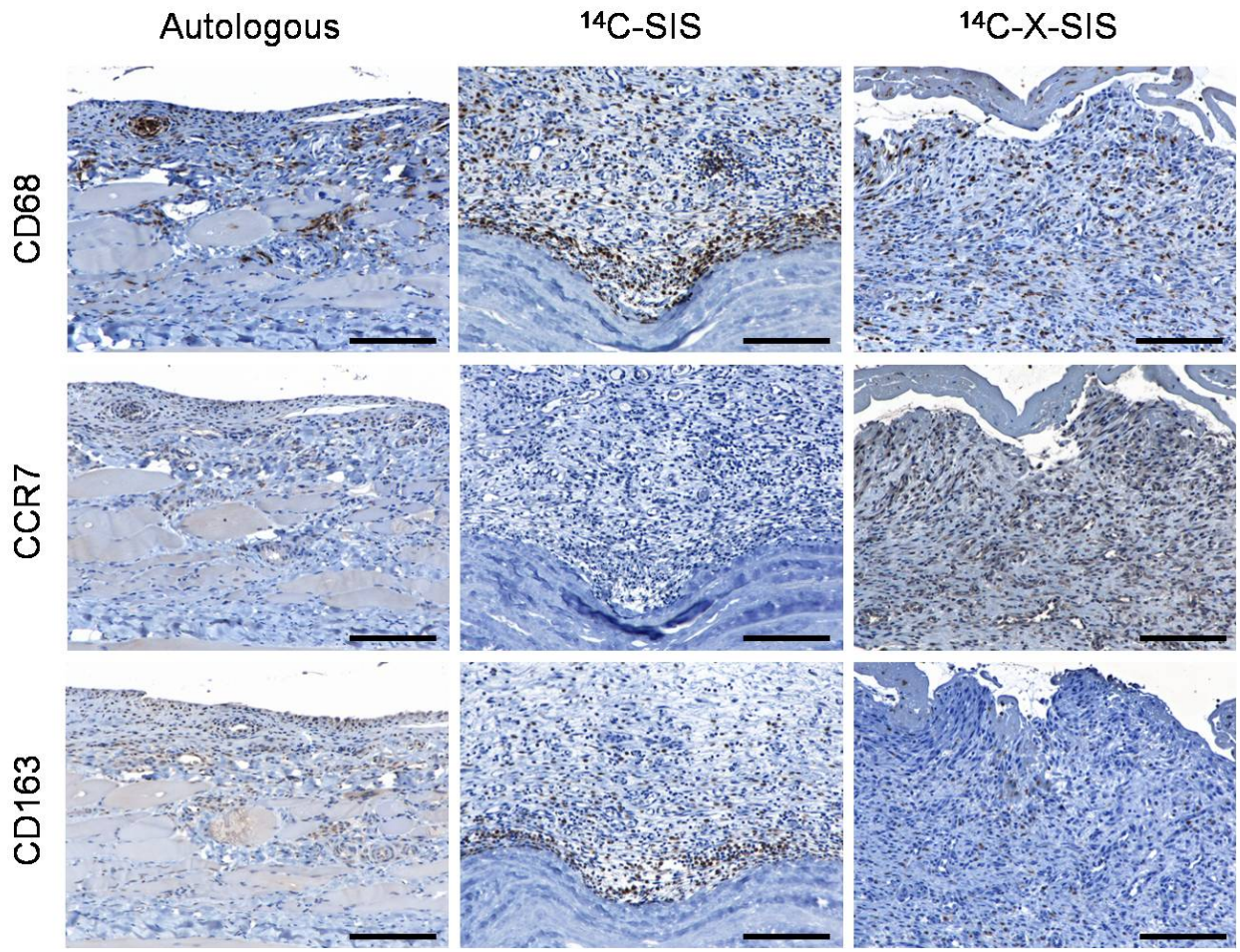

Figure 28: Representative photomicrographs of immunohistochemical staining for CD68 (pan macrophages), CCR7 (M1 macrophages), and CD163 (M2 macrophages) in autologous, ^{14C}-SIS, and ^{14}C-X-SIS scaffold repair sites from saline-treated animals at one week post-surgery. Scale bar = 300 µm.

A similar pattern of macrophage polarization was observed between the autologous tissue graft at one week and the ^{14}C-X-SIS scaffold at one and two weeks for most treatment groups (Figure 29D). In contrast, the autologous tissue graft at two weeks and the ^{14}C-SIS scaffold at one and two weeks were skewed toward the M2 (CD163+) phenotype for all treatment groups. The pattern of macrophage polarization for the treatment groups with respect to time showed that the remodeling sites of clodronate liposome-treated animals expressed a greater M2 (CD163+)

phenotype at two weeks compared to one week for the autologous and the ^{14}C-SIS scaffolds, but not for the ^{14}C-X-SIS scaffold. The remodeling sites from animals treated with PBS liposomes showed a switch from an M1 dominate to an M2 dominate phenotype at two weeks compared to one week for the autologous tissue graft, but no difference was observed between one and two weeks for the ^{14}C-SIS or the ^{14}C-X-SIS scaffolds. The graft sites from animals treated with saline showed a similar pattern of macrophage polarization between one and two weeks for all scaffold groups.

A preliminary analysis failed to indicate any effects due to area or the interactions of area with other factors, so the data were aggregated over area. For the M1 ratio, no statistically significant effects were found for the percentage of M1 polarized cells. For the percentage of M2 polarized cells, the statistically significant effects were the scaffold by time interaction ($P<0.03$). Further analysis of the M2 data indicated that there were no statistically significant differences in scaffolds at one week; but differences were evident at two weeks with ^{14}C-SIS greater than ^{14}C-X-SIS. For the autologous scaffold, percentage of M2 cells at one week was less than percentage of M2 cells at two weeks. No other comparisons were statistically significant.

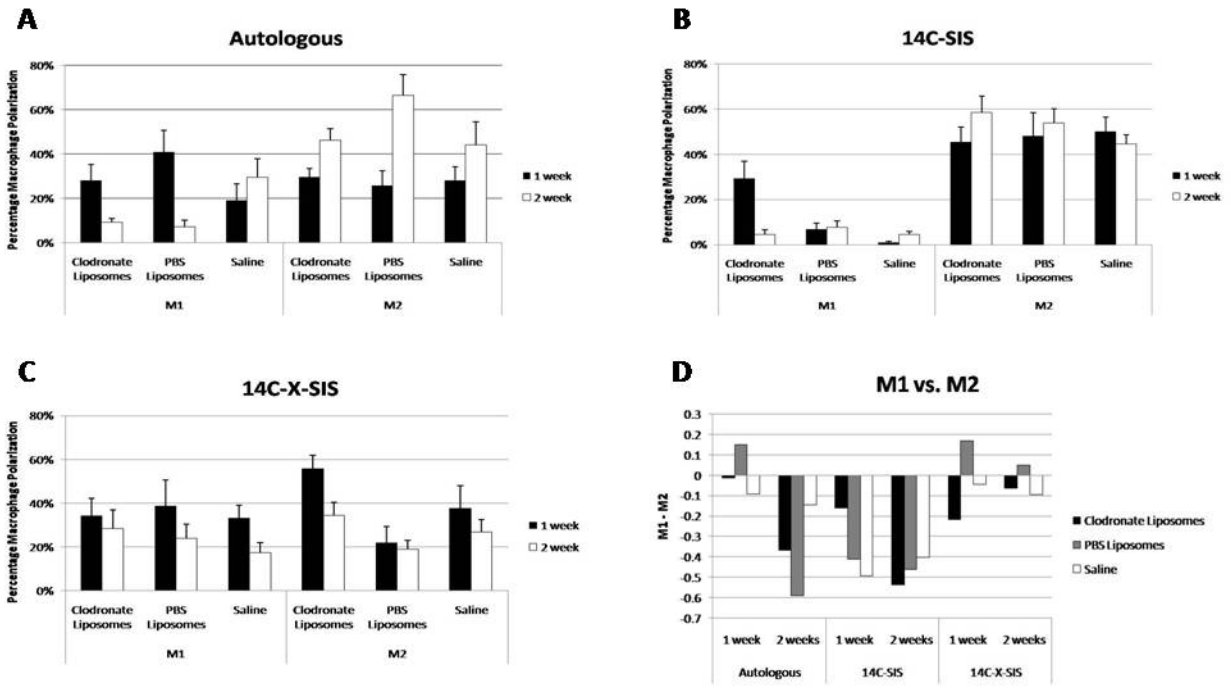

Figure 29: Percentage macrophage polarization at one and two weeks post-implantation of (A) autologous, (B) ^{14}C-SIS, and (C) ^{14}C-X-SIS scaffolds. All values are presented as mean ± SEM. For the percent of M1 cells, no statistically significant effects were found. For the percent of M2 cells, the statistically significant effects were the scaffold by time interaction ($P < 0.03$). (D) The percentage of M1 (CCR7+) macrophages was subtracted from the percentage of M2 (CD163+) macrophages for each scaffold and treatment group at one and two weeks post-implantation. Positive values are indicative of an M1 type response while negative values are indicative of an M2 type response.

5.2.6 Gene Expression Findings

The expression of *iNOS* (M1) and *ARG-1* (M2) was detected for all specimens. For the autologous tissue graft, the animals treated with saline showed low expression of *iNOS* and *ARG-1* at one week, but by two weeks the *iNOS* and *ARG-1* expression increased 1500 and 40-fold, respectively (Figure 30A). For the animals treated with the clodronate or the PBS-filled

liposomes, the gene expression for *iNOS* showed similar levels, but the *ARG-1* expression decreased, from one to two weeks. For the ^{14}C-SIS scaffolds, the animals treated with PBS-filled liposomes showed little *iNOS* expression at one week but an increase by two weeks, but no appreciable change in *ARG-1* expression was noted from one to two weeks. The *ARG-1* expression was higher for the saline-treated animals compared to the clodronate liposome-treated animals at one week (Figure 30B). The ^{14}C-X-SIS scaffold showed no significance within the scaffold group for the *iNOS* and *ARG-1* gene expressions for any treatment group (Figure 30C).

The gene expression markers *iNOS* and *ARG-1* use opposing pathways for arginine metabolism and therefore the expression can be directly compared (see 2.1.2) (Figure 30D). There was a mixed expression of *iNOS* and *ARG-1* for all implant groups treated with the clodronate liposomes with the exception of the M1 dominate profile of the autologous test article at two weeks post-implantation. The PBS liposome treated groups showed a mixed expression for most of the implant groups with the exception of the ^{14}C-SIS scaffold group at one week and ^{14}C-X-SIS scaffold group at two weeks. The saline treated groups showed a ratio of *iNOS:ARG-1* that was skewed toward M2 polarization for the autologous tissue graft at one week and the ^{14}C-SIS scaffold at one and two weeks.

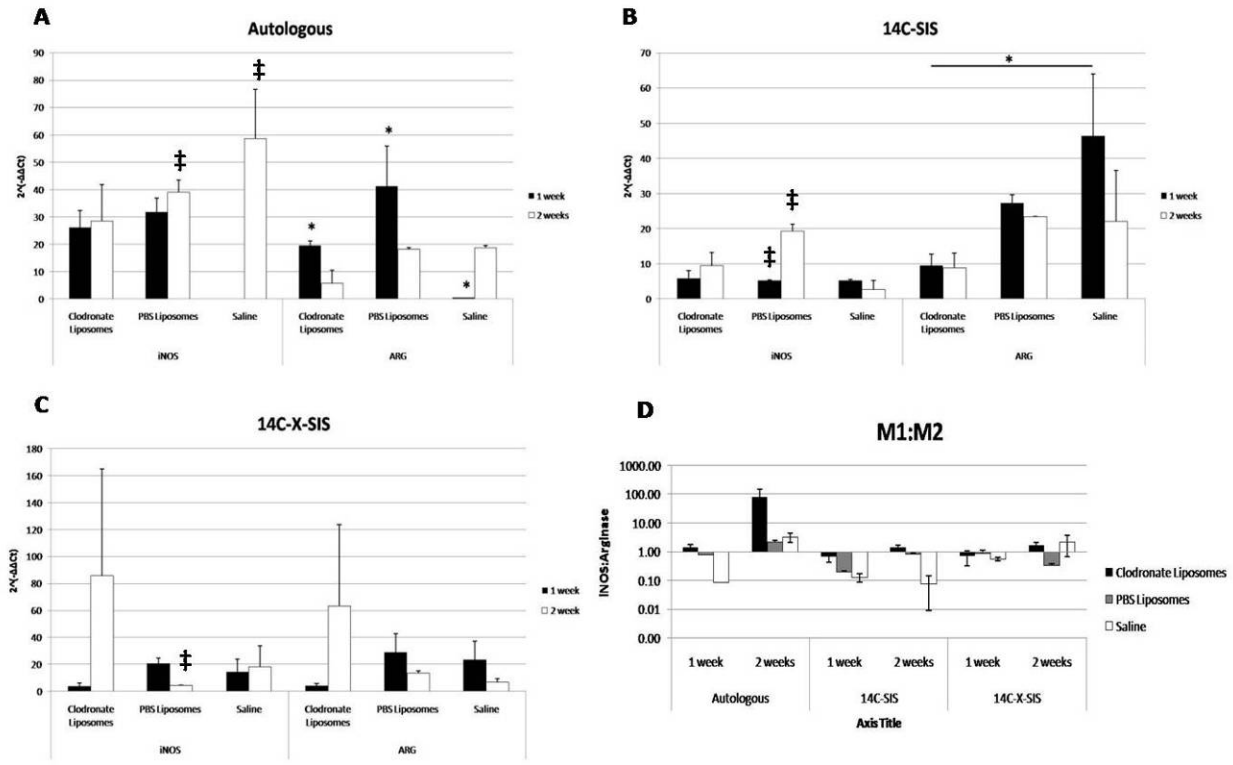

Figure 30: Gene expression of *iNOS* and *ARG-1* relative to the housekeeping gene and the native abdominal muscle at one and two weeks post implantation of (A) autologous, (B) ^{14}C-SIS, and (C) ^{14}C-X-SIS scaffolds. All values are presented as mean ± SEM. * indicates statistical significance ($p < 0.05$) within a scaffold group. ‡ indicates statistical significance ($p < 0.05$) between scaffold groups within a treatment group. (D) Ratio of *iNOS:ARG-1* expression for each scaffold and treatment group at one and two weeks post-implantation. Values above 1.0 are indicative of a predominance of *iNOS* expression while values less than 1.0 are indicative of a predominance of *ARG-1* expression.

The gene expression markers *IFN-γ* and *IL-10* are known inducers of M1 and M2 macrophages, respectively (see section 2.1.2) [108]. For the saline treatment group, the expression of *IFN-γ* increased in the autologous tissue graft but no change was detected for the ^{14}C-SIS and ^{14}C-X-SIS scaffolds from one to two weeks (Figure 31A). At two weeks, the sites repaired with the autologous tissue graft showed greater *IL-10* expression for the saline treated animals compared to ^{14}C-SIS (Figure 31B). For the ^{14}C-SIS scaffold group, the gene expression

of *IL-10* decreased from one to two weeks for the saline treatment group, but no change was detected for the clodronate or PBS-liposome treated animals (Figure 31B). Additionally, the saline treatment group showed higher expression of *IL-10* compared to the clodronate liposome-treated group at one week (Figure 31B).

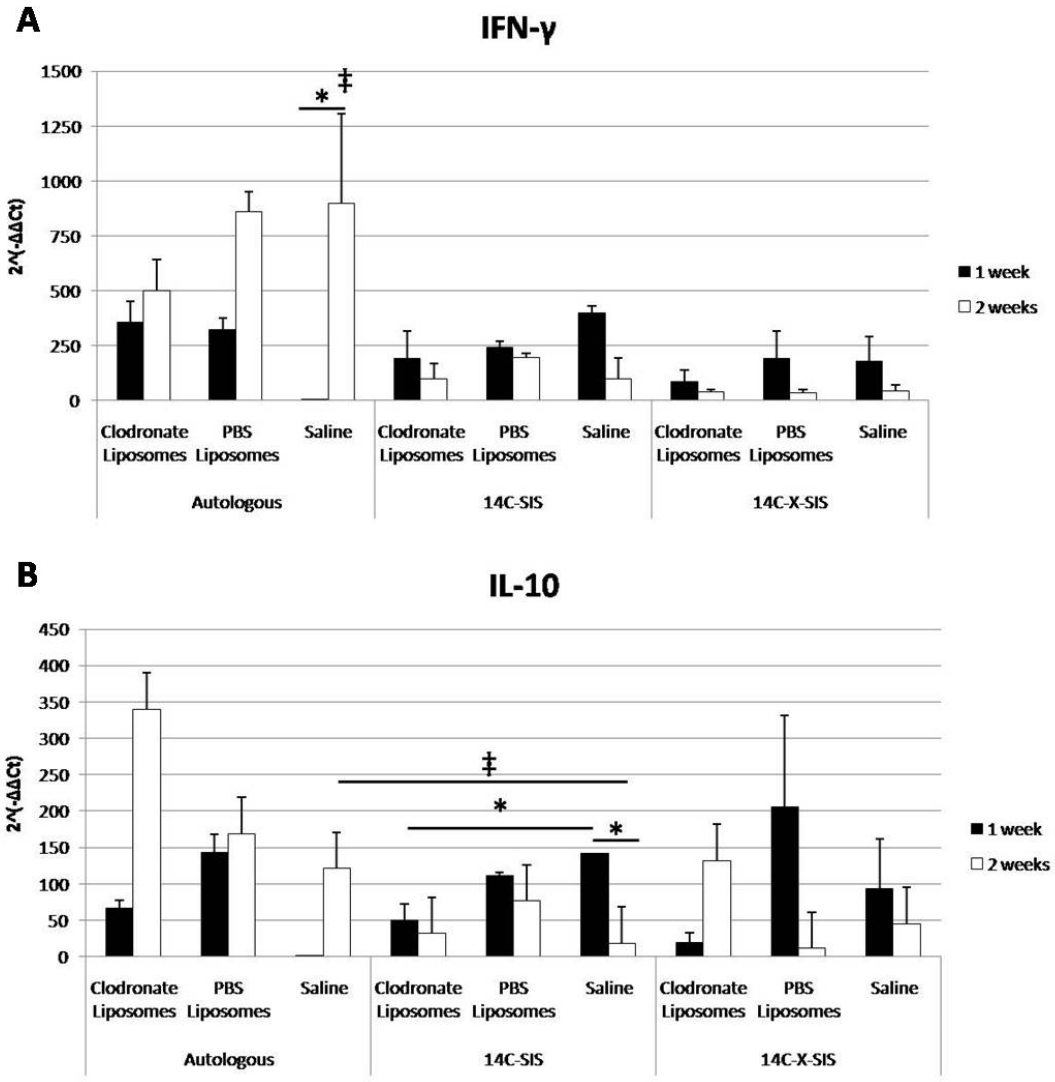

Figure 31: Gene expression of (A) *IFN-γ* and (B) *IL-10* relative to the housekeeping gene and the native abdominal muscle one and two weeks post-implantation for autologous, ^{14}C-SIS, and ^{14}C-X-SIS scaffolds. All values are presented as mean ± SEM. * indicates statistical significance ($p < 0.05$) within a scaffold group. ‡ indicates statistical significance ($p < 0.05$) between scaffold groups within a treatment group.

5.3 DISCUSSION

The results of Specific Aim 2 confirm the intuitive concept that blood-derived mononuclear macrophages play a necessary and important role in the early *in vivo* degradation process of ECM scaffolds and autologous tissue grafts, and that chemical crosslinking of the ECM by compounds such as CDI effectively inhibit the degradation process. These findings are important in the context of regenerative medicine and biologic scaffolds because the proposed mechanisms of the constructive remodeling response typically require scaffold degradation to realize the optimal beneficial effects. Degradation-dependent events such as the release of constituent growth factors, the production and release of matricryptic peptides and the recruitment of host progenitor cells and stem cells contribute to the well-documented dynamic histomorphologic changes that characterize the host response to such scaffold materials during this early post operative period [5, 7, 8, 36, 48, 49, 53, 55, 95, 96]. It is logical to speculate, based upon the results of the present study, that blood derived mononuclear macrophages are at least important, if not essential, mediators of these degradation dependent events. Such an interpretation is in stark contrast to the conclusion that a macrophage-rich tissue response following ECM scaffold implantation necessarily represents an adverse host-patient reaction [172]. Since the presence of mononuclear macrophages is usually associated with inflammatory processes and the expected downstream consequences of tissue necrosis and scar tissue formation, the findings of the present study emphasize the wisdom of evaluating the role of macrophages with an open mind at least with regard to ECM scaffold remodeling.

The host tissue response to a biomaterial is, by definition, the central factor in the eventual remodeling outcome. In a study described in Section 2.2, chemical crosslinking of the SIS scaffold with CDI resulted in a switch from an M2 dominant profile to an M1 dominant

profile and a change in the long-term (16 week) remodeling outcome from constructive remodeling to chronic inflammation [60]. The M2 response was associated with an organized, site-appropriate tissue remodeling outcome and an absence of persistent inflammation. CDI-crosslinking was associated with an M1 response, long-term inflammation and the formation of multinucleate giant cells and scar tissue. The present study showed that CDI effectively inhibited ECM scaffold degradation regardless of the presence of macrophages; in addition, the macrophages present at the remodeling site of ^{14}C-X-SIS for all treatment groups showed a mixed M1/M2 phenotype, and less M2 (CD163+) macrophages compared to ^{14}C-SIS. This finding was not unexpected and was consistent with recent studies that show a markedly altered, proinflammatory host tissue response to ECM scaffolds that were chemically crosslinked [42].

In the present study, it was observed for the noncrosslinked scaffolds that by two weeks the treatment with clodronate liposomes resulted in a host tissue response, but not macrophage cell surface marker expression, that skewed more toward a type I profile compared to the saline treatment groups. Stated differently, the systemic depletion of monocytes resulted in an altered remodeling response for the autologous and ^{14}C-SIS scaffolds, which may be at least partly due to the remaining cell populations that participated in the host response. Although not directly investigated in this study, the depletion of macrophages would logically alter the temporal and spatial response of other cell types towards an implanted scaffold material, including ECM scaffolds. The acute host tissue response to an implanted foreign material, as all of these materials represent, is typically characterized by the presence of neutrophils. After three to five days, the neutrophil population decreases and the mononuclear macrophage population becomes the predominant cell response. This balance of neutrophil departure and mononuclear macrophage arrival was disrupted by the depletion of macrophages in the present study.

Neutrophils were still the prominent feature of the host cell response two weeks following implantation in the animals that were implanted with the ^{14}C-SIS scaffold and that received clodronate-containing liposomes. The present results show that neutrophils do indeed participate in ECM scaffold remodeling, but do not appear to be major determinants of early scaffold degradation based upon the quantitative ^{14}C measurements. It is logical that at least a certain degree of neutrophil-mediated scaffold degradation should occur but the ability of neutrophils alone to provide for all of the biologic effects that are associated with ECM scaffold degradation remains to be investigated.

In summary, macrophages play an important and central role in biologic scaffold degradation and remodeling. Their presence within and surrounding scaffold materials following *in vivo* implantation should not only be expected but perhaps recognized as a favorable course of events and may predict a constructive remodeling outcome.

5.4 CONCLUSIONS

Macrophages that populated the ^{14}C-SIS scaffold following *in vivo* placement were at least partially responsible for scaffold degradation. The CDI crosslinking agent used to manufacture ^{14}C-X-SIS inhibited macrophage mediated scaffold degradation. The depletion of macrophages at the sites of ^{14}C-SIS, ^{14}C-X-SIS, and autologous graft implantation resulted in an attenuation of the host inflammatory response and slowed the rate of scaffold degradation. These findings show that macrophages are important contributors to biologic scaffold degradation and early remodeling events.

5.5 LIMITATIONS AND FUTURE WORK

There were several limitations in the present study. First, the determination of M1 versus M2 phenotype was based upon a limited number of cell surface markers. Although many markers exist to differentiate between M1 and M2 macrophages for murine and human tissues, most of these same markers are not available for the analysis of rat tissue, especially formalin-fixed tissue. Second, the results were confined to the early stages of scaffold remodeling; that is, two weeks. The marked depletion of mononuclear macrophages for longer periods of time places the host at great risk for sepsis and makes such studies difficult. Furthermore, repeated administration of clodronate was performed in order to insure that the results were not confounded by newly formed circulating macrophages later in the study period. It should also be noted that the present study is limited to a single type of biologic scaffold material, specifically the SIS, but the learned principles may be applicable to all biologic scaffold materials.

The present study characterized the macrophage population that participated in the remodeling response as a function of the M1 and M2 polarization schemes in a rat model. The sum of M1 and M2 immunopositive cells did not always equal the number of CD68 immunopositive cells [171]. It should be noted that CD68+ macrophages that were not yet determined to be an M1 or M2 phenotype would remain negative for the respective markers. It is presently not known what percentage (i.e., threshold) of M1 or M2 cells is required to influence the formation of scar tissue formation or constructive remodeling response, respectively. It is hypothesized in the present study that the comparison of M1 vs. M2 may be more important than the absolute number of cells or the absolute gene expression. There is a clear correlation of the M1/M2 relationship to remodeling outcomes in previous studies that investigated the remodeling response beyond two weeks [60, 151].

6.0 SPECIFIC AIM 3: TO DETERMINE THE HISTOMORPHOLOGY AND FUNCTIONALITY OF SIS-ECM SCAFFOLDS WHEN USED FOR THE RECONSTRUCTION OF MUSCULOSKELETAL TISSUE IN A RAT MODEL

6.1 INTRODUCTION

The biomechanical and biochemical properties of ECM scaffolds have been extensively characterized [52, 125, 173-175], but inevitably change after implantation due to the concurrent processes of scaffold degradation and host neomatrix deposition and remodeling [97, 99, 176]. Arguably, one of the most important merits for clinical success following use of an ECM scaffold is the functionality of the newly formed tissue. The functionality of remodeled ECM has been investigated in tendinous tissues, with the results showing a initial decrease in strength after implantation as the scaffold begins to degrade, followed by an increase in strength as new host tissue deposition occurs [35, 38, 44, 98]. However, no studies have quantitatively assessed the active contractility of remodeled ECM scaffold after repair of skeletal muscle tissue.

A previous study using the same animal model and the same test articles investigated the morphologic changes and the macrophage phenotype up to 16 weeks post-surgery, but did not explore the functional properties of the reconstructing tissue (see Sections 2.2.1.2 and 2.2.2.1) [42, 60]. The histomorphologic and active contraction experiments of Specific Aim 3 will complement and further characterize the remodeling response and associate the macrophage

phenotype during the early stages of the remodeling process to the downstream structural and functional properties of the reconstructed tissue. The objectives of Specific Aim 3 were: (1) to determine the functionality of skeletal muscle tissue that was repaired with one of three clinically relevant and commercially available test articles in a rat model; and (2) to characterize the histomorphologic appearance of the remodeled tissue. The hypothesis is that functional tissue will result from an outcome of constructive remodeling after repair with noncrosslinked scaffolds versus chronic inflammation after repair with crosslinked scaffolds.

6.2 MATERIALS AND METHODS

6.2.1 Overview of Experimental Design

Twenty-four male Sprague Dawley adult rats were randomly assigned to three groups of eight. Each rat was subjected to surgical partial thickness excision of a 1.5 cm x 1.5 cm section of the ventral lateral abdominal wall musculature. The defect was repaired with one of three test articles: Restore™, a 10 layer configuration of an ECM biologic scaffold composed of porcine SIS (n = 8); CuffPatch™, a 10 layer configuration of porcine SIS that was manufactured with CDI as a crosslinking agent (n = 8); or autologous body wall tissue (n = 8). The animals were survived to 26 weeks. The contractile properties of the remodeled tissue and of the contralateral native tissue were determined in-situ immediately prior to euthanasia. Following euthanasia and explantation of the remodeled scaffold materials, histologic and immunolabeling methods were used to determine the morphologic characteristics including the distribution of slow (Type I) and fast (Type II) skeletal muscle fibers, blood vessels, and nerves.

6.2.2 Test Articles

The ECM-derived scaffold materials that were used to repair the surgically created defect were derived from porcine SIS and differed mainly by the processing methods, i.e., the use of a chemical crosslinking agent. The Restore™ (DePuy Orthopaedics Inc., IN) device represents an ECM scaffold material that is not subjected to chemical crosslinking. The CuffPatch™ (Arthrotek, Inc., Warsaw, IN) device represents an SIS material that is crosslinked with CDI. Both of the ECM materials were purchased from the manufacturer. The handling of the materials after removal from the sterile package and prior to surgical implantation was performed according to the manufacturer's instructions as provided in the package insert. Skeletal muscle tissue excised from the abdominal wall of each animal in the last group served as the autograft.

6.2.3 Animal Care Compliance

All procedures were performed in accordance with the National Institute of Health (NIH) guidelines for care and use of laboratory animals, and with approval of the Institutional Animal Care and Use Committee (IACUC) at the University of Pittsburgh.

6.2.4 Animal Source and Husbandry

Twenty-four adult male Sprague-Dawley rats weighing approximately 300 grams were purchased from Charles River Laboratory (Wilmington, MA). Each animal was housed individually in shoebox cages. The rats were fed a diet of Purina Isopro rodent chow ad libitum (LabDiet ProLab Isopro RMH 3000, PMI Nutrition International, St. Louis, MO). The housing

environment was maintained at 68° to 76°C for twenty four hours a day and with a light:dark cycle of 12:12 hours.

6.2.5 Surgical Procedure

The partial thickness abdominal wall defect model for evaluation of muscular tissue remodeling was detailed in Section 5.1.5 but is briefly reviewed herein. Each animal was anesthetized by inhalation with 2% isoflurane in oxygen. The surgical site was prepared for sterile surgery. A ventral midline abdominal skin incision was created, and the skin and subcutaneous tissue were separated from the underlying muscle tissues on one side of the midline. A 1.5 cm x 1.5 cm section of the external and internal oblique layers of the ventral lateral abdominal wall was excised; the underlying transversalus fascia and peritoneum remained intact. The defect was repaired with a size-matched piece of the chosen test article. A single 4-0 Prolene suture was placed at each of the four corners of the test article to secure the device to the surrounding musculature, allow for mechanical loading of the test article, and to demarcate the implant for identification at the time of in-situ functional testing and necropsy. A subcuticular placement of 4-0 Vicryl suture was used to close the skin incision. Each animal was recovered from anesthesia and was returned to the housing unit.

Each rat received 0.02 mg Buprenex (buprenorphine hydrochloride) by subcutaneous injection the day of surgery and for two additional days. Baytril (20 mg) was given orally the day of surgery and for two additional days. The dietary habits, general health status, and the surgical site were monitored daily and recorded.

6.2.6 Measurement of Contractile Force In-Situ

6.2.6.1 Muscle Flap Preparation

Twenty-six weeks after the initial surgical procedure, each animal was prepared for functional testing of the implant site. Each rat was anesthetized with 2% isoflurane in oxygen by inhalation. A midline skin incision was created, and the skin and overlaying fascia was dissected from the underlying body wall at the site of test article implantation. The remodeled site was identified by the preplaced Prolene sutures at the four corners of the test article. A flap of tissue was created which contained the remodeled site plus 2 mm of adjacent native musculature. The origin and rib attachment of the external oblique muscle remained intact to maintain blood flow and innervation to the remodeled test article site. The muscle fibers on the remaining sides of the implantation site, including the insertion site at the linea alba were dissected free of all adjacent tissue attachment to isolate the tissue for contractile testing. The contralateral site, which did not receive a test article and was not surgically modified, was prepared in identical fashion to serve as a control for each animal (Figure 32).

The isolated tissue flap was positioned such that the direction of the muscle contraction was aligned along an axis from the costochonral arch toward the linea alba. Platinum electrodes were placed across the flap of tissue perpendicular to the direction of muscle contraction and at both the proximal and distal ends of the scaffold placement site as identified by the Prolene sutures. The distal (previous insertion end) tissue was secured to a force transducer (Sensotec, Columbus, OH; model 31) with silk suture. An analog to digital data acquision card (National Instruments [NI], Austin, TX; PCI-6023E) received signals from the force transducer (Figure 32). A custom-designed program was created in LabVIEW software (National Instruments) to monitor and record the forces measured by the force transducer.

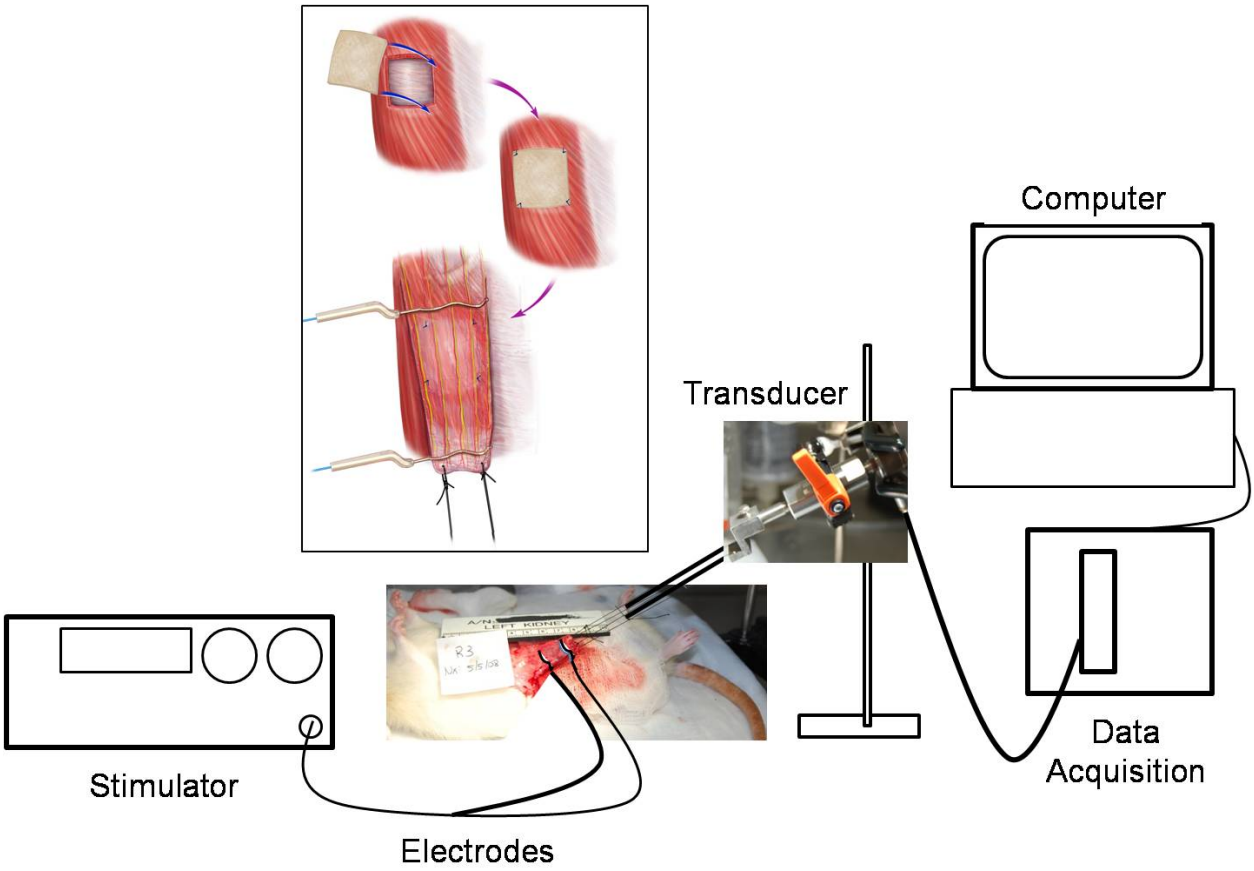

Figure 32: Representative schematic of the apparatus used to measure *in situ* tetanic force generation. Top illustration: the musculoskeletal defect was created by excising the external and internal oblique layers of the abdominal wall, leaving the transversalus fascia intact. Middle illustration: the test article was implanted in the defect site and secured with Prolene sutures at each of the four corners. Bottom illustration: twenty-six weeks post-implantation, a flap of tissue was created which contained the site of test article placement, identified by the preplaced Prolene sutures. The tissue flap maintained the muscular arteries and the thoracic spinal nerve branches that supplied the site of tissue remodeling. The muscle fibers on the remaining sides of the implantation site, including the insertion site at the linea alba, were dissected free from the surrounding adjacent tissue. The distal end of the flap was connected to the force transducer with silk suture, and positioned such that the direction of the function testing was aligned parallel to the rib origin. Platinum electrodes were placed across the flap proximal and distal to the scaffold placement site.

6.2.6.2 Contractile Force Testing

The isolated tissue flap was stimulated with a S88X Grass stimulator (Astro-Med, Inc., West Warwick, RI). Optimum length Lo was determined as the length at which the maximum twitch force was obtained using a 2 ms pulse at 50 pulses per second (pps). The maximum tetanic force (Pt-MAX) for the test site (Pt,S) and the contralateral native tissue (Pt,N) as a function of stimulation rate was determined by delivering 5, 10, 15, 20, 30, 40, 60, and 75 pps in 1-second trains with 2 minutes of rest between each test. The Pt,S was normalized to Pt,N and to the native Pt-MAX (Pt,N-MAX). The contractile force for each stimulation frequency was then calculated for each tetanic force and specific force was calculated for Pt-MAX by normalizing with the cross-sectional area of the tissue.

6.2.6.3 Fatigue Resistance Testing

The fatigue resistance of the tissue at the test site was determined by comparing the force generated at time t = 0 to t = 2 minutes. After a five minute rest period, pulses were delivered at the frequency at which the forces plateau during the tetanic force testing, in trains of 330 ms duration at a rate of 1 train per second, for a total of two minutes. The Fatigue Index was calculated as the ratio of the residual force at t = 2 to the initial force at t = 0.

6.2.7 Euthanasia and Specimen Harvest

Following completion of the functional testing, each rat was euthanized with 5% isoflurane in oxygen followed by an intracardiac injection of 5 mL of potassium chloride to induce cardiac arrest. The muscle flap was excised at the rib origin, mounted on a fixed support structure to maintain the size and shape of the tissue, and placed in 10% neutral buffered formalin (NFB).

6.2.8 Histologic and Immunohistochemical Analysis

The NBF-fixed specimens were sectioned perpendicular to the direction of contractile function testing at the implantation site in four separate locations. The tissue was embedded in paraffin, cut into 6-μm thick sections, and mounted for H&E or Masson's trichrome staining and immunohistochemical analysis. The primary antibodies used for immunohistochemical staining were: (1) monoclonal antimyosin (skeletal, slow, clone NOQ7.5.4D; Sigma-Aldrich, St. Louis, MO) at 1:4000 dilution for identification of slow (type I) skeletal muscle fibers; (2) monoclonal antimyosin (skeletal, fast, alkaline phosphatase conjugate, clone MY-32, Sigma-Aldrich) at 1:200 dilution for identification of fast (type II) skeletal muscle fibers; (3) rabbit polyclonal von Willebrand factor (Abcam, Cambridge, MA) at 1:1000 dilution for identification of endothelial cells and blood vessels; and (4) anti-neurofilament (DakoUSA, Carpinteria, CA) at 1:100 dilution for identification of neurons. The secondary antibodies used were biotinylated anti-mouse IgG (H+L, rat absorbed) (Vector, Burlingham, CA) at 1:200 dilution, and goat anti-rabbit IgG (H+L, rat absorbed) (Vector) at 1:200 dilution. NBF-fixed rat skeletal muscle tissue from the native abdominal wall was used as the positive control tissue for slow and fast antimyosin and for anti-neurofilament, and NFB-fixed rat liver was used as the positive control tissue for von Willebrand factor.

The antibodies to the fast and slow skeletal muscle fibers were visualized with two substrate staining systems on each section. Separate tissue sections were used for the von Willebrand factor and neurofilament staining.

The following protocol was used to identify fast and slow muscle fibers. Unstained sections were deparaffinized with xylene and rehydrated through a graded ethanol series. Heat-mediated antigen retrieval was performed with 0.1 mM EDTA buffer at 95-100 ºC for 25

minutes. After cooling for 15 minutes, enzyme-mediated antigen retrieval was performed with 0.1% trypsin/0.1% calcium chloride digestion at 37ºC for 10 minutes. Three washes in TBS, pH 7.6, were then performed. The slides were incubated for 10 minutes in a blocking solution containing 2% normal horse serum (Vector) and 2% normal goat serum (Vector) at room temperature to prevent non-specific antibody binding. To inhibit endogenous peroxidase activity, the slides were incubated with 3% hydrogen peroxide (Spectrum) in methanol for 10 minutes at room temperature. The slow anti-myosin antibody was applied for 30 minutes at room temperature. The slides were then incubated with the secondary antibody for 30 minutes at room temperature, followed by horseradish peroxidase solution (Vector) for 30 minutes at 37ºC. Diaminobenzidine (DAB) (Vector) was applied to detect positive staining cells. The blocking solution was then applied again for 10 minutes at room temperature, followed by the fast anti-myosin antibody for 60 minutes at room temperature. Red alkaline phosphatase substrate was applied to detect positive staining.

The following protocol was used to stain for von Willebrand factor and neurofilament. After deparaffinization and rehydration of the sections as described above, heat-mediated antigen retrieval was performed with 0.01M citrate buffer (Spectrum, New Brunswick, NJ), pH 6.0, at 95-100 ºC for 20 minutes. After cooling for 15 minutes, enzyme-mediated antigen retrieval was performed for the staining of von Willebrand factor using proteinase K in a buffer of 50mM Tris base and 1 mM EDTA, pH 8.0, at 60ºC for 10 minutes. Three washes in PBS were then performed. The slides were incubated for 30 minutes with 2% normal horse serum (Vector) at 37ºC to prevent non-specific antibody binding. To inhibit endogenous peroxidase activity, the slides were incubated with 3% hydrogen peroxide (Spectrum) in methanol for 30 minutes at room temperature. The slides were incubated with the secondary antibody for 30 minutes at

37ºC, followed by horseradish peroxidase solution (Vector) for 30 minutes at 37ºC. DAB (Vector) was applied to detect positive staining cells and the slides were counterstained with hematoxylin.

6.2.9 Statistical Analysis

A one-way analysis of variance (ANOVA) was performed, followed by the Tukey's post hoc test to determine significant differences between test articles for Pt-MAX, Specific Force, Fatigue Index, and the quantitative immunohistochemical analysis of blood vessels and muscle fibers. A *p* value of less than 0.05 was considered to be significant.

6.3 RESULTS

No complications occurred during the procedure, and all animals survived to the assigned timepoint of 26 weeks.

6.3.1 Contractile Properties of Remodeled Tissue

Tetanic contractile responses were observed in all of the contralateral native tissue specimens and all of the tissue specimens that were harvested from sites in which the Restore device was implanted (Figure 33). The tissue repaired with the Restore device generated approximately 82% of the tetanic force of native tissue (Figure 34, Figure 35). When normalized for cross-sectional area, the specific forces of the tissue repaired with Restore were similar to the native tissue

(Figure 36, Table 7). Four out of eight specimens harvested from the sites in which the CuffPatch device was placed and six out of eight specimens harvested from sites in which the autologous graft was placed generated a tetanic response (Figure 33). The CuffPatch device and the autologous tissue graft sites showed approximately 11% and 61%, respectively, of the tetanic force of native tissue (Figure 34, Figure 35).

The Fatigue Index for the native tissue was significantly lower than for the site implanted with the Restore device, despite the similar values for specific force (P = 0.93). The sites implanted with the CuffPatch device and the Restore device showed similar Fatigue Index values (P = 0.62), while the native tissue and sites implanted with the autologous tissue graft showed similar Fatigue Index values (P = 0.67) (Table 7).

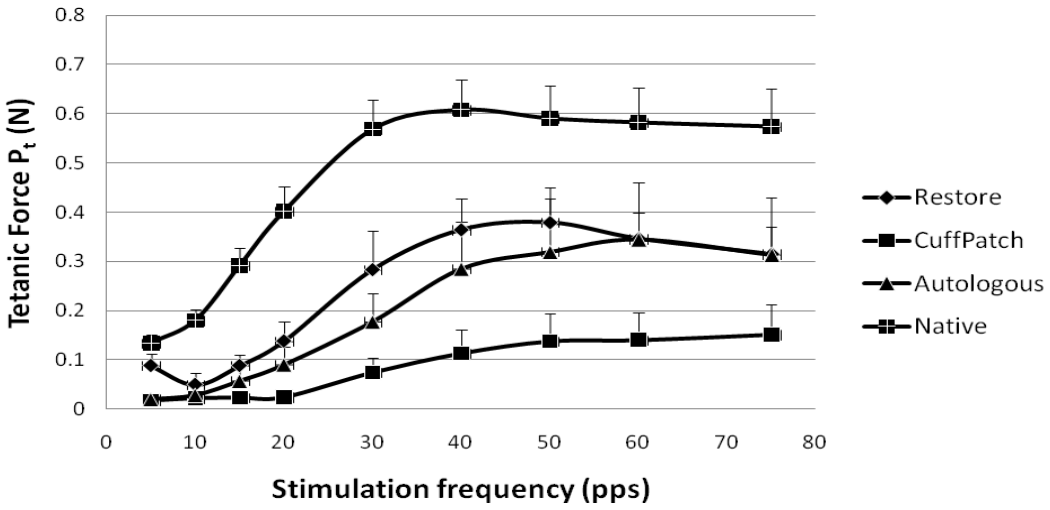

Figure 33: *In situ* muscle contraction studies were performed on muscle flaps from implants at 26 weeks post-surgery and compared to contralateral, native muscle. The tetanic forces (N) generated by remodeled and native tissue following electrical stimulation between 5 and 75 pps. Data expressed as mean ± standard error.

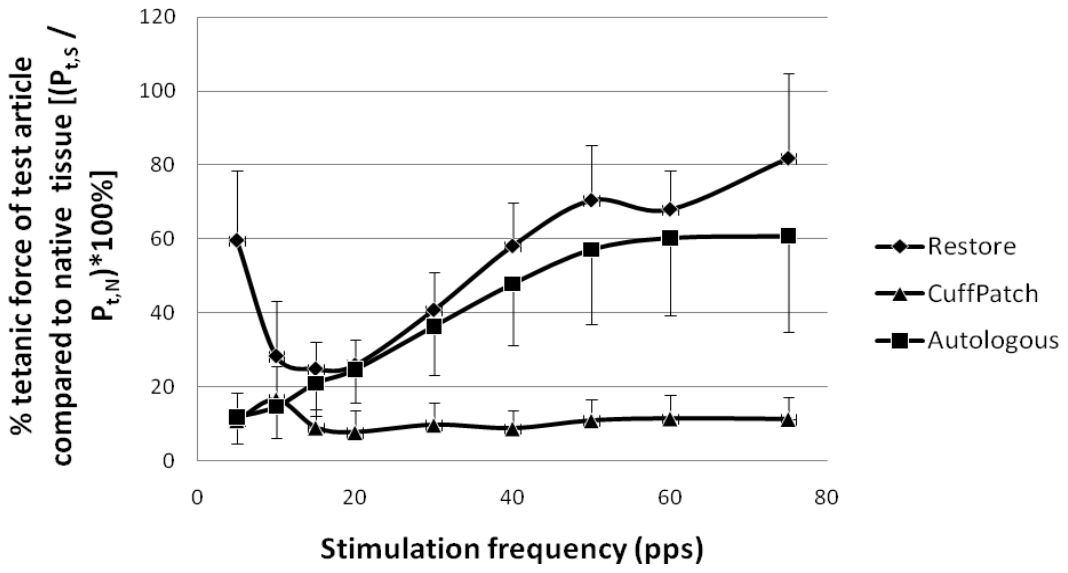

Figure 34: The percent tetanic force of the remodeled tissue compared to the contralateral native tissue with respect to the tetanic force at each stimulation frequency. Data expressed as mean ± standard error.

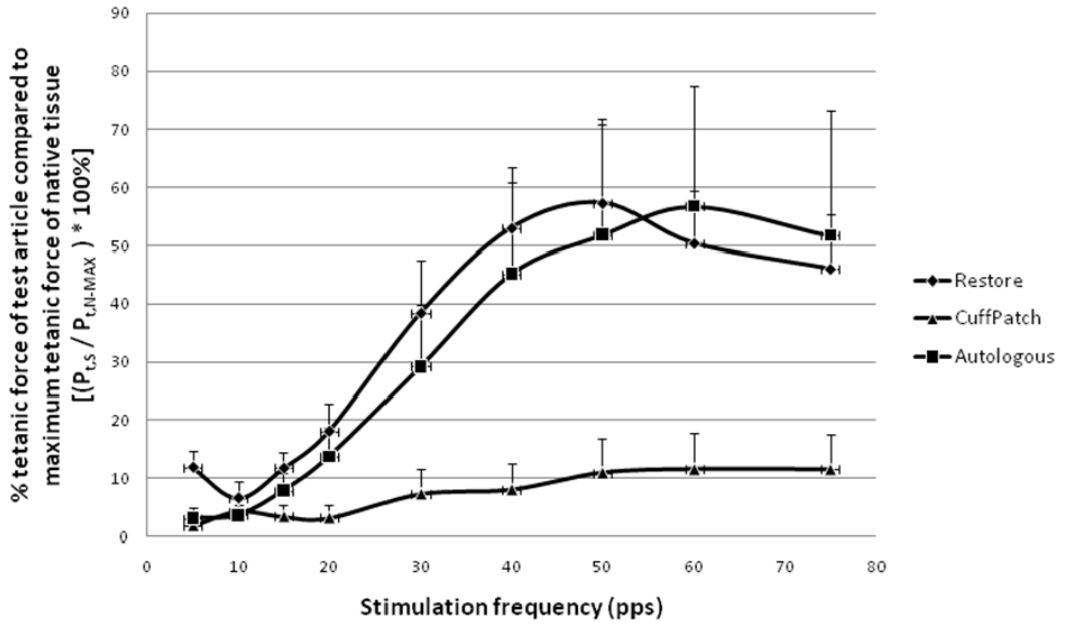

Figure 35: The percent tetanic force of the remodeled tissue compared to the contralateral native tissue with respect to the maximum tetanic force. Data expressed as mean ± standard error.

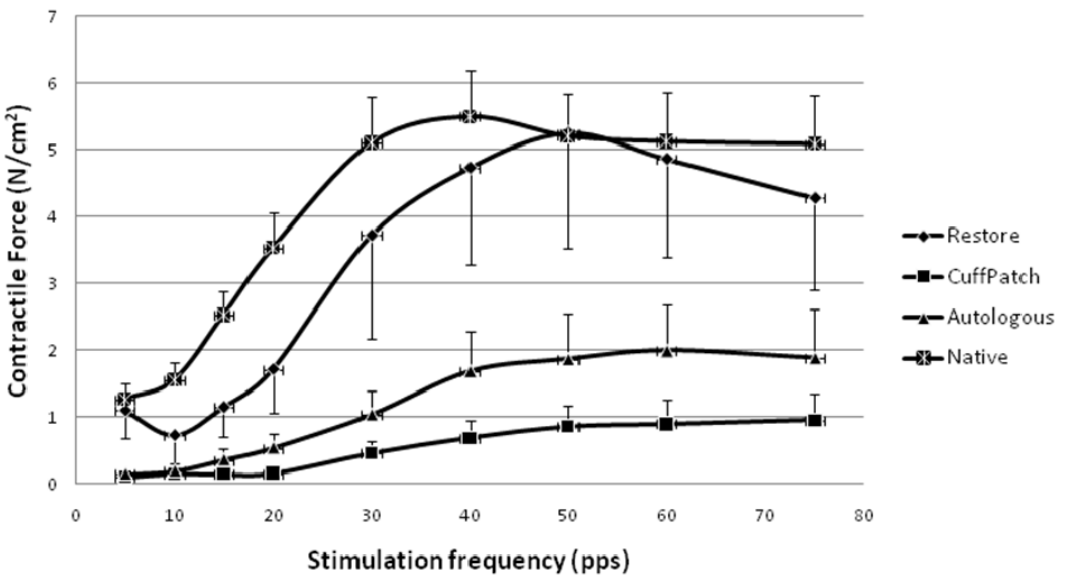

Figure 36: Contractile forces (N/cm^2) of tissue, which peaked at 40 pps for the native tissue, and 50 pps for the remodeled tissue. Data expressed as mean ± standard error.

Table 7: The contractile properties for each scaffold group and the contralateral native tissue.

Scaffold	$\frac{Lo - Ln}{Lo}$	*Maximum Tetanic Force (N)*	*Specific Force (N/cm²)*	*Fatigue Index*
Restore™	0.248 ± 0.056	0.401 ± 0.175[a]	5.723 ± 4.822[a,b]	0.407 ± 0.181[a,b]
CuffPatch™	0.218 ± 0.044	0.142 ± 0.176[a]	0.888 ± 1.081[a,c]	0.349 ± 0.228[c]
Autologous	0.227 ± 0.053	0.342 ± 0.332	2.020 ± 2.064[b,d]	0.201 ± 0.229[b]
Native	0.219 ± 0.044	0.669 ± 0.309*	5.895 ± 3.080[c,d]	0.155 ± 0.095[a,c]

Values reported as mean ± standard deviation. Superscripts a, b, or c show significance between implant pairs, and * show significance compared to all scaffolds ($p<0.05$).

6.3.2 Histomorphologic and Immunolabeling Findings

6.3.2.1 Native tissue

The native tissue harvested from the contralateral abdominal wall showed myofibers that were organized into muscle bundles, with sparse collagenous connective tissue and adipose connective tissue (Figure 37). Mature blood vessels and capillaries (Figure 41A) and nerve fibers (Figure 41E) were located adjacent to the muscle bundles. The number of blood vessels and muscle types (i.e., slow type I and fast type II) were quantified by positive immunostaining (Table 8). The native tissue showed fewer blood vessels and a high density of fast type II and slow type I fibers compared to all other test articles. The majority of the myofibers were immunopositive for fast type II myosin, and the fibers that stained positive for slow type I myosin were evenly distributed between the fast fibers (Figure 42A).

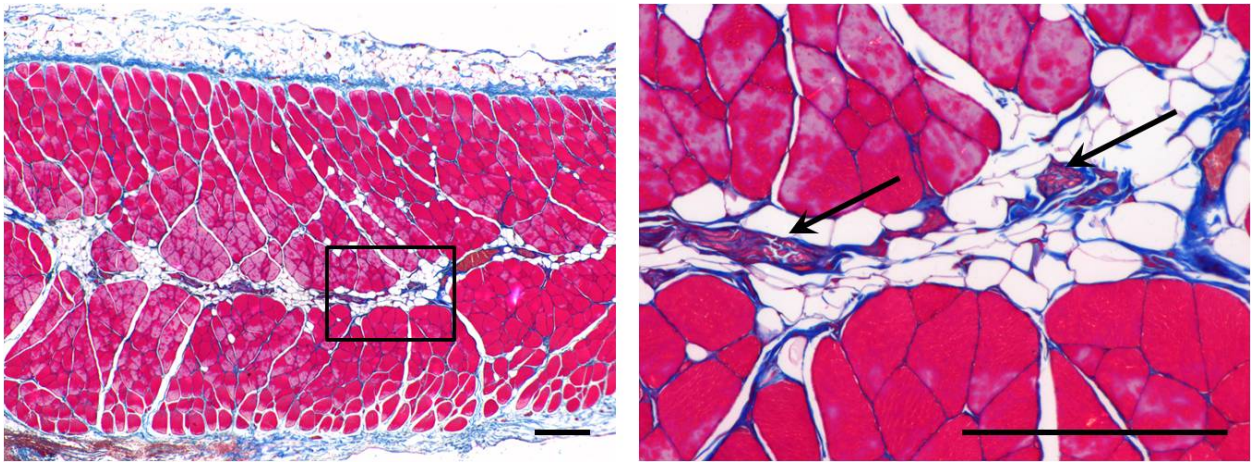

Figure 37: At 26 weeks post surgery, the native tissue was composed mainly of muscle cells organized into tight bundles and mature blood vessels and nerves (arrows) were adjacent to the muscle bundles. Tissue sections were stained with Masson's trichrome. Higher magnification image was acquired from the lower magnification image in the area outlined by the rectangle. Scale bars = 300 µm.

6.3.2.2 Restore device

The sites in which the Restore device was placed showed no histologic evidence of the originally implanted device 26 weeks after implantation and replacement with new host tissue that contained organized bundles of skeletal muscle cells, and partially organized collagenous connective tissue and adipose connective tissue surrounding the muscle bundles (Figure 38). There was no evidence of chronic inflammation. A moderate number of mature vessels and capillaries (Figure 41B, Table 8) and nerve fibers (Figure 41E) were located adjacent to the muscle bundles. Similar to the native tissue, the majority of the muscle fibers stained positive for fast type II myosin, and the muscle fibers that stained positive for slow type I myosin were dispersed equally alongside the fast fibers (Figure 42B, Table 8).

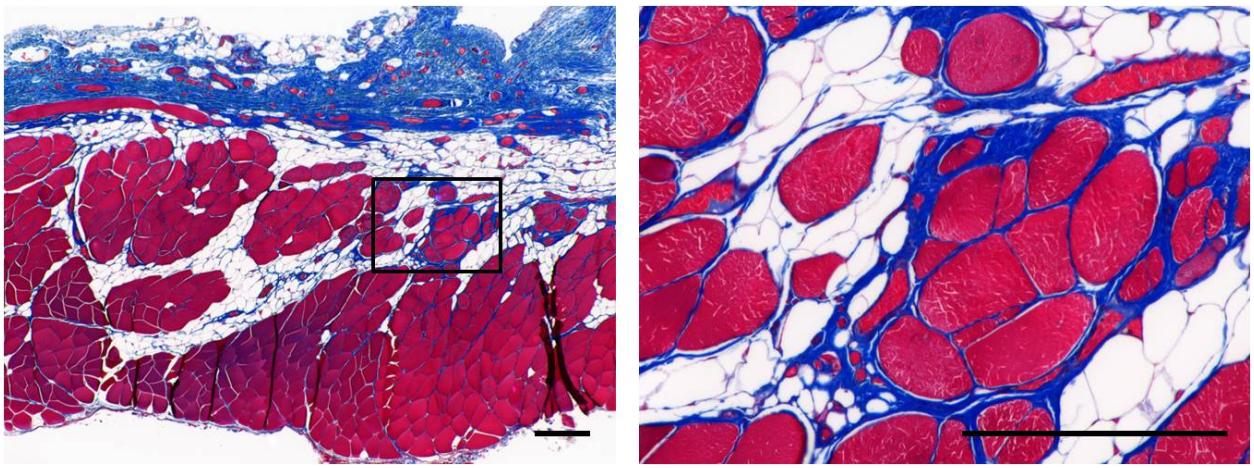

Figure 38: At 26 weeks post implantation, the Restore device completely remodeled into new host tissue which was comprised of bundles of muscle fibers surrounded by vascularized, organized collagenous connective tissue. Tissue sections were stained with Masson's trichrome. Higher magnification image was acquired from the lower magnification image in the area outlined by the rectangular. Scale bars = 300 µm.

6.3.2.3 CuffPatch device

At 26 weeks, the surgical site in which the CuffPatch device was placed showed that remnants of the original device were surrounded by mononuclear cells and multinucleate giant cells (Figure 39). The tissue surrounding the implantation site contained a robust capillary presence (Figure 41D, Table 8) and densely organized collagenous connective tissue. Neurons were identified adjacent to the blood vessels at the host-implant interface (Figure 41G). No nerve fibers were identified within the implantation site. The muscle fibers showed a low density of fast type II fibers, which were located peripheral to the site of scaffold placement (Figure 42C, Table 8).

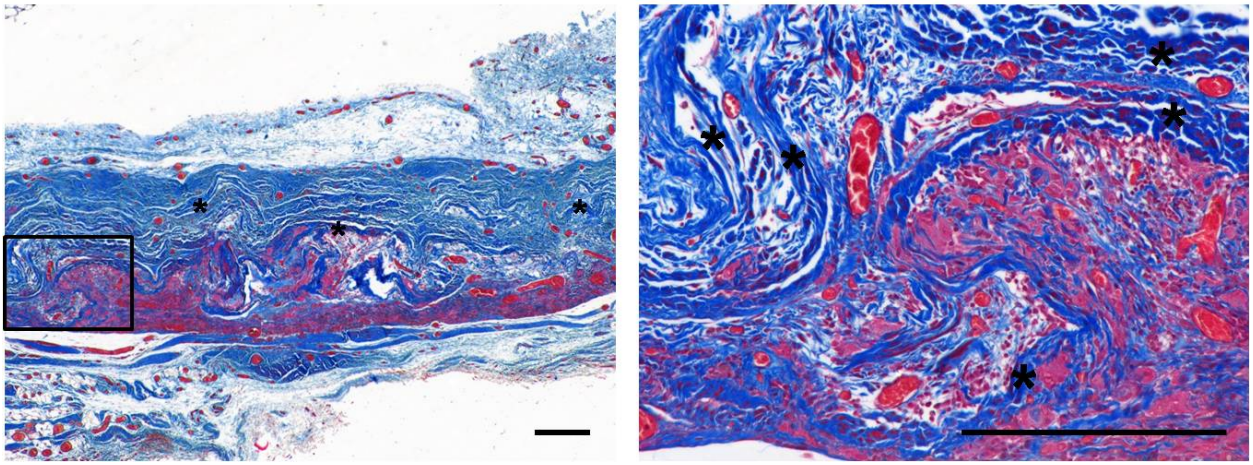

Figure 39: After 26 weeks post surgery, the tissue treated with the CuffPatch device contained identifiable remnants of the originally implanted device (*), which were surrounded by dense collagenous tissue, numerous blood vessels, and inflammatory cells including multinucleate giant cells. Tissue sections were stained with Masson's trichrome. Higher magnification image was acquired from the lower magnification image in the area outlined by the rectangle. Scale bars = 300 µm.

6.3.2.4 Autologous tissue graft

The sites in which the autologous tissue graft was placed showed replacement of the graft by islands of muscle fibers that were surrounded by a moderate amount of collagenous connective tissue and adipose tissue (Figure 40). There was no evidence of chronic inflammation. The new muscle bundles and adipose tissue contained nerve fibers and a moderate amount of mature blood vessels and capillaries (Figure 41D, Figure 41H, Table 8). There was a high density of fast type II fibers, and the slow type I muscle fibers were organized in clusters among the fast type II muscle fibers (Figure 42D, Table 8).

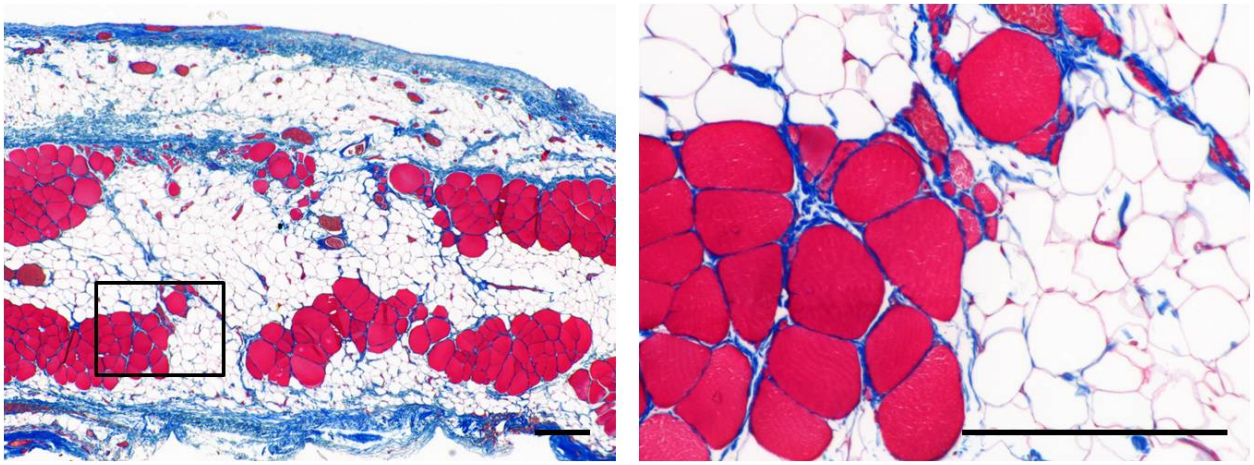

Figure 40: At 26 weeks post surgery, the tissue treated with the autologous graft showed randomly dispersed muscle bundles surrounded by fibrous connective tissue and adipose connective tissue. Tissue sections were stained with Masson's trichrome. Higher magnification image was acquired from the lower magnification image in the area outlined by the rectangle. Scale bars = 300 µm.

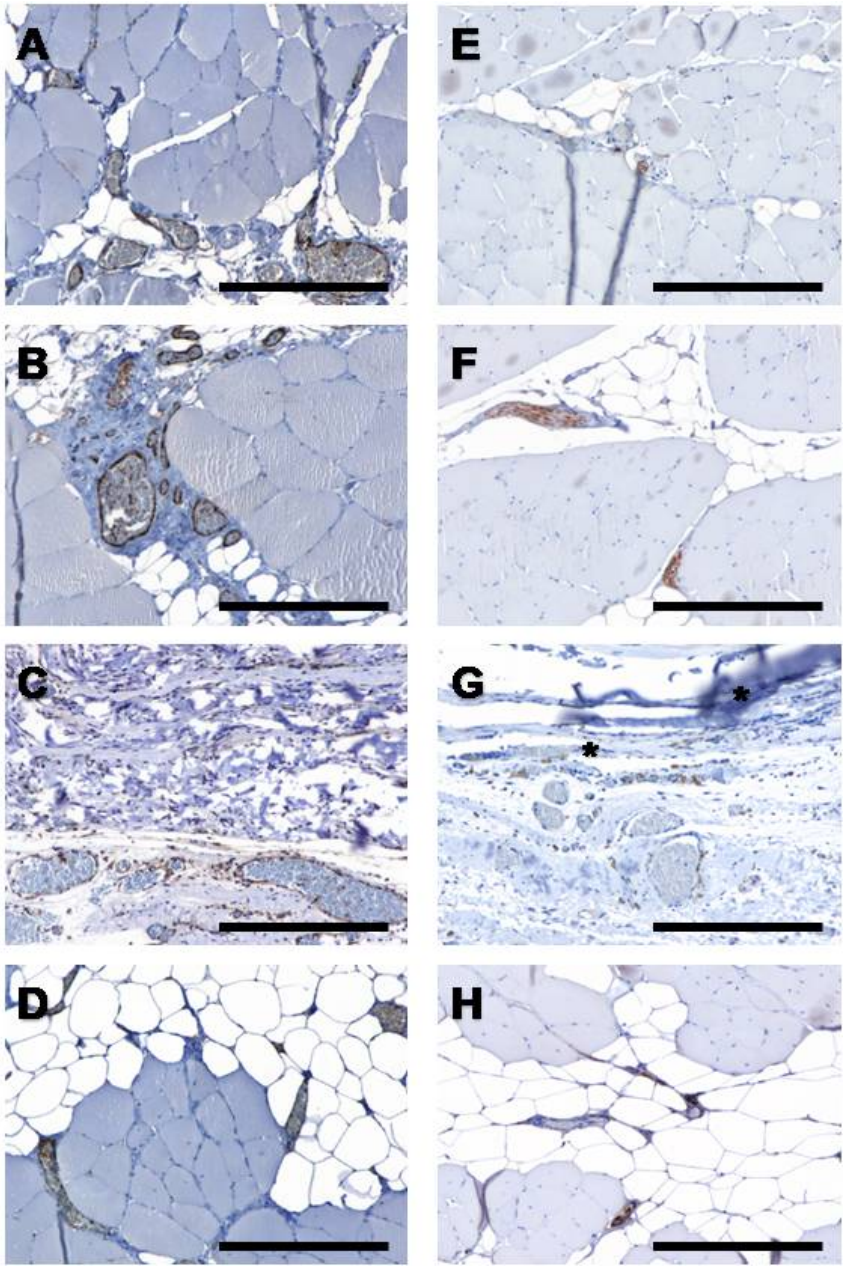

Figure 41: Blood vessel distribution and innervation of native and remodeled tissue. Tissue sections at 26 weeks post surgery were immunolabeled for Von Willibrand Factor to identify endothelial cells associated with the lumen of blood vessels (A-D), and anti-neurofilament was used to identify nerve structures (E-H) in the native and remodeled tissue sections. Mature blood vessels (A) and nerves (E) were located adjacent to the muscle bundles for the native tissue. The tissue repaired with the Restore device (B,F), and the tissue repaired with the autologous graft (D,H) showed nerves adjacent to the new muscle cells, and larger blood vessels were identified throughout the implantation site. The remnants of the original CuffPatch device (indicated by *) (C) were surrounded by a substantial amount of capillaries and larger vessels; individual neurons were located in close proximity to new blood vessels that surrounded the remnants of the CuffPatch device (G). Scale bars = 300 µm.

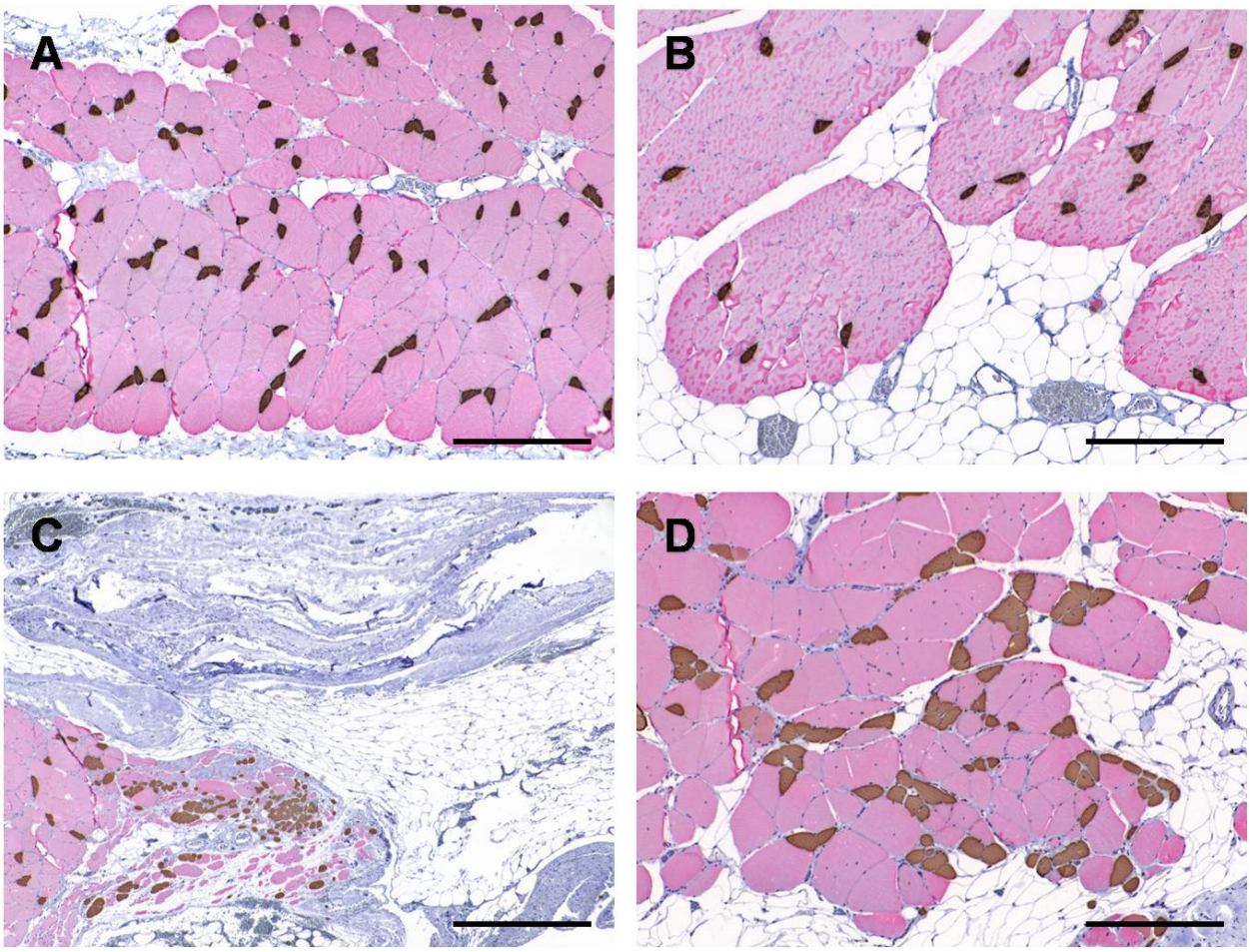

Figure 42: Distribution of slow and fast skeletal muscle fibers in native tissue and remodeled tissue at 26 weeks post surgery. Tissue sections were double-labeled for antimyosin slow (type I) skeletal muscle (brown stain) and antimyosin fast (type II) skeletal muscle (red stain). The native tissue (A) and the tissue repaired with the Restore device (B) showed that the slow muscle fibers were uniformly distributed between the fast muscle fibers. Skeletal muscle fibers surrounded the proximal edges of the CuffPatch device (C) but were not located within the graft site. (D) In the autologous tissue graft, the slow muscle fibers were distributed in an irregular pattern among the fast muscle fibers in the remodeling site, in that the slow fibers were sporadically distributed in some areas and arranged in clusters for other areas. Scale bars = 300 µm.

Table 8: Quantitative IHC analysis for each scaffold group and the contralateral native tissue

Scaffold	*# Blood Vessels per FOV*	*Slow Fibers per FOV*	*Fast Fibers per FOV*	*% Slow Fibers*
Restore™	25.3 ± 20.8	24.9 ± 16.9	98.4 ± 53.9*	20.0 ± 6.9
CuffPatch™	56.4 ± 23.2*	23.1 ± 50.9	52.1 ± 68.8‡	26.4 ± 21.5*
Autologous	27.7 ± 18.8	34.1 ± 24.2	147.8 ± 69.2	19.2 ± 10.5
Native	11.0 ± 4.9*	62.2 ± 10.5*	143.1 ± 30.9	30.7 ± 5.4*

Immunopositive blood vessels and slow (Type I) and fast (Type II) muscle fibers were counted per 100× field of view (FOV), 6 fields per graft site, examined at the implantation site. % slow fibers were compared to total number of muscle fibers (slow + fast) in same tissue section. Values reported as mean ± standard deviation. Superscripts *,‡ show significance ($p<0.05$).

6.4 DISCUSSION

Surgical mesh remodeling has commonly been assessed by passive mechanical characteristics, such as ultimate tensile strength, failure load, tangent modulus, and stiffness when used for the repair of tissues such as tendons and ligaments [99, 176-178] but repair of muscular tissue requires assessment of the active contractile force of the repair site to determine whether function is restored [18, 179].

Sections 2.2.1.2 and 2.2.2.1 showed that tissue remodeled with non-crosslinked SIS elicited a macrophage phenotype indicative of a tissue remodeling (M2) response in the early remodeling period, and constructive remodeling was the consequential outcome. Alternatively, tissue remodeled with CDI-SIS elicited predominately a pro-inflammatory macrophage (M1) response by four weeks after surgical placement, and resulted in chronic inflammation and the deposition of dense connective tissue and/or scarring. The histomorphologic and active contraction results of the current study support the hypothesis that functional tissue resulted from

an outcome of constructive remodeling after repair with noncrosslinked scaffolds versus chronic inflammation after repair with crosslinked scaffolds.

The tissue engineering approach for muscle reconstruction typically uses a myogenic progenitor cell population such as mesenchymal stem cells or satellite cells, in combination with scaffolds that may or may not include bioactive factors to support growth and differentiation [180]. Synthetic scaffold materials such as polylactic-co-glycolic acid (PGA) have been designed with nano- or microscale topographic features [181] or maintained under tension [182] for the purpose of parallel alignment of myoblasts and cytoskeletal proteins, an important requirement for functional skeletal muscle. Organic conducting polymers such as polypyrrole have the potential to promote the differentiation of electrically excitable cell types such as myoblasts and nerves by transmitting electrical and mechanical stimulation directly to the cell surface [183]. A number of strategies have been applied to engineer contractile skeletal muscle tissue using in-vitro or *in vivo* matrix-based approaches, but none have shown specific forces that approximate native muscle [184-186]. Pioneering work by Vanderburgh and colleagues [187] designed a mechanical cell stimulator device to apply mechanical stimulation to "human bioartificial muscles" (i.e., skeletal muscle cells suspended in Matrigel:collagen), resulting in improved myofibers diameter and alignment, increased elasticity of the muscle fibers, and improved cell-generated passive force. A study by Borschel et al. showed that constructs that were composed of C2C12 myoblasts (satellite cells of C3H mice) seeded onto an acellular scaffold harvested from the mouse extensor digitorum longus muscle produced specific forces that were approximately 5% of that observed for the native muscle after 3 weeks of culture [188]. In a similar fashion, Yoo and colleagues seeded primary human muscle precursor cells onto acellular bladder submucosa and subjected the constructs to cyclic strain for up to 4 weeks, followed by

subcutaneous implantation of the cell-seeded construct onto the latissimus dorsi of mice. This study demonstrated that specific forces of 1% of that observed for native latissimus dorsi were produced when the constructs were preconditioned in an in-vitro bioreactor [189]. The present study showed that vascularized, contractile skeletal muscle resulted from ECM scaffold reconstruction without prior cell or mechanical preconditioning.

For successful reconstruction of muscle, the remodeled tissue must be vascularized, innervated, and contain aligned muscle fibers in the direction of stress. Previous studies have shown that ECM scaffolds can effectuate constructive remodeling in reconstruction models of skeletal [97], cardiac [18, 179], and smooth muscle repair [21, 27, 100, 190]. In a study conducted in our laboratory, a canine model of musculotendinous repair showed that SIS facilitated the regeneration of functional musculotendinous tissue, including innervated muscle that histologically and functionally resembled native muscle tissue following the catastrophic loss of the gastrocnemius muscle/Achilles tendon junction. In a retrospective study conducted by Agrawal and colleagues, nerve tissue, including mature nerve, immature nerve, and Schwann cells were identified in specimens repaired with a non-crosslinked ECM scaffold as early as 28 days in a rat abdominal wall repair model and in specimens 91 days post-surgery from a canine model of esophageal repair [152]. In the current study, nerve tissue and blood vessels were found adjacent to the newly formed muscle bundles in tissues repaired with the non-crosslinked ECM scaffold and the autologous tissue graft, further supporting the hypothesis that ECM scaffolds can be used to facilitate the regeneration of muscular tissue for functional restoration.

Skeletal muscle is usually made up of a mixture of types I and II muscle fibers, and the fiber type composition and distribution can affect the speed of contraction, fatigability, and degree of force production. Slow type I fibers have slower maximum shortening velocities, lower

force production, and are more resistant to fatigue when compared to fast type II fibers [180]. In adult Sprague Dawley rats, the muscles with the highest percentage of the slow type I fibers are the soleus (84%), adductor longus (87%), and quadratus femoris (87%); the muscles with the lowest percentage of type I fibers are the gastrocnemius muscle (superficial-white portion) (<0.1%), tibialis anterior (2.5%) and the extensor digitorum longus (5%) [191, 192]. In the present study, muscle fiber content from sites repaired with the non-crosslinked SIS scaffold showed similar percentages of slow type I fibers to the repair sites of the autologous tissue graft but a lower percentage of slow type I fibers compared to the native tissue. However, the noncrosslinked SIS device showed a higher fatigue resistance than the native tissue, a finding that contradicts the percentage slow type I fiber data. The CDI-SIS scaffold and the native tissue showed a similar slow type I fiber percentage, which may be due to the high slow type I fiber content found in the native tissue and the low fast type II fiber found at the repair site of the crosslinked SIS scaffold. For CDI-SIS, it is most likely that the force generated and the fatigue index both indicate the influence of the surrounding native muscle and the new muscle that formed only peripherally to the scaffold, rather than specific characteristics of the site of remodeling. Furthermore, although statistical significance was detected between the scaffold groups, the percentage of slow type I fibers were within a range of 20 – 30%, a finding that is consistent to data reported by Delp and Duan [191]. In the present study, the percentage of slow type I fibers did not show a clear relationship with the fatigue index values, suggesting that the fiber type distribution may not have reached a certain threshold percentage to affect the fatigue resistance in a meaningful way.

6.5 CONCLUSION

We have shown that non-crosslinked ECM scaffolds remodeled into functional skeletal muscle tissue that produced a contractile response and histomorphologic characteristics that were similar to the native muscle, including the presence of newly formed muscle fibers and nerve tissue. By introducing a crosslinking agent into the manufacturing protocol, the contractile response was drastically reduced, and the histomorphologic profile represented a foreign body reaction rather than a reconstructive response.

6.6 LIMITATIONS AND FUTURE WORK

A limitation to the current study was the lack of temporal evaluation of the contractile response to the scaffolds. Previous studies using the same animal model have investigated the morphologic changes of the scaffolds up to 16 weeks post-surgery, but did not explore the functional properties of the reconstructing tissue (see Appendix A) [36, 42, 151]. The histomorphologic and active contraction results of the current study support the hypothesis of the previous studies, in that functional tissue resulted from an outcome of constructive remodeling after repair with noncrosslinked scaffolds versus chronic inflammation after repair with crosslinked scaffolds.

It is unclear whether the regenerative capacity of the remodeling tissue observed after ECM scaffold repair in the current study resulted from the local activation of satellite cells or muscle-derived stem cells [193], the homing and differentiation of early myeloid precursors from the bone marrow to the site of injury [193], the physical and biochemical signals released by the

degrading ECM scaffold while subjected to mechanical load, or a combination of the aforementioned. The source of cells that participated in the remodeling of new contractile skeletal tissue was not a focus of the current study, but would be an interesting endeavor for future investigations.

7.0 DISSERTATION SYNOPSIS

This dissertation examined macrophage phenotype in the context of constructive remodeling with ECM scaffold remodeling, and attempted to correlate the remodeling events in the early post-operative period to downstream remodeling outcomes. Such an analysis is critical to understand the role that regenerative medicine plays in the efforts to change the default healing mechanism of scar tissue formation into reconstruction and functionality.

In Specific Aim 1, the phenotype of monocyte-derived macrophages cultured on the surfaces of noncrosslinked SIS showed a phenotype that resembled a type 2 response, while the presence of chemical crosslinking to the same SIS scaffold changed the macrophage phenotype to a type 1 response. It was also discovered that low oxygen tension did not alter the gene expression and the protein secretion of most markers important to the differentiation of macrophages toward a type 1 or 2 response. In Specific Aim 2, the systemic depletion of monocytes *in vivo* showed that macrophages are necessary for the degradation of noncrosslinked ECM scaffolds, and that the tissue remodeling response was skewed toward a type 1 response. This study also showed that other cell types, including neutrophils, are affected at least in their temporal response pattern when macrophages are depleted from the surgical site. Specific Aim 3 showed that the interpretation of constructive remodeling as an outcome to ECM scaffold placement correlated with active contractile functionality of the reconstructed tissue.

It is currently unknown whether macrophages uncommitted to either the M1 or M2 phenotype were recruited to the site of scaffold remodeling and then stimulated to differentiate locally, or whether phenotype-committed macrophages were selectively recruited to sites of remodeling depending upon the antigens or substrates that were present. In either case, the findings of this dissertation suggest that strategies for tissue engineering and regenerative medicine that promote an M2 response are associated with a favorable remodeling response. Therefore it is important not only to consider the simple presence of macrophages at the site of scaffold remodeling but also the phenotype of this important cell population when attempting to predict downstream remodeling outcomes.

APPENDIX A

EXTRACELLULAR MATRIX BIOSCAFFOLDS FOR ORTHOPAEDIC APPLICATIONS: A COMPARATIVE HISTOLOGIC STUDY

ECM scaffolds differ in their species and tissue of origin, methods of processing, and methods of terminal sterilization. The purpose of this study was to evaluate the host tissue morphologic response to five commercially available ECM-derived biologic scaffolds used for orthopaedic soft tissue repair in a rodent model. The temporal sequence of remodeling events, including the rapidity of scaffold degradation and extent of new tissue deposition by the host, would logically be predictive of the clinical course, determination of the optimal rehabilitation protocol, and functional outcome.

A.1 INTRODUCTION

During the past decade, off-the-shelf biologic scaffold materials composed of ECM have become available for the repair and reconstruction of damaged or missing orthopaedic soft tissues. The clinical products currently available include GraftJacket® (Wright Medical Technology, Inc., Arlington, TN), Restore™ (DePuy Orthopaedics®, Inc., Warsaw, IN), CuffPatch™ (Arthrotek®,

Warsaw, IN), TissueMend® (TEI Biosciences, Inc., Boston, MA), and Permacol™ (Tissue Science Laboratories plc. Covington, GA). Each of the above-mentioned ECM-derived scaffold materials has been the subject of pre-clinical studies but little clinical outcome data is available; the partial cause of which is the relatively recent market introduction of these devices. These ECM-based products differ in the source species, tissue of origin, and the processing and sterilization procedures used to prepare each material for human clinical use. It is not clear how these differences can alter the host tissue remodeling response, clinical course and clinical outcome.

A.2 MATERIALS AND METHODS

A.2.1 Overview of Study Design

One hundred twenty-six rats were randomly divided into six equal groups of twenty-one. Each rat was subjected to surgical excision of a 1.0-cm^2 section of the musculotendinous portion of the ventral lateral abdominal wall leaving the abdominal fascia, transversus abdominis, and peritoneum intact. The defect was then repaired with one of five different ECM-derived scaffold materials or autologous tissue, depending upon the assigned group. The animals in each group were subdivided into seven subgroups based upon survival time: 2, 4, 7, 14, 28, 56 or 112 days. The surgical site plus an equal amount of surrounding tissue was collected at the time of sacrifice for histological examination.

A.2.2 Test Articles

The five ECM-derived scaffold materials that were used to repair the surgically created defect were all derived from biologic sources and differed in species of origin, tissue of origin, processing methods, and/or method of terminal sterilization (Table 9). Freshly harvested autologous excised abdominal wall tissue served as the control device. The commercially available devices are processed by methods that disrupt cell membranes and cytoplasmic organelles, denature cytoplasmic proteins, and largely eliminate these components from the remaining ECM.

Each of the test articles evaluated in this study (excluding autologous abdominal wall tissue) was purchased from the respective manufacturer. The handling of the materials after removal from the package and prior to surgical implantation was performed according to manufacturer's instructions as provided in the package insert.

Table 9: Source tissue, configuration, and processing methods for each of the five commercially available ECM materials.

Test Article	Species/ Tissue of Origin	Device Composition	Processing Methods	Sterilization Method
GraftJacket (Wright Medical Technology)	Human dermis	Single layer	Cryogenic, proprietary	None, regulated as tissue transplant by Food and Drug Administration
Restore (DePuy Orthopaedics)	Porcine small intestinal submucosa	10 layers, supplied dehydrated	Peracetic acid, vacuum-dried, minimally processed	Electron-beam radiation
CuffPatch (Arthrotek)	Porcine small intestinal submucosa	8 layers, supplied hydrated	Vacuum-dried, chemically crosslinked: carbodiimide	25-kGy gamma irradiation
TissueMend (TEI Biosciences)	Fetal bovine skin	Single layer	Proprietary	Ethylene oxide
Permacol (Tissue Science Laboratories)	Porcine dermis	Single layer, supplied hydrated	Chemically crosslinked: isocyanate	Gamma irradiation

A.2.3 Animal Model

An established rat model of abdominal wall repair was used to evaluate the host morphologic response to each implanted biomaterial. This model includes muscle and tendon tissue (i.e., the musculotendinous junction), the presence of a variable and multidirectional load, and a clinically obvious failure outcome (i.e., hernia). All procedures described in this study were performed in accordance with the National Institute of Health (NIH) guidelines for care and use of laboratory animals. All procedures were approved by the Institutional Animal Care and Use Committee.

Sprague Dawley rats in the weight range of 300-500 grams were purchased from Charles River Laboratories (Wilmington, MA). The animals were housed individually in shoebox cages and fed a diet of Purina Iso Pro ad libitum. The bedding was changed at least once per week. The animals were examined by a veterinarian prior to surgery and determined to be in good health. The housing environment was maintained at a temperature of 68 to 76° F.

Each animal was anesthetized with isoflurane (2% in oxygen) in an inhalation chamber. The surgical site was clipped, shaved and prepared for sterile surgery with a betadine scrub. Sterile technique was used at all times. A ventral midline abdominal incision was made and the skin and subcutaneous tissue were separated from the underlying muscle tissues on one side of the midline for a distance of approximately 4.0 cm. The incision in the ventral midline of the abdominal skin was retracted to expose the ventral lateral wall adjacent to the linea alba, including the musculotendinous junction of the abdominal wall musculature.

A 1.0-cm^2 defect of the musculotendinous portion of the ventral lateral abdominal wall was excised leaving the underlying transversalus fascia and peritoneum intact. The defect was then replaced with a size-matched piece of the test article chosen for that animal. Autologous excised abdominal wall tissue served as the control implant. One 4-0 Prolene suture was placed

at each of the four corners of the test article to secure attachment to the adjacent abdominal wall and to demarcate the implant. Securing the test articles in this manner provided a mechanism by which the test article was subjected to the mechanical forces delivered by the adjacent native abdominal wall musculature. A total of only four sutures were used for each device to avoid the predominance of a host tissue reaction to the suture material rather than the test article. A subcuticular placement of 4-0 Vicryl was used to close the skin incision. Each animal was recovered from anesthesia on a heating pad and returned to its housing unit.

Each rat received 0.02 mg Buprenex SQ and 2 mg Gentamicin SQ immediately after surgery and for two and three days afterward, respectively. The surgical site was evaluated daily for the duration of the study, and any signs of swelling, discoloration, or herniation at the operative site were recorded. The dietary habits and general health status of each animal were recorded daily.

On the scheduled date of sacrifice, each rat was anesthetized with Isoflurane (5% in oxygen) followed by an intracardiac injection of 5 ml potassium chloride to induce immediate cardiac arrest.

A.2.4 Specimen Collection and Histopathology

Immediately following euthanasia, the defect site with an equal amount of adjacent native tissue was excised, mounted on a fixed support structure, and placed in 10% neutral buffered formalin. The specimens were then sectioned through their entire thickness and length, including generous amounts of the adjacent normal body wall. The tissues were embedded in paraffin, cut into 6 μm thick sections and mounted upon glass slides. Tissues were stained with either H&E or Masson's trichrome stain before coverslipping.

Semiquantitative analysis included evaluation of: 1) amount of cellular infiltration, 2) presence or absence of multinucleate giant cells, 3) vascularity, and 4) degree of organization of the replacement connective tissue. At 40x magnification, the cellular infiltration counts were based on ten preselected sites at the host-device interface. Multinucleate giant cells, vascularity, and the connective tissue organization were evaluated at the same tissue sites as the cellular infiltration counts. The areas surrounding suture placement were avoided as part of the analysis because of the potential confounding foreign body response that is typically observed with Prolene suture material. The scoring criteria are listed in Table 10. Since specific phenotypic markers to distinguish between mononuclear macrophages and lymphoid lineage cells were not used in the present study, the generic and more conservative term "mononuclear cells" was used in the analysis and in the description of the host response to all test articles.

Table 10: Scoring criteria of the semiquantitative histological analysis*.

Criterion	0	1	2	3
Cellular infiltration	Between 0 and 50 cells per HPF	Between 51 and 100 cells per HPF	Between 101 and 150 cells per HPF	More than 150 cells per HPF
Multinucleated giant cells	No multinucleated giant cells per HPF	Between 1 and 2 multinucleated giant cells per HPF	Between 3 and 4 multinucleated giant cells per HPF	More than 5 multinucleated giant cells per HPF
Vascularity	Either 0 or 1 blood vessel per HPF	Between 2 and 5 blood vessels per HPF	Between 6 and 10 blood vessels per HPF	More than 10 blood vessels per HPF
Connective-tissue organization	Original scaffold intact	Original scaffold disrupted, poorly organized new host extracellular matrix present	Moderately organized connective tissue present	Dense, highly organized connective tissue present

*HPF = high-power field (×40).

A.2.5 Statistical Methods

For each of the four response variables (cellularity, multinucleate giant cells, vascularity, and degree of connective tissue organization), ten fields were scored on an integer scale of 0 to 3 (Table 10). Averages of the ten scores for each animal were the raw data that were analyzed statistically using a two-way analysis of variance (ANOVA) model. The factors were type of scaffold material with six levels (autologous control graft plus the five biologic scaffold materials) and time with seven levels. There were three animals for each type by time treatment combination. Although the raw data were not normally distributed, the robustness of the ANOVA methods was sufficient to guarantee the validity of the results obtained using this methodology.

A.3 RESULTS

All but one animal survived the surgical procedure without problems. Three rats developed age related problems that required euthanasia prior to the scheduled time. These 4 rats were replaced in the study to maintain an equal n-value for each group and subgroup.

A.3.1 Histopathologic Findings

The mean score for the three animals in each group by time treatment combination are provided in Table 11. For each response variable, both main effects and the interaction were statistically significant with $P<0.001$ in the analysis of variance.

The most intense cellular response was observed with GraftJacket, Restore and CuffPatch but the temporal appearance of the cell response differed for each of the test articles. Multinucleate giant cells were present at some point during the host response with GraftJacket, CuffPatch and Permacol but were never seen with Restore, TissueMend or autologous tissue. The most intense vascular response was observed with autologous muscle, Restore and CuffPatch, but the appearance of this vascular response differed with respect to time for each of the devices. The greatest degree of connective tissue organization at the four-month endpoint was seen with the Restore device.

Table 11: Mean rounded scores for each group according to time-treatment combination*.

Criterion	Time-Period *(day)*						
	2	4	7	14	28	56	112
Cellularity							
Control	1	1	2	2	1^{a}	0^{b}	0
GraftJacket	1	1	3	3	2^{b}	2^{a}	0
Restore	1	1	2	3	2^{b}	1^{b}	0^{b}
CuffPatch	1	1	2	2	2	$3^{a,c}$	1^{a}
TissueMend	1	2	2	2	2	1^{d}	0
Permacol	1	2	2	1	1^{a}	0^{b}	0^{b}
Multinucleated giant cells							
Control	0	0	0^{b}	0^{b}	0^{b}	0^{b}	0^{b}
GraftJacket	0	0	1^{a}	0^{b}	0^{b}	0^{d}	0^{b}
Restore	0	0	0^{b}	0^{b}	0^{b}	0^{b}	0^{b}
CuffPatch	0	0	0^{b}	1^{a}	1^{a}	$1^{a,c}$	1^{a}
TissueMend	0	0	0^{b}	0^{b}	0^{b}	0^{b}	0^{b}
Permacol	0	0	1^{a}	1^{a}	1^{a}	1^{a}	0
Vascularity							
Control	1	1	2	$3^{a,c}$	$2^{a,c}$	1^{d}	$1^{a,d}$
GraftJacket	1	1	2	1^{b}	2	1^{d}	1^{d}
Restore	1	1	2	3^{a}	2^{a}	2^{a}	$2^{a,c}$
CuffPatch	1	1	1	1^{b}	2	$3^{a,c}$	2^{a}
TissueMend	1	1	1	1^{b}	1^{b}	1^{b}	1^{b}
Permacol	1	1	1	1^{d}	1^{d}	1^{b}	0^{b}
Connective-tissue organization							
Control	1	1	1^{a}	2^{a}	2^{a}	$2^{a,c}$	$2^{a,c}$
GraftJacket	0	0	0^{b}	0^{b}	1^{b}	0^{b}	1^{b}
Restore	0	0	1	2^{a}	2^{a}	$3^{a,d}$	$3^{a,d}$
CuffPatch	0	0	0^{b}	0^{b}	0^{b}	$2^{a,c}$	$2^{a,c}$
TissueMend	0	0	0^{b}	0^{b}	0^{b}	0^{b}	1^{b}
Permacol	0	0	0^{b}	0^{b}	0^{b}	0^{b}	0^{b}

*The scores for each implant at each time-point were tabulated according to the criteria in Table II. Each score was averaged and rounded to obtain the final score provided in this table. Superscripts a-b and c-d show significance between implant pairs for each time-point and variable; that is, implants with superscript "a" are significantly different from implants with superscript "b," and implants with superscript "c" are significantly different from implants with superscript "d" ($p < 0.01$).

A.3.2 Morphologic Findings

At two days, the grafts were surrounded by a moderate accumulation of neutrophils. At four days, the neutrophil and mononuclear cell populations increased in number for all grafts.

For the autologous abdominal wall tissue graft, there was progressive necrosis of skeletal muscle fibers and an increased number of both neutrophils and mononuclear cells that peaked in number at the seven-day timepoint (Figure 43A). Tissue edema and necrosis with complete loss of tissue and cellular architecture occurred by fourteen days, at which time there was also new collagenous connective tissue deposition and prominent angiogenesis. At twenty-eight days, a moderate amount of disorganized connective tissue was present at the implant site, consistent with scar tissue formation. Remnants of muscle fibers were scattered randomly throughout the tissue with a small number of mononuclear cells. The fifty-six and 112-day timepoints showed replacement of the autologous graft by dense, poorly organized collagenous connective tissue and scattered islands of adipose tissue. (Figure 43B).

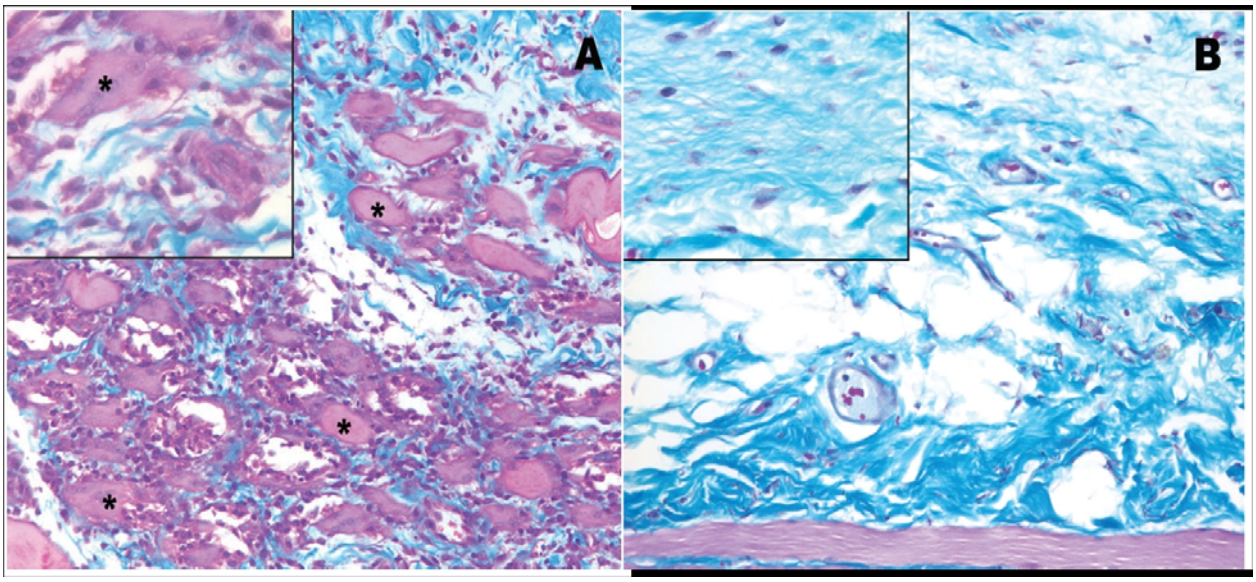

Figure 43: Histologic appearance of the autologous tissue graft at (A) seven and (B) 112 days. At seven days, necrotic skeletal muscle fiber bundles (*), a dense infiltration of neutrophils, and mononuclear cells were present. At 112 days the autograft was replaced by moderately dense scar tissue, characterized by fibrous connective tissue and adipose connective tissue. The red-staining muscle fibers at the bottom of the image represent the underlying transversalis (Masson's trichrome, X200, insets, X400).

At 7 days, the cellular response for GraftJacket consisted primarily of dense accumulations of mononuclear cells (Figure 44A). Occasional multinucleate giant cells surrounded the graft site at the 7-day timepoint, and by fourteen days, the cellular infiltrate was dense and consisted exclusively of mononuclear cells. The GraftJacket architecture was disrupted at the edges of the material with deposition of small amounts of new extracellular matrix at fourteen days. By twenty-eight days, the mononuclear cell population increased slightly from that observed at fourteen days and a small amount of new host connective tissue was present at the edges of the GraftJacket device. Moderate angiogenesis, minimal graft degradation, and a prominent cellular infiltrate were observed. By fifty-six days, the new host connective tissue at the edges of the graft material was moderately dense, the cellular infiltrate had subsided, and the majority of the graft material was unchanged from the appearance of the original scaffold article and was not yet infiltrated or populated by cells. At 112 days post surgery, there was partial degradation of the GraftJacket device and replacement with dense, partially organized collagenous connective tissue (Figure 44B).

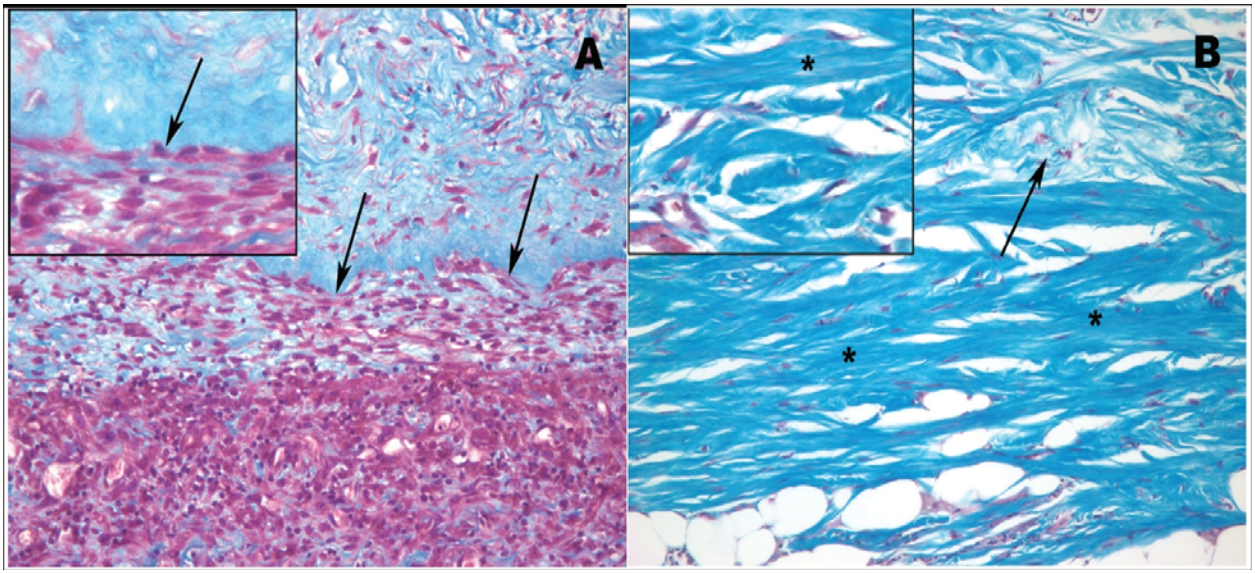

Figure 44: Histologic appearance of the GraftJacket device (stained blue) at (A) seven and (B) 112 days after surgery. At seven days, a dense mononuclear cell infiltration was limited almost exclusively to the edge of the device (arrows). Inset: The arrow represents the lower edge of the GraftJacket-host tissue interface, which is bordered by dense, red-staining mononuclear cell infiltrate. At 112 days, there was partial degradation of the GraftJacket device, with replacement by moderately organized dense collagenous connective tissue. The original device is marked with *, and newly deposited collagenous connective tissue is marked with an arrow (Masson's trichrome, X200, insets, X400).

For the Restore device, the cell population was mostly mononuclear in morphology and was distributed throughout the graft material. The individual layers of the Restore device were still distinct and identifiable at 7 days but new host-derived ECM was deposited between the layers of the original Restore device (Figure 45A). By fourteen days, there was abundant angiogenesis and extensive infiltration of the ECM scaffold material by sheets of mononuclear cells. A loss of the distinct 10-layer multilaminate device architecture occurring at twenty-eight days, and only remnants of the Restore device were still identifiable. By fifty-six days, islands of muscle cells and adipose connective tissue cells were found within the implant site and partially

organized connective tissue replaced almost the entirety of the Restore device. Nerve cells were present on the exterior surface of the implant, and only occasional inflammatory cells could still be found at fifty-six days post surgery. By the 112-day timepoint, the vascularity of the implant site was still very prominent and the Restore device appeared to be completely degraded and replaced with a mixture of organized muscle cells, collagenous connective tissue, and small islands of adipose connective tissue (Figure 45B).

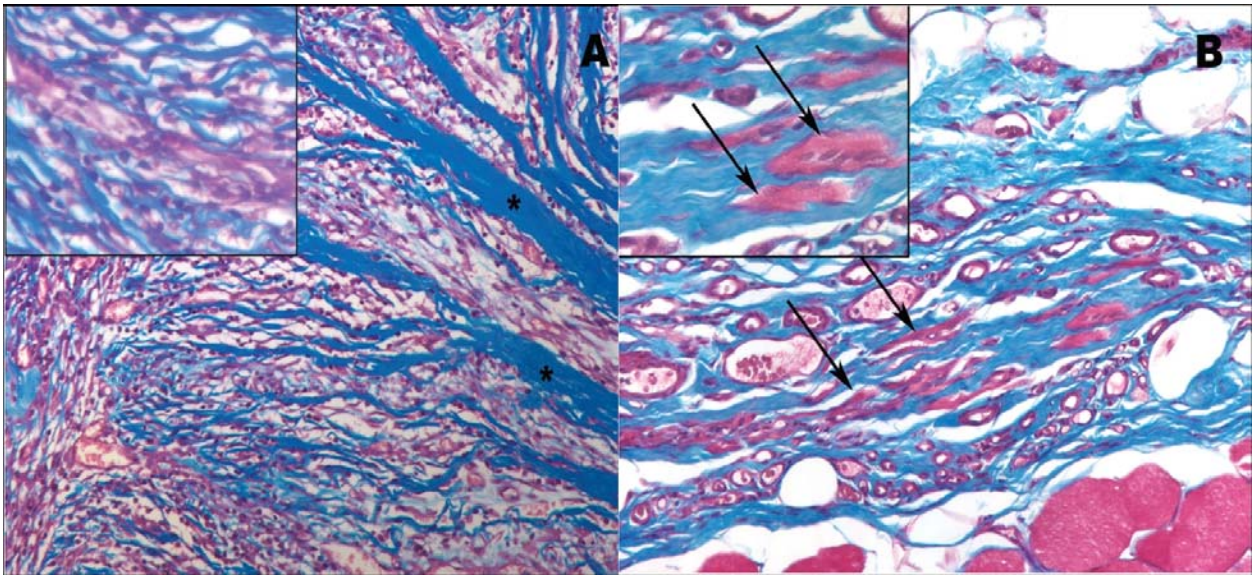

Figure 45: Histologic appearance of the Restore device (A) seven and (B) 112 days after surgery. At seven days, a dense mononuclear cell infiltration separated the individual layers of the device (blue-staining material marked with *). At 112 days, the Restore device had been replaced by a vascularized connective tissue with islands of skeletal muscle scattered randomly throughout the tissue (arrows) (Masson's trichrome, X200, insets, X400).

The CuffPatch device showed an increased neutrophil population by seven days, with a moderate amount of tissue edema that extended into the adjacent native abdominal wall tissue (Figure 46A). There was minimal infiltration of cells beyond the edges of the test article at fourteen days, and new host extracellular matrix and fibrous connective tissue was deposited in the space immediately surrounding the implant. Multinucleate giant cells were scattered throughout the periphery of the implant site at fourteen and twenty-eight days. By fifty-six days post surgery, neutrophils and mononuclear cells separated the individual layers of the CuffPatch device in the central regions of the graft site and the vascularity of the surrounding tissue was very prominent. Scaffold degradation was apparent by the fifty-six day timepoint, and a robust inflammatory cell reaction, primarily mononuclear in nature, infiltrated the entirety of the scaffold material. By 112 days, a typical foreign body tissue response was present, including the presence of multinucleate giant cells. As seen in Figure 46B, remnants of the originally implanted biomaterial were still identifiable with little organization of new host connective tissue at the implant site.

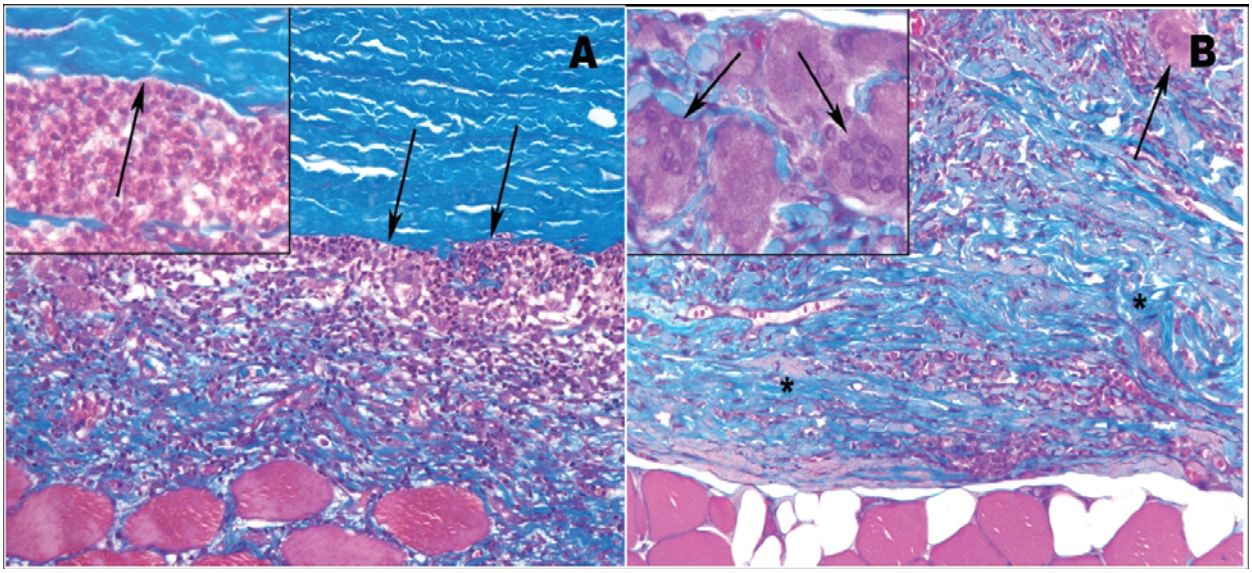

Figure 46: Histologic appearance of the CuffPatch device at (A) seven and (B) 112 days post implantation. At seven days, a dense accumulation of neutrophils and mononuclear cells were located primarily at the edge of the implanted device (the arrows indicate the edge of CuffPatch, the blue-stained material). The native abdominal wall skeletal muscle tissue can be seen in the lower left-hand portion. Inset: The interface between the dense cellular accumulation and the edge of the CuffPatch device. 112 days, there were a moderate number of inflammatory cells, including multinucleate giant cells (arrow) within the graft site. Remnants of the originally implanted CuffPatch device could still be identified (blue material marked with *) (Masson's trichrome, X200, insets, X400).

For the TissueMend device, there was an absence of host cell invasion by seven days, and small amounts of fibrous connective tissue were deposited at the periphery of the device (Figure 47A). The vascularity at the interface between the native host tissue and the TissueMend device was increased above that of the surrounding normal tissue and it remained increased for the entire 112-day study period. By twenty-eight and fifty-six days post surgery, the fibrous capsule had increased in thickness with little infiltration of the TissueMend device by host cells. By 112 days there was degradation of scaffold material at the edges of the device. Adipose connective

tissue accumulated near the borders of the TissueMend device, and a dense, highly organized connective tissue capsule was present (Figure 47B).

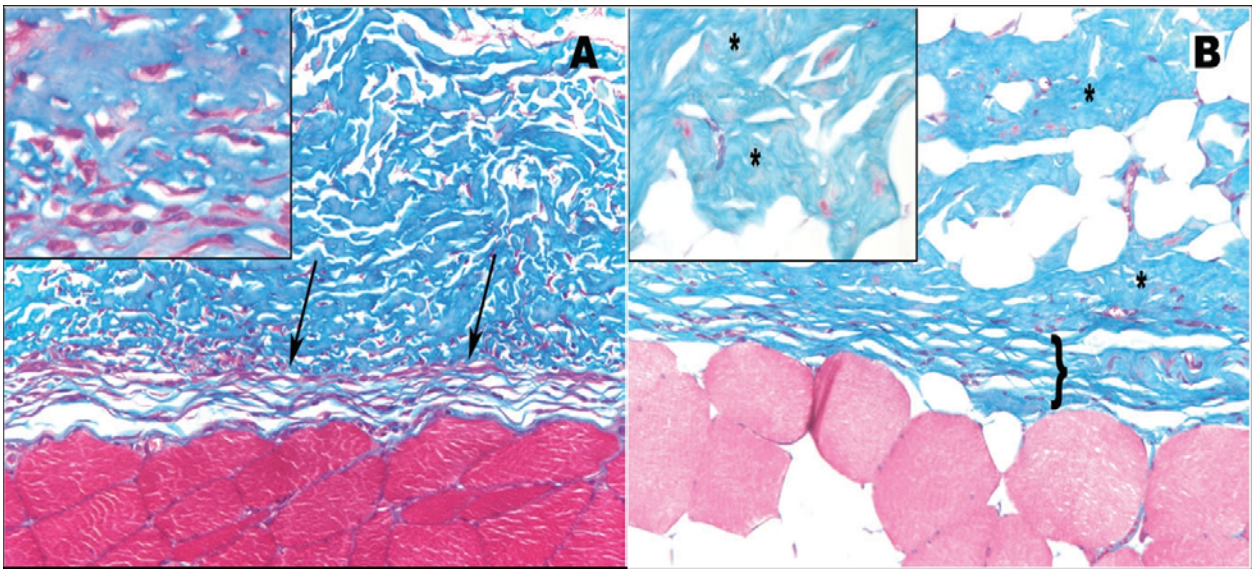

Figure 47: Histologic appearance of the TissueMend device at (A) seven and (B) 112 days after implantation. At seven days, there was very little infiltration of the edge of the device by host inflammatory cells (the arrows show the lower edge of the TissueMend, the solid blue-stained material). At 112 days, the device-implant site showed an accumulation of adipose connective tissue (circular white areas) at the edges of the TissueMend device (internal to the surrounding capsule, as indicated by the bracket), but the remainder of the device (blue materials marked with *) remained virtually unchanged from the time of implantation (Masson's trichrome, X200, insets, X400).

For the Permacol device, poorly organized fibrous connective tissue deposition was noted as early as four days. From fourteen to fifty-six days, the fibrous connective tissue capsule around the device was the predominant morphologic finding. Small numbers of mononuclear cells were present at the edges of the scaffold material and multinucleate giant cells were present from 7 days (Figure 48A) until fifty-six days. By fifty-six and 112 days, the host cellular

response was minimal. There was almost no evidence for scaffold degradation at the 112-day timepoint and a thin fibrous connective tissue capsule surrounded the device (Figure 48B).

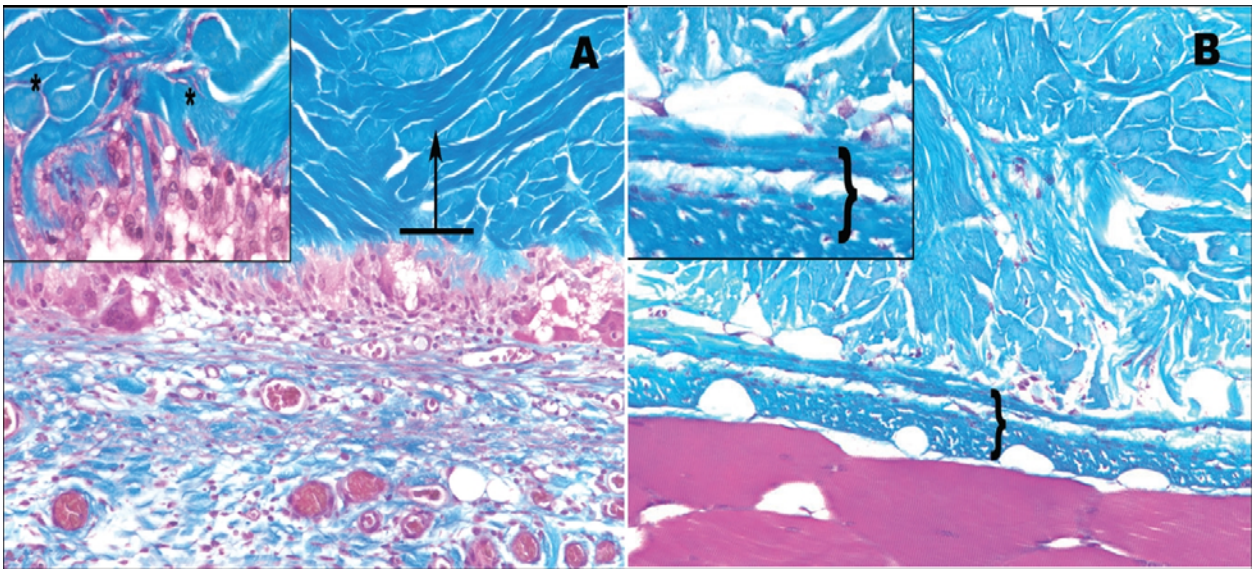

Figure 48: Histologic appearance of the Permacol device at (A) seven and (B) 112 days after surgery. At seven days, there was an accumulation of both neutrophils and mononuclear cells mixed with a thin fibrous capsule surrounding the device. The solid blue-staining material above the horizontal line is the Permacol device. Inset: Inflammatory cells at the periphery of the Permacol device (*). At 112 days, a dense fibrous tissue (brackets) encapsulates the Permacol device (blue staining material located above the bracket). There was almost no evidence of scaffold degradation or remodeling (Masson's trichrome, X200, insets, X400).

A.4 DISCUSSION

The host tissue response to five different commercially available ECM-based scaffold materials and autologous tissue was evaluated in an established rodent model of body wall repair. The marketing literature for all devices claims host acceptance and intact functionality. The host

response in which all variables were equal showed that there were clear differences in the amount and temporal appearance of inflammatory cells, the morphologic structural integrity of the devices over time, and the type of host tissue that either replaced or surrounded the ECM-derived devices.

The 16-week remodeling outcome of the present study differed markedly between the devices. The autologous control tissue showed typical scar tissue formation. The 16-week host tissue response to GraftJacket showed replacement of the device with fibrous connective tissue and a persistent low-grade chronic inflammatory response. The Restore device was replaced by a mixture of muscle cells and organized connective tissue. The CuffPatch device showed a slower remodeling process as compared to either the autologous control tissue or Restore. An accumulation of dense collagenous tissue and a persistent foreign body response was present at the 16-week timepoint. The host response to TissueMend and Permacol was consistent with the typical response to a non-resorbable foreign material; that is, a response characterized by low-grade chronic inflammation, minimal scaffold degradation, and fibrous encapsulation.

A.5 CONCLUSIONS

This study represents the first head-to-head comparison of the clinically available ECM scaffold materials in an animal model, and showed that the five different scaffold devices currently used for musculotendinous repair are distinct with regard to the host tissue response. A limitation of the present study is that it was conducted in a rodent model, which may or may not be predictive of the response seen in humans.

BIBLIOGRAPHY

1. Badylak SF, Record R, Lindberg K, Hodde J, Park K. Small intestinal submucosa: a substrate for in vitro cell growth. J Biomater Sci Polym Ed 1998;9(8):863-878.

2. Beattie AJ, Gilbert TW, Guyot JP, Yates AJ, Badylak SF. Chemoattraction of Progenitor Cells by Remodeling Extracellular Matrix Scaffolds. Tissue Eng Part A 2008 Oct 6.

3. Hodde J, Record R, Tullius R, Badylak S. Fibronectin peptides mediate HMEC adhesion to porcine-derived extracellular matrix. Biomaterials 2002 Apr;23(8):1841-1848.

4. Hodde JP, Record RD, Tullius RS, Badylak SF. Retention of endothelial cell adherence to porcine-derived extracellular matrix after disinfection and sterilization. Tissue Eng 2002 Apr;8(2):225-234.

5. Li F, Li W, Johnson S, Ingram D, Yoder M, Badylak S. Low-molecular-weight peptides derived from extracellular matrix as chemoattractants for primary endothelial cells. Endothelium 2004 May-Aug;11(3-4):199-206.

6. Lindberg K, Badylak SF. Porcine small intestinal submucosa (SIS): a bioscaffold supporting in vitro primary human epidermal cell differentiation and synthesis of basement membrane proteins. Burns 2001 May;27(3):254-266.

7. Reing JE, Zhang L, Myers-Irvin J, Cordero KE, Freytes DO, Heber-Katz E, et al. Degradation Products of Extracellular Matrix Affect Cell Migration and Proliferation. Tissue Eng Part A 2008 Jul 24.

8. Zantop T, Gilbert TW, Yoder MC, Badylak SF. Extracellular matrix scaffolds are repopulated by bone marrow-derived cells in a mouse model of achilles tendon reconstruction. J Orthop Res 2006 Jun;24(6):1299-1309.

9. Hodde JP, Johnson CE. Extracellular matrix as a strategy for treating chronic wounds. Am J Clin Dermatol 2007;8(2):61-66.

10. Ansaloni L, Cambrini P, Catena F, Di Saverio S, Gagliardi S, Gazzotti F, et al. Immune response to small intestinal submucosa (surgisis) implant in humans: preliminary observations. J Invest Surg 2007 Jul-Aug;20(4):237-241.

11. Brigido SA, Boc SF, Lopez RC. Effective management of major lower extremity wounds using an acellular regenerative tissue matrix: a pilot study. Orthopedics 2004 Jan;27(1 Suppl):s145-149.

12. Griffiths M, Ojeh N, Livingstone R, Price R, Navsaria H. Survival of Apligraf in acute human wounds. Tissue Eng 2004 Jul-Aug;10(7-8):1180-1195.

13. Kim MS, Hong KD, Shin HW, Kim SH, Lee MS, Jang WY, et al. Preparation of porcine small intestinal submucosa sponge and their application as a wound dressing in full-thickness skin defect of rat. Int J Biol Macromol 2005 Jul;36(1-2):54-60.

14. Mostow EN, Haraway GD, Dalsing M, Hodde JP, King D. Effectiveness of an extracellular matrix graft (OASIS Wound Matrix) in the treatment of chronic leg ulcers: a randomized clinical trial. J Vasc Surg 2005 May;41(5):837-843.

15. Badylak S, Obermiller J, Geddes L, Matheny R. Extracellular matrix for myocardial repair. Heart Surg Forum 2003;6(2):E20-26.

16. Badylak SF, Coffey AC, Lantz GC, Tacker WA, Geddes LA. Comparison of the resistance to infection of intestinal submucosa arterial autografts versus polytetrafluoroethylene arterial prostheses in a dog model. J Vasc Surg 1994 Mar;19(3):465-472.

17. Badylak SF, Kochupura PV, Cohen IS, Doronin SV, Saltman AE, Gilbert TW, et al. The use of extracellular matrix as an inductive scaffold for the partial replacement of functional myocardium. Cell Transplant 2006;15 Suppl 1:S29-40.

18. Kochupura PV, Azeloglu EU, Kelly DJ, Doronin SV, Badylak SF, Krukenkamp IB, et al. Tissue-engineered myocardial patch derived from extracellular matrix provides regional mechanical function. Circulation 2005 Aug 30;112(9 Suppl):I144-149.

19. Shell DHt, Croce MA, Cagiannos C, Jernigan TW, Edwards N, Fabian TC. Comparison of small-intestinal submucosa and expanded polytetrafluoroethylene as a vascular conduit in the presence of gram-positive contamination. Ann Surg 2005 Jun;241(6):995-1001; discussion 1001-1004.

20. Yavuz K, Geyik S, Pavcnik D, Uchida BT, Corless CL, Hartley DE, et al. Comparison of the endothelialization of small intestinal submucosa, dacron, and expanded polytetrafluoroethylene suspended in the thoracoabdominal aorta in sheep. J Vasc Interv Radiol 2006 May;17(5):873-882.

21. Badylak SF, Vorp DA, Spievack AR, Simmons-Byrd A, Hanke J, Freytes DO, et al. Esophageal reconstruction with ECM and muscle tissue in a dog model. J Surg Res 2005 Sep;128(1):87-97.

22. Nieponice A, Gilbert TW, Badylak SF. Reinforcement of esophageal anastomoses with an extracellular matrix scaffold in a canine model. Ann Thorac Surg 2006 Dec;82(6):2050-2058.

23. Nieponice A, McGrath K, Qureshi I, Beckman EJ, Luketich JD, Gilbert TW, et al. An extracellular matrix scaffold for esophageal stricture prevention after circumferential EMR. Gastrointest Endosc 2008 Jul 25.

24. Badylak SF, Kropp B, McPherson T, Liang H, Snyder PW. Small intestional submucosa: a rapidly resorbed bioscaffold for augmentation cystoplasty in a dog model. Tissue Eng 1998 Winter;4(4):379-387.

25. Cannon TW, Sweeney DD, Conway DA, Kamo I, Yoshimura N, Sacks M, et al. A tissue-engineered suburethral sling in an animal model of stress urinary incontinence. BJU Int 2005 Sep;96(4):664-669.

26. Kropp BP, Ludlow JK, Spicer D, Rippy MK, Badylak SF, Adams MC, et al. Rabbit urethral regeneration using small intestinal submucosa onlay grafts. Urology 1998 Jul;52(1):138-142.

27. Boruch AV, Nieponice A, Qureshi IR, Gilbert TW, Badylak SF. Constructive Remodeling of Biologic Scaffolds is Dependent on Early Exposure to Physiologic Bladder Filling in a Canine Partial Cystectomy Model. J Surg Res 2009 Mar 20.

28. Chen F, Yoo JJ, Atala A. Acellular collagen matrix as a possible "off the shelf" biomaterial for urethral repair. Urology 1999 Sep;54(3):407-410.

29. Kimuli M, Eardley I, Southgate J. In vitro assessment of decellularized porcine dermis as a matrix for urinary tract reconstruction. BJU Int 2004 Oct;94(6):859-866.

30. Wood JD, Simmons-Byrd A, Spievack AR, Badylak SF. Use of a particulate extracellular matrix bioscaffold for treatment of acquired urinary incontinence in dogs. J Am Vet Med Assoc 2005 Apr 1;226(7):1095-1097.

31. Musahl V, Abramowitch SD, Gilbert TW, Tsuda E, Wang JH, Badylak SF, et al. The use of porcine small intestinal submucosa to enhance the healing of the medial collateral ligament--a functional tissue engineering study in rabbits. J Orthop Res 2004 Jan;22(1):214-220.

32. Woo SL, Takakura Y, Liang R, Jia F, Moon DK. Treatment with bioscaffold enhances the the fibril morphology and the collagen composition of healing medial collateral ligament in rabbits. Tissue Eng 2006 Jan;12(1):159-166.

33. De Deyne PG, Kladakis SM. Bioscaffolds in tissue engineering: a rationale for use in the reconstruction of musculoskeletal soft tissues. Clin Podiatr Med Surg 2005 Oct;22(4):521-532, v.

34. Aurora A, McCarron J, Iannotti JP, Derwin K. Commercially available extracellular matrix materials for rotator cuff repairs: state of the art and future trends. J Shoulder Elbow Surg 2007 Sep-Oct;16(5 Suppl):S171-178.

35. Badylak S, Arnoczky S, Plouhar P, Haut R, Mendenhall V, Clarke R, et al. Naturally occurring extracellular matrix as a scaffold for musculoskeletal repair. Clin Orthop Relat Res 1999 Oct(367 Suppl):S333-343.

36. Badylak S, Kokini K, Tullius B, Simmons-Byrd A, Morff R. Morphologic study of small intestinal submucosa as a body wall repair device. J Surg Res 2002 Apr;103(2):190-202.

37. Crow BD, Haltom JD, Carson WL, Greene WB, Cook JL. Evaluation of a novel biomaterial for intrasubstance muscle laceration repair. J Orthop Res 2007 Mar;25(3):396-403.

38. Dejardin LM, Arnoczky SP, Ewers BJ, Haut RC, Clarke RB. Tissue-engineered rotator cuff tendon using porcine small intestine submucosa. Histologic and mechanical evaluation in dogs. Am J Sports Med 2001 Mar-Apr;29(2):175-184.

39. Derwin K, Androjna C, Spencer E, Safran O, Bauer TW, Hunt T, et al. Porcine small intestine submucosa as a flexor tendon graft. Clin Orthop Relat Res 2004 Jun(423):245-252.

40. Gilbert TW, Stewart-Akers AM, Simmons-Byrd A, Badylak SF. Degradation and remodeling of small intestinal submucosa in canine Achilles tendon repair. J Bone Joint Surg Am 2007 Mar;89(3):621-630.

41. Nicholson GP, Breur GJ, Van Sickle D, Yao JQ, Kim J, Blanchard CR. Evaluation of a cross-linked acellular porcine dermal patch for rotator cuff repair augmentation in an ovine model. J Shoulder Elbow Surg 2007 Sep-Oct;16(5 Suppl):S184-190.

42. Valentin JE, Badylak JS, McCabe GP, Badylak SF. Extracellular matrix bioscaffolds for orthopaedic applications. A comparative histologic study. J Bone Joint Surg Am 2006 Dec;88(12):2673-2686.

43. Badylak SF. The extracellular matrix as a biologic scaffold material. Biomaterials 2007 Sep;28(25):3587-3593.

44. Badylak SF, Freytes DO, Gilbert TW. Extracellular matrix as a biological scaffold material: Structure and function. Acta Biomater 2009 Jan;5(1):1-13.

45. Brown B, Lindberg K, Reing J, Stolz DB, Badylak SF. The basement membrane component of biologic scaffolds derived from extracellular matrix. Tissue Eng 2006 Mar;12(3):519-526.

46. Hodde J. Naturally occurring scaffolds for soft tissue repair and regeneration. Tissue Eng 2002 Apr;8(2):295-308.

47. Hodde JP, Badylak SF, Brightman AO, Voytik-Harbin SL. Glycosaminoglycan Content of Small Intestinal Submucosa: A Bioscaffold for Tissue Replacement. Tissue Eng 1996;2(3):209-217.

48. Hodde JP, Record RD, Liang HA, Badylak SF. Vascular endothelial growth factor in porcine-derived extracellular matrix. Endothelium 2001;8(1):11-24.

49. McDevitt CA, Wildey GM, Cutrone RM. Transforming growth factor-beta1 in a sterilized tissue derived from the pig small intestine submucosa. J Biomed Mater Res A 2003 Nov 1;67(2):637-640.

50. McPherson TB, Badylak SF. Characterization of Fibronectin Derived from Porcine Small Intestinal Submucosa. Tissue Eng 1998;4(1):75-83.

51. Chun SY, Lim GJ, Kwon TG, Kwak EK, Kim BW, Atala A, et al. Identification and characterization of bioactive factors in bladder submucosa matrix. Biomaterials 2007 Oct;28(29):4251-4256.

52. Derwin KA, Baker AR, Spragg RK, Leigh DR, Iannotti JP. Commercial extracellular matrix scaffolds for rotator cuff tendon repair. Biomechanical, biochemical, and cellular properties. J Bone Joint Surg Am 2006 Dec;88(12):2665-2672.

53. Badylak SF, Park K, Peppas N, McCabe G, Yoder M. Marrow-derived cells populate scaffolds composed of xenogeneic extracellular matrix. Exp Hematol 2001 Nov;29(11):1310-1318.

54. Badylak SF, Wu CC, Bible M, McPherson E. Host protection against deliberate bacterial contamination of an extracellular matrix bioscaffold versus Dacron mesh in a dog model of orthopedic soft tissue repair. J Biomed Mater Res B Appl Biomater 2003 Oct 15;67(1):648-654.

55. Brennan EP, Reing J, Chew D, Myers-Irvin JM, Young EJ, Badylak SF. Antibacterial activity within degradation products of biological scaffolds composed of extracellular matrix. Tissue Eng 2006 Oct;12(10):2949-2955.

56. Sarikaya A, Record R, Wu CC, Tullius B, Badylak S, Ladisch M. Antimicrobial activity associated with extracellular matrices. Tissue Eng 2002 Feb;8(1):63-71.

57. Jernigan TW, Croce MA, Cagiannos C, Shell DH, Handorf CR, Fabian TC. Small intestinal submucosa for vascular reconstruction in the presence of gastrointestinal contamination. Ann Surg 2004 May;239(5):733-738; discussion 738-740.

58. Allman AJ, McPherson TB, Badylak SF, Merrill LC, Kallakury B, Sheehan C, et al. Xenogeneic extracellular matrix grafts elicit a TH2-restricted immune response. Transplantation 2001 Jun 15;71(11):1631-1640.

59. Badylak SF, Gilbert TW. Immune response to biologic scaffold materials. Semin Immunol 2008 Apr;20(2):109-116.

60. Badylak SF, Valentin JE, Ravindra AK, McCabe GP, Stewart-Akers AM. Macrophage phenotype as a determinant of biologic scaffold remodeling. Tissue Eng Part A 2008 Nov;14(11):1835-1842.

61. Hodde J, Janis A, Ernst D, Zopf D, Sherman D, Johnson C. Effects of sterilization on an extracellular matrix scaffold: part I. Composition and matrix architecture. J Mater Sci Mater Med 2007 Apr;18(4):537-543.

62. Whitlock PW, Smith TL, Poehling GG, Shilt JS, Van Dyke M. A naturally derived, cytocompatible, and architecturally optimized scaffold for tendon and ligament regeneration. Biomaterials 2007 Oct;28(29):4321-4329.

63. Record RD, Hillegonds D, Simmons C, Tullius R, Rickey FA, Elmore D, et al. In vivo degradation of 14C-labeled small intestinal submucosa (SIS) when used for urinary bladder repair. Biomaterials 2001 Oct;22(19):2653-2659.

64. Gilbert TW, Stewart-Akers AM, Badylak SF. A quantitative method for evaluating the degradation of biologic scaffold materials. Biomaterials 2007 Jan;28(2):147-150.

65. Davis GE, Bayless KJ, Davis MJ, Meininger GA. Regulation of tissue injury responses by the exposure of matricryptic sites within extracellular matrix molecules. Am J Pathol 2000 May;156(5):1489-1498.

66. Adair-Kirk TL, Senior RM. Fragments of extracellular matrix as mediators of inflammation. Int J Biochem Cell Biol 2008;40(6-7):1101-1110.

67. Brennan EP, Tang XH, Stewart-Akers AM, Gudas LJ, Badylak SF. Chemoattractant activity of degradation products of fetal and adult skin extracellular matrix for keratinocyte progenitor cells. J Tissue Eng Regen Med 2008 Dec;2(8):491-498.

68. Ueno T, Pickett LC, de la Fuente SG, Lawson DC, Pappas TN. Clinical application of porcine small intestinal submucosa in the management of infected or potentially contaminated abdominal defects. J Gastrointest Surg 2004 Jan;8(1):109-112.

69. Anderson JM, Rodriguez A, Chang DT. Foreign body reaction to biomaterials. Semin Immunol 2008 Apr;20(2):86-100.

70. Ratner BD. Biomaterials science : an introduction to materials in medicine. 2nd ed. Amsterdam ; Boston: Elsevier Academic Press, 2004.

71. Frid MG, Brunetti JA, Burke DL, Carpenter TC, Davie NJ, Reeves JT, et al. Hypoxia-induced pulmonary vascular remodeling requires recruitment of circulating mesenchymal precursors of a monocyte/macrophage lineage. Am J Pathol 2006 Feb;168(2):659-669.

72. Yoder MC. Blood cell progenitors: insights into the properties of stem cells. Anat Rec A Discov Mol Cell Evol Biol 2004 Jan;276(1):66-74.

73. Ingram DA, Caplice NM, Yoder MC. Unresolved questions, changing definitions, and novel paradigms for defining endothelial progenitor cells. Blood 2005 Sep 1;106(5):1525-1531.

74. Chan RJ, Yoder MC. The multiple facets of hematopoietic stem cells. Curr Neurovasc Res 2004 Jul;1(3):197-206.

75. George J, Shmilovich H, Deutsch V, Miller H, Keren G, Roth A. Comparative analysis of methods for assessment of circulating endothelial progenitor cells. Tissue Eng 2006 Feb;12(2):331-335.

76. Hunting CB, Noort WA, Zwaginga JJ. Circulating endothelial (progenitor) cells reflect the state of the endothelium: vascular injury, repair and neovascularization. Vox Sang 2005 Jan;88(1):1-9.

77. Ingram DA, Mead LE, Moore DB, Woodard W, Fenoglio A, Yoder MC. Vessel wall-derived endothelial cells rapidly proliferate because they contain a complete hierarchy of endothelial progenitor cells. Blood 2005 Apr 1;105(7):2783-2786.

78. Rehman J, Li J, Orschell CM, March KL. Peripheral blood "endothelial progenitor cells" are derived from monocyte/macrophages and secrete angiogenic growth factors. Circulation 2003 Mar 4;107(8):1164-1169.

79. Frid MG, Brunetti JA, Burke DL, Carpenter TC, Davie NJ, Stenmark KR. Circulating mononuclear cells with a dual, macrophage-fibroblast phenotype contribute robustly to hypoxia-induced pulmonary adventitial remodeling. Chest 2005 Dec;128(6 Suppl):583S-584S.

80. Metz CN. Fibrocytes: a unique cell population implicated in wound healing. Cell Mol Life Sci 2003 Jul;60(7):1342-1350.

81. Quan TE, Cowper S, Wu SP, Bockenstedt LK, Bucala R. Circulating fibrocytes: collagen-secreting cells of the peripheral blood. Int J Biochem Cell Biol 2004 Apr;36(4):598-606.

82. Varcoe RL, Mikhail M, Guiffre AK, Pennings G, Vicaretti M, Hawthorne WJ, et al. The role of the fibrocyte in intimal hyperplasia. J Thromb Haemost 2006 May;4(5):1125-1133.

83. Elsheikh E, Uzunel M, He Z, Holgersson J, Nowak G, Sumitran-Holgersson S. Only a specific subset of human peripheral-blood monocytes has endothelial-like functional capacity. Blood 2005 Oct 1;106(7):2347-2355.

84. Jabs A, Moncada GA, Nichols CE, Waller EK, Wilcox JN. Peripheral blood mononuclear cells acquire myofibroblast characteristics in granulation tissue. J Vasc Res 2005 Mar-Apr;42(2):174-180.

85. Smith PD, Ochsenbauer-Jambor C, Smythies LE. Intestinal macrophages: unique effector cells of the innate immune system. Immunol Rev 2005 Aug;206:149-159.

86. Smythies LE, Sellers M, Clements RH, Mosteller-Barnum M, Meng G, Benjamin WH, et al. Human intestinal macrophages display profound inflammatory anergy despite avid phagocytic and bacteriocidal activity. J Clin Invest 2005 Jan;115(1):66-75.

87. Sellaro TL, Ravindra AK, Stolz DB, Badylak SF. Maintenance of hepatic sinusoidal endothelial cell phenotype in vitro using organ-specific extracellular matrix scaffolds. Tissue Eng 2007 Sep;13(9):2301-2310.

88. Vakonakis I, Campbell ID. Extracellular matrix: from atomic resolution to ultrastructure. Curr Opin Cell Biol 2007 Oct;19(5):578-583.

89. Xiaohui T, Wujun X, Xiaoming D, Xinlu P, Yan T, Puxun T, et al. Small intestinal submucosa improves islet survival and function in vitro culture. Transplant Proc 2006 Jun;38(5):1552-1558.

90. Gilbert TW, Stewart-Akers AM, Sydeski J, Nguyen TD, Badylak SF, Woo SL. Gene expression by fibroblasts seeded on small intestinal submucosa and subjected to cyclic stretching. Tissue Eng 2007 Jun;13(6):1313-1323.

91. Zhang Y, Kropp BP, Moore P, Cowan R, Furness PD, 3rd, Kolligian ME, et al. Coculture of bladder urothelial and smooth muscle cells on small intestinal submucosa: potential applications for tissue engineering technology. J Urol 2000 Sep;164(3 Pt 2):928-934; discussion 934-925.

92. Woods EJ, Walsh CM, Sidner RA, Zieger MA, Lakey JR, Ricordi C, et al. Improved in vitro function of islets using small intestinal submucosa. Transplant Proc 2004 May;36(4):1175-1177.

93. Malda J, Klein TJ, Upton Z. The roles of hypoxia in the in vitro engineering of tissues. Tissue Eng 2007 Sep;13(9):2153-2162.

94. Valentin JE, Freytes DO, Grasman JM, Pesyna C, Freund J, Gilbert TW, et al. Oxygen diffusivity of biologic and synthetic scaffold materials for tissue engineering. J Biomed Mater Res A 2008 Dec 18.

95. Hodde JP, Ernst DM, Hiles MC. An investigation of the long-term bioactivity of endogenous growth factor in OASIS Wound Matrix. J Wound Care 2005 Jan;14(1):23-25.

96. Voytik-Harbin SL, Brightman AO, Kraine MR, Waisner B, Badylak SF. Identification of extractable growth factors from small intestinal submucosa. J Cell Biochem 1997 Dec 15;67(4):478-491.

97. Badylak S, Kokini K, Tullius B, Whitson B. Strength over time of a resorbable bioscaffold for body wall repair in a dog model. J Surg Res 2001 Aug;99(2):282-287.

98. Badylak SF, Tullius R, Kokini K, Shelbourne KD, Klootwyk T, Voytik SL, et al. The use of xenogeneic small intestinal submucosa as a biomaterial for Achilles tendon repair in a dog model. J Biomed Mater Res 1995 Aug;29(8):977-985.

99. Liang R, Woo SL, Takakura Y, Moon DK, Jia F, Abramowitch SD. Long-term effects of porcine small intestine submucosa on the healing of medial collateral ligament: a functional tissue engineering study. J Orthop Res 2006 Apr;24(4):811-819.

100. Kropp BP, Sawyer BD, Shannon HE, Rippy MK, Badylak SF, Adams MC, et al. Characterization of small intestinal submucosa regenerated canine detrusor: assessment of reinnervation, in vitro compliance and contractility. J Urol 1996 Aug;156(2 Pt 2):599-607.

101. Cotran RS, Kumar V, Collins T, Robbins SL. Robbins pathologic basis of disease. 6th ed. Philadelphia: Saunders, 1999.

102. Burke B, Lewis CE. The macrophage. 2nd ed. Oxford ; New York: Oxford University Press, 2002.

103. Gordon S, Taylor PR. Monocyte and macrophage heterogeneity. Nat Rev Immunol 2005 Dec;5(12):953-964.

104. Kumar V, Abbas AK, Fausto N, Robbins SL, Cotran RS. Robbins and Cotran pathologic basis of disease. 2005 [cited; 7th:[xv, 1525]. Available from:

105. Anderson CF, Mosser DM. A novel phenotype for an activated macrophage: the type 2 activated macrophage. J Leukoc Biol 2002 Jul;72(1):101-106.

106. Daley JM, Reichner JS, Mahoney EJ, Manfield L, Henry WL, Jr., Mastrofrancesco B, et al. Modulation of macrophage phenotype by soluble product(s) released from neutrophils. J Immunol 2005 Feb 15;174(4):2265-2272.

107. Lewis C, Murdoch C. Macrophage responses to hypoxia: implications for tumor progression and anti-cancer therapies. Am J Pathol 2005 Sep;167(3):627-635.

108. Mantovani A, Sica A, Sozzani S, Allavena P, Vecchi A, Locati M. The chemokine system in diverse forms of macrophage activation and polarization. Trends Immunol 2004 Dec;25(12):677-686.

109. Porcheray F, Viaud S, Rimaniol AC, Leone C, Samah B, Dereuddre-Bosquet N, et al. Macrophage activation switching: an asset for the resolution of inflammation. Clin Exp Immunol 2005 Dec;142(3):481-489.

110. Schnoor M, Cullen P, Lorkowski J, Stolle K, Robenek H, Troyer D, et al. Production of type VI collagen by human macrophages: a new dimension in macrophage functional heterogeneity. J Immunol 2008 Apr 15;180(8):5707-5719.

111. Stout RD, Jiang C, Matta B, Tietzel I, Watkins SK, Suttles J. Macrophages sequentially change their functional phenotype in response to changes in microenvironmental influences. J Immunol 2005 Jul 1;175(1):342-349.

112. Mills CD, Kincaid K, Alt JM, Heilman MJ, Hill AM. M-1/M-2 macrophages and the Th1/Th2 paradigm. J Immunol 2000 Jun 15;164(12):6166-6173.

113. Song E, Ouyang N, Horbelt M, Antus B, Wang M, Exton MS. Influence of alternatively and classically activated macrophages on fibrogenic activities of human fibroblasts. Cell Immunol 2000 Aug 25;204(1):19-28.

114. Verreck FA, de Boer T, Langenberg DM, van der Zanden L, Ottenhoff TH. Phenotypic and functional profiling of human proinflammatory type-1 and anti-inflammatory type-2 macrophages in response to microbial antigens and IFN-gamma- and CD40L-mediated costimulation. J Leukoc Biol 2006 Feb;79(2):285-293.

115. Moore KW, de Waal Malefyt R, Coffman RL, O'Garra A. Interleukin-10 and the interleukin-10 receptor. Annu Rev Immunol 2001;19:683-765.

116. Buechler C, Ritter M, Orso E, Langmann T, Klucken J, Schmitz G. Regulation of scavenger receptor CD163 expression in human monocytes and macrophages by pro- and antiinflammatory stimuli. J Leukoc Biol 2000 Jan;67(1):97-103.

117. Sulahian TH, Hogger P, Wahner AE, Wardwell K, Goulding NJ, Sorg C, et al. Human monocytes express CD163, which is upregulated by IL-10 and identical to p155. Cytokine 2000 Sep;12(9):1312-1321.

118. Mantovani A, Sozzani S, Locati M, Allavena P, Sica A. Macrophage polarization: tumor-associated macrophages as a paradigm for polarized M2 mononuclear phagocytes. Trends Immunol 2002 Nov;23(11):549-555.

119. Hagemann T, Wilson J, Burke F, Kulbe H, Li NF, Pluddemann A, et al. Ovarian cancer cells polarize macrophages toward a tumor-associated phenotype. J Immunol 2006 Apr 15;176(8):5023-5032.

120. Hesse M, Modolell M, La Flamme AC, Schito M, Fuentes JM, Cheever AW, et al. Differential regulation of nitric oxide synthase-2 and arginase-1 by type 1/type 2 cytokines in vivo: granulomatous pathology is shaped by the pattern of L-arginine metabolism. J Immunol 2001 Dec 1;167(11):6533-6544.

121. Wynn TA. Fibrotic disease and the T(H)1/T(H)2 paradigm. Nat Rev Immunol 2004 Aug;4(8):583-594.

122. Rauh MJ, Ho V, Pereira C, Sham A, Sly LM, Lam V, et al. SHIP represses the generation of alternatively activated macrophages. Immunity 2005 Oct;23(4):361-374.

123. Gilbert TW, Sellaro TL, Badylak SF. Decellularization of tissues and organs. Biomaterials 2006 Jul;27(19):3675-3683.

124. Badylak S, Liang A, Record R, Tullius R, Hodde J. Endothelial cell adherence to small intestinal submucosa: an acellular bioscaffold. Biomaterials 1999 Dec;20(23-24):2257-2263.

125. Freytes DO, Tullius RS, Valentin JE, Stewart-Akers AM, Badylak SF. Hydrated versus lyophilized forms of porcine extracellular matrix derived from the urinary bladder. J Biomed Mater Res A 2008 Jan 28.

126. Feili-Hariri M, Falkner DH, Morel PA. Polarization of naive T cells into Th1 or Th2 by distinct cytokine-driven murine dendritic cell populations: implications for immunotherapy. J Leukoc Biol 2005 Sep;78(3):656-664.

127. Krook H, Hagberg A, Song Z, Landegren U, Wennberg L, Korsgren O. A distinct Th1 immune response precedes the described Th2 response in islet xenograft rejection. Diabetes 2002 Jan;51(1):79-86.

128. Sanchez-Madrid F, del Pozo MA. Leukocyte polarization in cell migration and immune interactions. EMBO J 1999 Feb 1;18(3):501-511.

129. Palmer EM, Beilfuss BA, Nagai T, Semnani RT, Badylak SF, van Seventer GA. Human helper T cell activation and differentiation is suppressed by porcine small intestinal submucosa. Tissue Eng 2002 Oct;8(5):893-900.

130. Allman AJ, McPherson TB, Merrill LC, Badylak SF, Metzger DW. The Th2-restricted immune response to xenogeneic small intestinal submucosa does not influence systemic protective immunity to viral and bacterial pathogens. Tissue Eng 2002 Feb;8(1):53-62.

131. Palmer EM, Baum LG, van Seventer GA. Small intestinal submucosa induces loss of mitochondrial integrity and caspase-dependent apoptosis in human T cells. Tissue Eng 2003 Apr;9(2):307-314.

132. Billiar K, Murray J, Laude D, Abraham G, Bachrach N. Effects of carbodiimide crosslinking conditions on the physical properties of laminated intestinal submucosa. J Biomed Mater Res 2001 Jul;56(1):101-108.

133. Hafemann B, Ghofrani K, Gattner HG, Stieve H, Pallua N. Cross-linking by 1-ethyl-3-(3-dimethylaminopropyl)-carbodiimide (EDC) of a collagen/elastin membrane meant to be used as a dermal substitute: effects on physical, biochemical and biological features in vitro. J Mater Sci Mater Med 2001 May;12(5):437-446.

134. Markowicz MP, Steffens GC, Fuchs PC, Pallua N. Enhanced dermal regeneration using modified collagen scaffolds: experimental porcine study. Int J Artif Organs 2006 Dec;29(12):1167-1173.

135. Harper C. Permacol: clinical experience with a new biomaterial. Hosp Med 2001 Feb;62(2):90-95.

136. Kim KM. Cells, rather than extracellular matrix, nucleate apatite in glutaraldehyde-treated vascular tissue. J Biomed Mater Res 2002 Mar 15;59(4):639-645.

137. Valente M, Laborde F, Thiene G, Milano A, Talenti E, Gallix P. Glutaraldehyde-fixed bovine iliac veins used as bioprosthetic conduits: an experimental animal study. J Card Surg 1992 Jun;7(2):156-162.

138. Hsu SY, Cheng JC, Chong YW, Leung PC. Glutaraldehyde-treated bioprosthetic substitute for rabbit Achilles tendon. Biomaterials 1989 May;10(4):258-264.

139. MacLeod TM, Sarathchandra P, Williams G, Sanders R, Green CJ. Evaluation of a porcine origin acellular dermal matrix and small intestinal submucosa as dermal replacements in preventing secondary skin graft contraction. Burns 2004 Aug;30(5):431-437.

140. Macleod TM, Sarathchandra P, Williams G, Sanders R, Green CJ. The diamond CO2 laser as a method of improving the vascularisation of a permanent collagen implant. Burns 2004 Nov;30(7):704-712.

141. Macleod TM, Williams G, Sanders R, Green CJ. Histological evaluation of Permacol as a subcutaneous implant over a 20-week period in the rat model. Br J Plast Surg 2005 Jun;58(4):518-532.

142. Belcher HJ, Zic R. Adverse effect of porcine collagen interposition after trapeziectomy: a comparative study. J Hand Surg [Br] 2001 Apr;26(2):159-164.

143. Cheung D, Brown L, Sampath R. Localized inferior orbital fibrosis associated with porcine dermal collagen xenograft orbital floor implant. Ophthal Plast Reconstr Surg 2004 May;20(3):257-259.

144. Saray A. Porcine dermal collagen (Permacol) for facial contour augmentation: preliminary report. Aesthetic Plast Surg 2003 Sep-Oct;27(5):368-375.

145. Liang HC, Chang Y, Hsu CK, Lee MH, Sung HW. Effects of crosslinking degree of an acellular biological tissue on its tissue regeneration pattern. Biomaterials 2004 Aug;25(17):3541-3552.

146. Courtman DW, Errett BF, Wilson GJ. The role of crosslinking in modification of the immune response elicited against xenogenic vascular acellular matrices. J Biomed Mater Res 2001 Jun 15;55(4):576-586.

147. Sung HW, Chang WH, Ma CY, Lee MH. Crosslinking of biological tissues using genipin and/or carbodiimide. J Biomed Mater Res A 2003 Mar 1;64(3):427-438.

148. Brown BN, Barnes CA, Kasick RT, Michel R, Gilbert TW, Beer-Stolz D, et al. Surface characterization of extracellular matrix scaffolds. Biomaterials 2009 Oct 12.

149. Jones JA, Chang DT, Meyerson H, Colton E, Kwon IK, Matsuda T, et al. Proteomic analysis and quantification of cytokines and chemokines from biomaterial surface-adherent macrophages and foreign body giant cells. J Biomed Mater Res A 2007 Dec 1;83(3):585-596.

150. Luttikhuizen DT, Dankers PY, Harmsen MC, van Luyn MJ. Material dependent differences in inflammatory gene expression by giant cells during the foreign body reaction. J Biomed Mater Res A 2007 Dec 1;83(3):879-886.

151. Brown BN, Valentin JE, Stewart-Akers AM, McCabe GP, Badylak SF. Macrophage phenotype and remodeling outcomes in response to biologic scaffolds with and without a cellular component. Biomaterials 2008 Dec 31.

152. Agrawal V, Brown BN, Beattie AJ, Gilbert TW, Badylak SF. Evidence of innervation following extracellular matrix scaffold-mediated remodelling of muscular tissues. J Tissue Eng Regen Med 2009 Aug 21.

153. Eitan Y, Sarig U, Dahan N, Machluf M. Acellular cardiac extracellular matrix as a scaffold for tissue engineering: In-vitro cell support, remodeling and biocompatibility. Tissue Eng Part C Methods 2009 Sep 25.

154. Wainwright JM, Czajka CA, Patel UB, Freytes DO, Tobita K, Gilbert TW, et al. Preparation of Cardiac Extracellular Matrix from an Intact Porcine Heart. Tissue Eng Part C Methods 2009 Aug 25.

155. Freytes DO, Badylak SF, Webster TJ, Geddes LA, Rundell AE. Biaxial strength of multilaminated extracellular matrix scaffolds. Biomaterials 2004 May;25(12):2353-2361.

156. Martinez FO, Gordon S, Locati M, Mantovani A. Transcriptional profiling of the human monocyte-to-macrophage differentiation and polarization: new molecules and patterns of gene expression. J Immunol 2006 Nov 15;177(10):7303-7311.

157. Schmittgen TD, Livak KJ. Analyzing real-time PCR data by the comparative C(T) method. Nat Protoc 2008;3(6):1101-1108.

158. Livak KJ, Schmittgen TD. Analysis of relative gene expression data using real-time quantitative PCR and the 2(-Delta Delta C(T)) Method. Methods 2001 Dec;25(4):402-408.

159. Chiang CS, Chen FH, Hong JH, Jiang PS, Huang HL, Wang CC, et al. Functional phenotype of macrophages depends on assay procedures. Int Immunol 2008 Feb;20(2):215-222.

160. Pham TN, Brown BL, Dobson PR, Richardson VJ. Protein kinase C-eta (PKC-eta) is required for the development of inducible nitric oxide synthase (iNOS) positive phenotype in human monocytic cells. Nitric Oxide 2003 Nov;9(3):123-134.

161. Pham TN, Rahman P, Tobin YM, Khraishi MM, Hamilton SF, Alderdice C, et al. Elevated serum nitric oxide levels in patients with inflammatory arthritis associated with co-expression of inducible nitric oxide synthase and protein kinase C-eta in peripheral blood monocyte-derived macrophages. J Rheumatol 2003 Dec;30(12):2529-2534.

162. Murdoch C, Muthana M, Lewis CE. Hypoxia regulates macrophage functions in inflammation. J Immunol 2005 Nov 15;175(10):6257-6263.

163. Bosco MC, Puppo M, Blengio F, Fraone T, Cappello P, Giovarelli M, et al. Monocytes and dendritic cells in a hypoxic environment: Spotlights on chemotaxis and migration. Immunobiology 2008;213(9-10):733-749.

164. Turner L, Scotton C, Negus R, Balkwill F. Hypoxia inhibits macrophage migration. Eur J Immunol 1999 Jul;29(7):2280-2287.

165. Csete M. Oxygen in the cultivation of stem cells. Ann N Y Acad Sci 2005 May;1049:1-8.

166. Coons DA, Alan Barber F. Tendon graft substitutes-rotator cuff patches. Sports Med Arthrosc 2006 Sep;14(3):185-190.

167. Van Rooijen N, Sanders A. Liposome mediated depletion of macrophages: mechanism of action, preparation of liposomes and applications. J Immunol Methods 1994 Sep 14;174(1-2):83-93.

168. van Rooijen N, Sanders A. Elimination, blocking, and activation of macrophages: three of a kind? J Leukoc Biol 1997 Dec;62(6):702-709.

169. van Rooijen N, Sanders A, van den Berg TK. Apoptosis of macrophages induced by liposome-mediated intracellular delivery of clodronate and propamidine. J Immunol Methods 1996 Jun 14;193(1):93-99.

170. van Rooijen N, van Kesteren-Hendrikx E. "In vivo" depletion of macrophages by liposome-mediated "suicide". Methods Enzymol 2003;373:3-16.

171. Stewart-Akers AM, Krasnow JS, Brekosky J, DeLoia JA. Endometrial leukocytes are altered numerically and functionally in women with implantation defects. Am J Reprod Immunol 1998 Jan;39(1):1-11.

172. Zheng MH, Chen J, Kirilak Y, Willers C, Xu J, Wood D. Porcine small intestine submucosa (SIS) is not an acellular collagenous matrix and contains porcine DNA: possible implications in human implantation. J Biomed Mater Res B Appl Biomater 2005 Apr;73(1):61-67.

173. Freytes DO, Stoner RM, Badylak SF. Uniaxial and biaxial properties of terminally sterilized porcine urinary bladder matrix scaffolds. J Biomed Mater Res B Appl Biomater 2008 Feb;84(2):408-414.

174. Gilbert TW, Wognum S, Joyce EM, Freytes DO, Sacks MS, Badylak SF. Collagen fiber alignment and biaxial mechanical behavior of porcine urinary bladder derived extracellular matrix. Biomaterials 2008 Dec;29(36):4775-4782.

175. Sacks MS, Gloeckner DC. Quantification of the fiber architecture and biaxial mechanical behavior of porcine intestinal submucosa. J Biomed Mater Res 1999 Jul;46(1):1-10.

176. Ko R, Kazacos EA, Snyder S, Ernst DM, Lantz GC. Tensile strength comparison of small intestinal submucosa body wall repair. J Surg Res 2006 Sep;135(1):9-17.

177. Konstantinovic ML, Lagae P, Zheng F, Verbeken EK, De Ridder D, Deprest JA. Comparison of host response to polypropylene and non-cross-linked porcine small intestine serosal-derived collagen implants in a rat model. BJOG 2005 Nov;112(11):1554-1560.

178. Schlegel TF, Hawkins RJ, Lewis CW, Motta T, Turner AS. The effects of augmentation with Swine small intestine submucosa on tendon healing under tension: histologic and mechanical evaluations in sheep. Am J Sports Med 2006 Feb;34(2):275-280.

179. Ota T, Gilbert TW, Badylak SF, Schwartzman D, Zenati MA. Electromechanical characterization of a tissue-engineered myocardial patch derived from extracellular matrix. J Thorac Cardiovasc Surg 2007 Apr;133(4):979-985.

180. Koning M, Harmsen MC, van Luyn MJ, Werker PM. Current opportunities and challenges in skeletal muscle tissue engineering. J Tissue Eng Regen Med 2009 Aug;3(6):407-415.

181. Yan W, George S, Fotadar U, Tyhovych N, Kamer A, Yost MJ, et al. Tissue engineering of skeletal muscle. Tissue Eng 2007 Nov;13(11):2781-2790.

182. Thorrez L, Shansky J, Wang L, Fast L, VandenDriessche T, Chuah M, et al. Growth, differentiation, transplantation and survival of human skeletal myofibers on biodegradable scaffolds. Biomaterials 2008 Jan;29(1):75-84.

183. Gilmore KJ, Kita M, Han Y, Gelmi A, Higgins MJ, Moulton SE, et al. Skeletal muscle cell proliferation and differentiation on polypyrrole substrates doped with extracellular matrix components. Biomaterials 2009 Oct;30(29):5292-5304.

184. Dhawan V, Lytle IF, Dow DE, Huang YC, Brown DL. Neurotization improves contractile forces of tissue-engineered skeletal muscle. Tissue Eng 2007 Nov;13(11):2813-2821.

185. Huang YC, Dennis RG, Larkin L, Baar K. Rapid formation of functional muscle in vitro using fibrin gels. J Appl Physiol 2005 Feb;98(2):706-713.

186. Khodabukus A, Baar K. Regulating Fibrinolysis to Engineer Skeletal Muscle from the C2C12 Cell Line. Tissue Eng Part C Methods 2009 Feb 3.

187. Powell CA, Smiley BL, Mills J, Vandenburgh HH. Mechanical stimulation improves tissue-engineered human skeletal muscle. Am J Physiol Cell Physiol 2002 Nov;283(5):C1557-1565.

188. Borschel GH, Dennis RG, Kuzon WM, Jr. Contractile skeletal muscle tissue-engineered on an acellular scaffold. Plast Reconstr Surg 2004 Feb;113(2):595-602; discussion 603-594.

189. Moon du G, Christ G, Stitzel JD, Atala A, Yoo JJ. Cyclic mechanical preconditioning improves engineered muscle contraction. Tissue Eng Part A 2008 Apr;14(4):473-482.

190. Lopes MF, Cabrita A, Ilharco J, Pessa P, Paiva-Carvalho J, Pires A, et al. Esophageal replacement in rat using porcine intestinal submucosa as a patch or a tube-shaped graft. Dis Esophagus 2006;19(4):254-259.

191. Delp MD, Duan C. Composition and size of type I, IIA, IID/X, and IIB fibers and citrate synthase activity of rat muscle. J Appl Physiol 1996 Jan;80(1):261-270.

192. Staron RS, Kraemer WJ, Hikida RS, Fry AC, Murray JD, Campos GE. Fiber type composition of four hindlimb muscles of adult Fisher 344 rats. Histochem Cell Biol 1999 Feb;111(2):117-123.

193. Ehrhardt J, Morgan J. Regenerative capacity of skeletal muscle. Curr Opin Neurol 2005 Oct;18(5):548-553.